THORIUM UTILIZATION PROGRAM

QUARTERLY PROGRESS REPORT FOR THE PERIOD ENDING NOVEMBER 30, 1974

Prepared under
Contract AT(04-3)-167
Project Agreement No. 53
for the
San Francisco Operations Office
U.S. Atomic Energy Commission

DATE PUBLISHED - FEBRUARY 15, 1975

Printed in the United States of America
Available from
National Technical Information Service
U.S. Department of Commerce
5285 Port Royal Road
Springfield, Virginia 22161
Price: Printed Copy $5.45; Microfiche $2.25

DISCLAIMER

GA-A13255
UC-77

THORIUM UTILIZATION PROGRAM

QUARTERLY PROGRESS REPORT
FOR THE PERIOD ENDING NOVEMBER 30, 1974

Prepared under
Contract AT(04-3)-167
Project Agreement No. 53
for the
San Francisco Operations Office
U.S. Atomic Energy Commission

GENERAL ATOMIC PROJECT 0852 DATE PUBLISHED - FEBRUARY 15, 1975

QUARTERLY REPORT SERIES*

GA-A13178 - June 1974 through August 1974

*Prior to GA-A13178, the Thorium Utilization Program was reported in the Base Program Quarterly Progress Report.

ABSTRACT

This publication is the second of a quarterly series presenting results of work performed under the National HTGR Fuel Recycle Program (also known as the Thorium Utilization Program) at General Atomic Company. Results of work on this program were previously included in a quarterly series on the HTGR Base Program.

The work reported includes the development of unit processes and equipment for reprocessing of High-Temperature Gas-Cooled Reactor (HTGR) fuel and the design and development of an integrated line to demonstrate the head end of HTGR reprocessing using unirradiated fuel materials. Work is also described on the evaluation of alternate techniques for fuel reprocessing to surmount possible operating problems with the reference flow sheet and the development of the conceptual design of a target recycle facility to identify the requirements of large-scale recycle of HTGR fuels.

INTRODUCTION

This report covers the work performed by General Atomic Company under U.S. Atomic Energy Commission Contract AT(04-3)-167, Project Agreement No. 53. The work done under this project agreement is part of the program for development of recycle technology for High-Temperature Gas-Cooled Reactor (HTGR) fuels described in the "National HTGR Fuel Recycle Development Program" (ORNL 4702).

The objective of the program is to provide the necessary technology, development, engineering, and demonstration of the steps required in the economic recycle of HTGR fuels utilizing thorium as a fertile material. Work at General Atomic Company is concentrating on the development of reprocessing methods (subtask 110 of the National Program), engineering and economic studies (subtask 310), and the application of recycle technology to the conceptual design of a large-scale recycle facility (subtask 320).

The objectives of subtask 110, Reprocessing Development, are to develop the necessary technology for the construction and operation of a prototype reprocessing facility which will process irradiated fuel materials and to provide the capability for commercial recycle of HTGR fuels. The output of this subtask includes (1) definition of process flow sheets, (2) development of equipment components, and (3) definition of operating data.

The objectives of subtask 310 are to guide the development program from the viewpoint of overall recycle needs and to obtain an economical HTGR fuel recycle method for early recovery and use of bred U-233. Alternate methods and options for reprocessing and refabrication are evaluated, and recommendations are made for possible further experimental development.

The objectives of subtask 320 are to develop a conceptual design of a target-size recycle plant for the reprocessing and refabrication of HTGR fuels and to use the results developed in the preparation of this design to guide the development work. The output of this task is in the form of design criteria, reference process flow sheets, and equipment sizing for a target recycle facility.

CONTENTS

FIGURES

FIGURES (continued)

TABLES

1. SUMMARY

In recent months direction has been received to expand the original scope of work for development of the UNIFRAME concept for head-end fuel element size reduction. A more comprehensive review of the concept than was previously necessary has therefore been undertaken and is partially complete.

The definition of an appropriate solids properties measurement program was completed during the reporting period.

A General Atomic topical report on the experimental classification of TRISO/TRISO fuel blends is in progress and is scheduled for publication in January.

Due to a lack of data on the pneumatic transport of solids specific to HTGR fuel reprocessing, an experimental pneumatic transport system will be assembled to obtain information to supplement known transport techniques.

Both the 10-cm and 20-cm primary fluidized-bed burners were operated to obtain development data to support the design of the 40-cm prototype primary burner. The 10-cm burner was utilized to determine the effect of feed size distribution and maximum feed size on burner operation. Also, the burner was operated with a bed height-to-diameter ratio approximating the conditions necessary to achieve the design burn rate of the prototype burner. The 20-cm burner is presently being used to study pneumatic fines injection as the technique for fines recycle. Pneumatic fines injection is the reference technique for the prototype primary burner.

The 10-cm secondary fluidized-bed burner presently incorporates all of the process considerations that are included in the reference prototype

design. Maximum burner capacity, bed size, and fluidizing velocity have been established, and an automatic control system for the burner is currently being installed for testing.

A fluidized-bed drying system was designed for drying the insoluble silicon carbide hulls received from the centrifuge separation of the product from the secondary burner ash dissolvers.

Eight solvent extraction run summaries were completed; the flowsheets tested indicated no problems that cannot be solved by changes in either flowsheet design or column design.

Studies were initiated concerning alternate reprocessing techniques. The first experiments will be aimed at a graphite/fuel separation method in which the majority of the graphite is mechanically removed.

2. FUEL ELEMENT CRUSHING

2.1. UNIFRAME PROTOTYPE FUEL ELEMENT SIZE REDUCTION SYSTEM

In recent months the UNIFRAME concept for head-end fuel element size reduction has received new direction requiring a more comprehensive review of the concept than was previously necessary. This review was continued during the reporting period and is partially completed.

2.1.1. Structural and Mechanical Design Analysis

The majority of the design calculations for the structural properties of the primary and secondary crushers has been completed. Some of the forces imposed on these components proved excessive and a redesign was initiated. As an example, the pushing block and its support were redesigned for "zero" torque.

Structural analysis of the UNIFRAME support structure will continue following approval of the concept. Further analysis will include a seismic loading distribution, with an acceleration-time history typical of those specified in AEC Regulatory Guide 1.60, and soil elasticity determinations.

Design calculations for the pin-joint connections for the pitman toe, toggles, and their respective bushings (see Fig. 1) were made according to the following procedure:

1. Assume a "tight" interference fit (Ref. 1) between the bearings and sleeves.

2. Calculate hoop stress (Ref. 2) between the sleeves and bronze bearings.

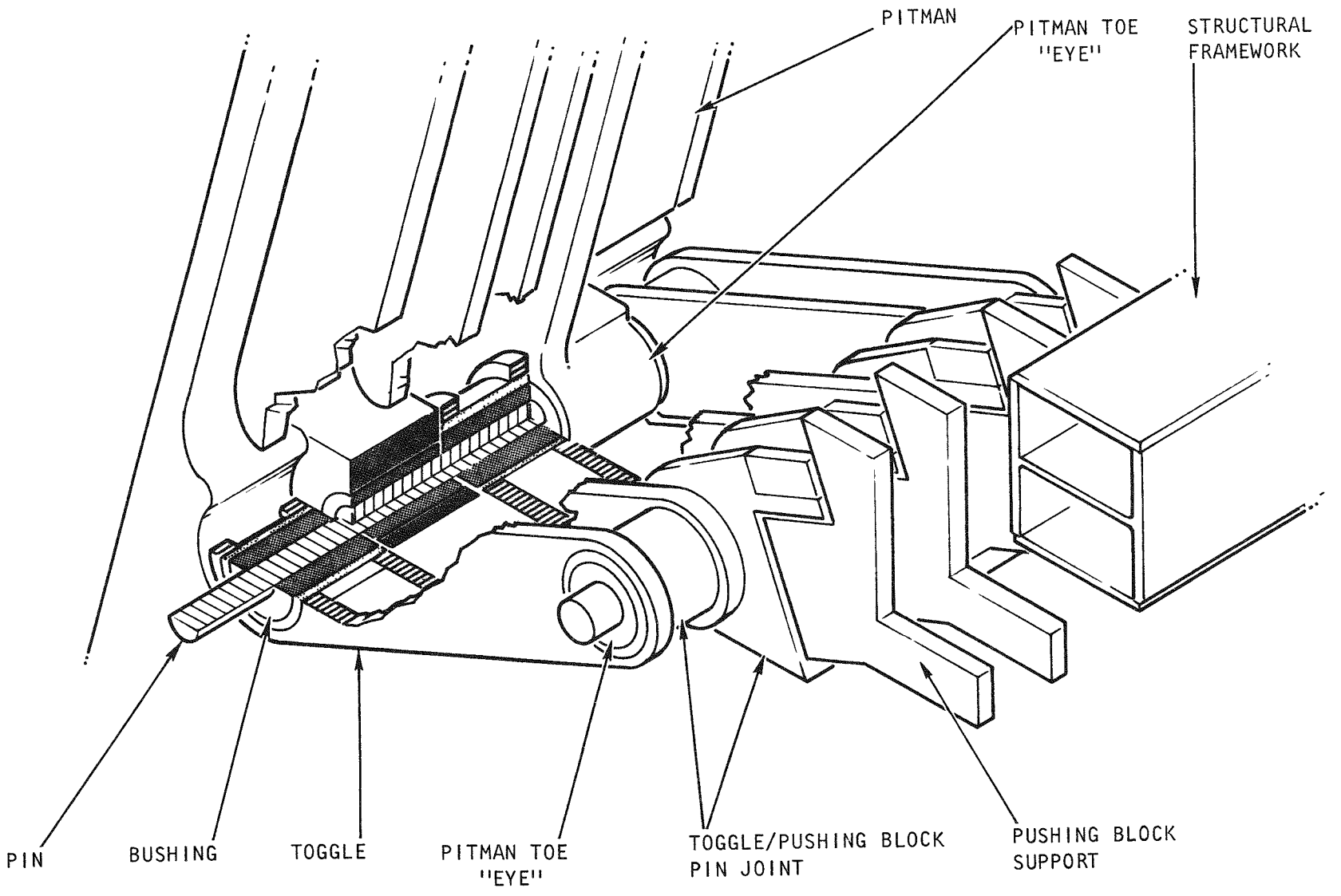

Fig. 1. Pin-joint connection

3. Calculate the stresses imposed by pins on sleeves and bearings (Ref. 3) by determining the contact angle of the pins on the bearings (Fig. 3 of Ref. 4) and subsequently obtaining the stress by finding the contact area on which the force acts.

4. Add the stresses obtained in steps (2) and (3) algebraically.

5. Calculate the "eye" strength (Fig. 2 of Ref. 4).

6. Calculate the compressive and radial crushing strength of the bronze bearings (Ref. 5).

The relative motion and velocity between the pitman toe, toggle, and pin were calculated by representing the jaw crusher assembly as a four-bar mechanism. In calculating the relative velocities in the motion of the mechanism, the following equation was developed for the relative velocity between the toggle and the pitman toe:

$$\dot{\theta}_4 = \frac{\ell_2}{\ell_4} \dot{\theta}_2 \frac{\sin (\theta_2 - \theta_3)}{\sin (\theta_3 - \theta_4)}$$

The mechanism is depicted in Fig. 2.

By measurements of each dimension and initial value in Fig. 2 at two extreme velocities of the pitman toe, the approximate relative velocity between the toggle and the pitman toe was found to be 16 rpm. This value was used as the basis for calculations of the corresponding wear and lubrication characteristics of the bushings.

The pins connecting the toggles, pitman toe, and pushing block are necessarily designed with "windows" on the shaft to accommodate wear debris resulting from the small relative oscillations between these moving parts (see Fig. 3). This phenomenon is known as fretting and is characteristic

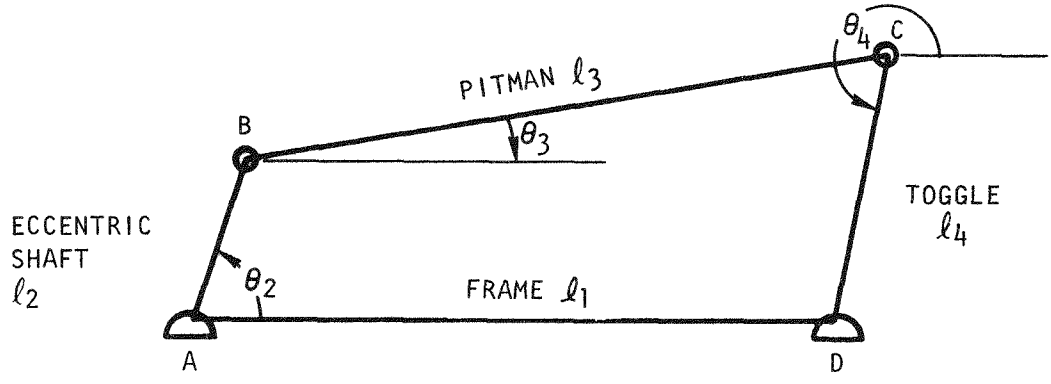

Fig. 2. Four-bar representation of an overhead eccentric jaw crusher

NOTES

1 DIMENSIONS & TOLERANCES PER ANSI Y14.5
2 REMOVE ALL BURRS & SHARP EDGES
3 REFERENCE LINES 1 & 2 IN ITEM 1 and 3 TO PERTAIN TO INSTALLATION OF PART
4 SURFACE FINISH AND TOLERANCES OF ITEMS 1, 2, 3 & 4 CALLED OUT IN TABLE
5 ONLY ITEMS 1 & 3, SHAFT TO HAVE CUT-OUTS AS SHOWN.

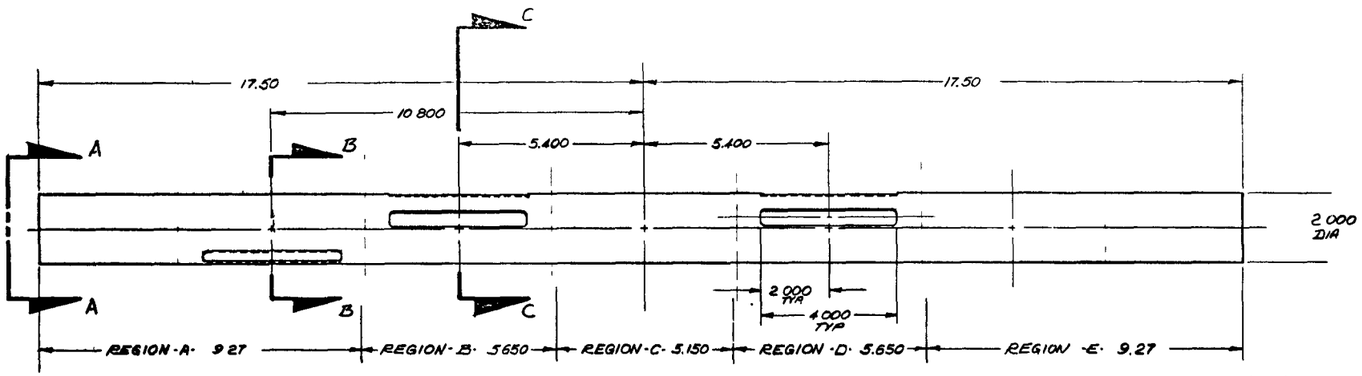

SHAFT, ½ SCALE

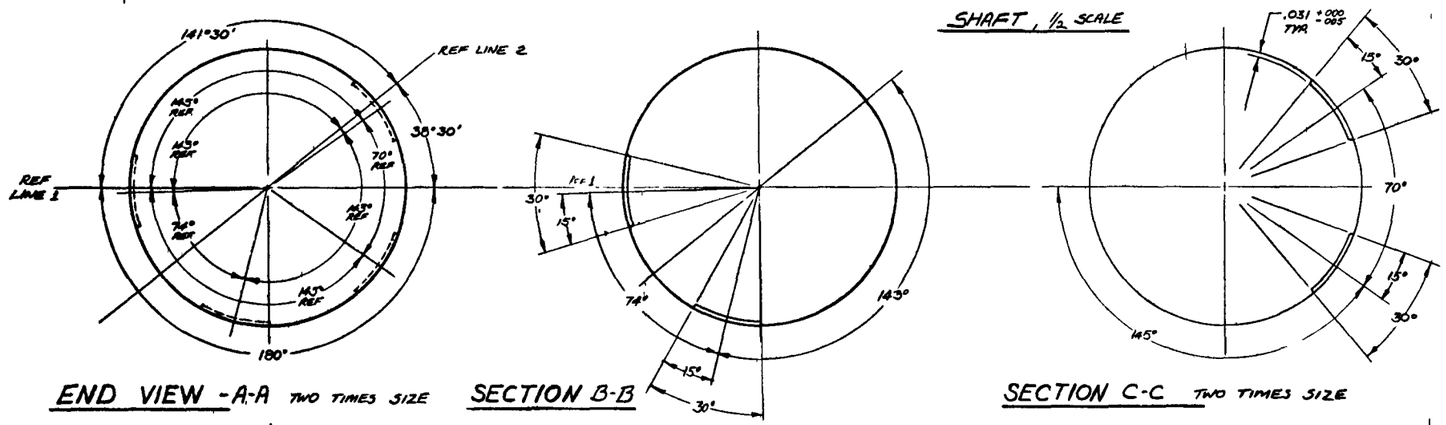

END VIEW -A-A TWO TIMES SIZE

SECTION B-B

SECTION C-C TWO TIMES SIZE

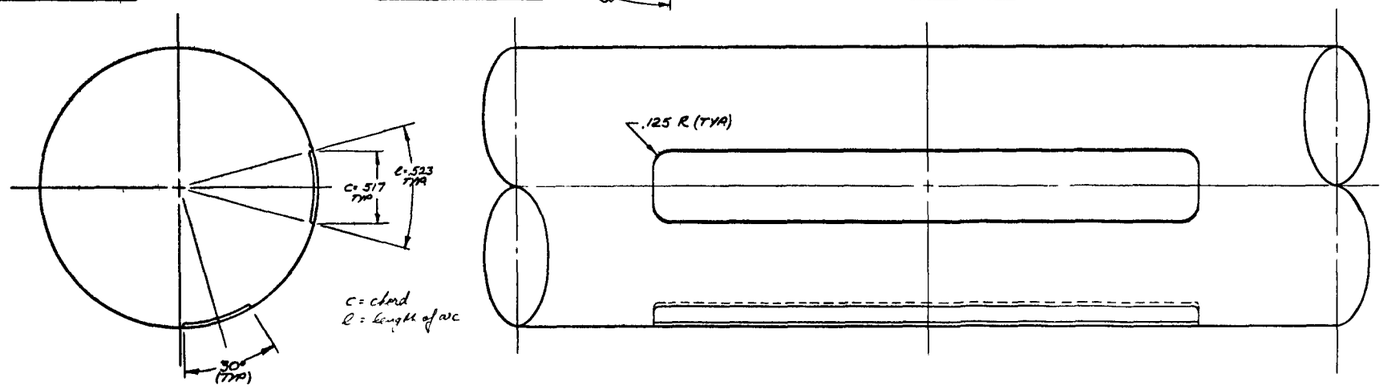

SECTION ROTATED 178°30' TWO TIMES SIZE

SHAFT ITEM	SURFACE FINISH IN RMS REGION					SHAFT DIA. & TOLERANCE
	A	B	C	D	E	
1	32	16	63	32	16	1.997 ± .001
2	32	32	16	63	63	1.997 ± 001
3	63	32	125	63	32	1.995 ± .002
4	63	63	32	125	125	1.995 ± .002

REQD/ASSEMBLY	ITEM	PART NO	DESCRIPTION	MATL	
			LIST OF MATERIAL		
	1	4	5210 152-4	SECONDARY CRUSHER TOGGLE-PUSHING BLOCK SHAFT	
	1	3	-3	SECONDARY CRUSHER PITMAN-TOGGLE SHAFT	
	1	2	-2	PRIMARY CRUSHER TOGGLE-PUSHING BLOCK SHAFT	
	1	1	5210 152-1	PRIMARY CRUSHER PITMAN-TOGGLE SHAFT	

Fig. 3. Toggle shaft, jaw crusher

of such systems. The dimensions and location of the "windows" were determined from the contact angle previously calculated in the design of the pitman toe.

In addition to accommodating the fretting phenomenon, the design must account for bending fatigue. Future evaluations of these problems include calculations to determine if the pin connection to the toggle and/or pitman should be an interference or clearance fit; this condition is identical to that at the pushing-block/toggle pin-joint connection. Also, since bolts are not desirable for anchoring the ends of the pin joints (due to the creation of bending moments on the pins), a fabricated end plate will be designed to satisfy this consideration.

A study, using Shell Turbo Oil-41 as the reference, was made of the lubrication system for the pitman-toe/toggle pin-joint connection. The reference oil was chosen because of its known successful use on machinery operating in an atmosphere contaminated by radioactivity.

Calculations indicated that the reference oil was sufficient for lubrication of the eccentric shaft of the pitman but insufficient for the bushings and pins of the pitman-toe and pushing-block toggles. The reason for this was the low (16 rpm) relative velocity between the toggle and pitman toe, which resulted in a lack of squeeze film generation. The squeeze film of lubricant generated between a shaft and a bushing is dependent on the power stroke duration, which is one-half of the period of motion in this application. Other lubricants, as well as a nonlubricated type bushing, are being considered for this application.

2.1.2. Maintainability and Reliability Analysis

A frequency of failure report was compiled using repair histories of the 15 ft by 28 ft Pacific jaw crusher. Histories were supplied by the manufacturer (Industrial Supply Company).

Using data compiled for the failure rates of specific components as a statistical base, maintainability and reliability analyses were calculated for the primary crusher to demonstrate application of the technique to the entire UNIFRAME system.

From the failure rates, assumptions were made as to the approximate remote repair or replacement time for each component. Using these approximations and the maximum time allowable for the maintenance actions, curves were generated for the probability of survival, equipment availability, and mission availability, and a value for the maintainability of the system was determined.

These mathematical techniques have been consolidated into a report for presentation at the ACC design review scheduled for December 15, 1974.

2.2. CRUSHED PRODUCT MONITORING SYSTEM

A comparative analysis was made of commercially offered screener separators. The purpose of the analysis was to determine which separators, if any, would best satisfy the UNIFRAME design criteria. These criteria consist of the following two mechanical considerations: (1) an in-line motion generator and motor assembly to provide symmetry of crushed product flow through the screener framework, and (2) easy access and adjustment of the motion generator in order to determine the optimum flow pattern of the oversized crushed product on the screen. A standard unit that meets our design requirements has not yet been completely developed. Other requirements for commercial screeners, in addition to the two above, are being considered in the design for a prototype screener. One of these considerations is the development of a support "spider" type framework for maximum sweep-down "air" flow characteristics of the <3/16-in. ring size crushed product through the screen to the pneumatic transport line. A second development is modification of the design for remote maintenance. The screen of the separator is a high maintenance item and, as such, must be easily replaced. Some type of shielding will be required for the motor and electrical connections.

Preliminary design calculations on the static and dynamic loading of the screen shown in Fig. 4 included the following:

1. Determination of the weight of the motion generator, motor, and supporting "spider" assembly.

2. Determination of the properties and generated static stresses of the springs.

3. Assumption of a model in which the motor and motion generator are represented as one mass with the three support spiders as cantilevered beams.

4. Treatment of the spiders as cantilevered at the end welded to the motor housing and free guided at the other end.

5. Calculation of the dynamic loading on the spider and welds assuming an equation of motion of the form $M\ddot{x} + Kx = F_o \sin \omega t$, where M = mass, K = spring constant, and F_o = initial force.

6. Determination of the moments and forces on the spiders at the welds.

7. Calculation of the weld requirements.

In addition, calculations will be done on the effect of the centrifugal force generated by the off-set or eccentric motion of the weights and the corresponding effect on the separator body.

2.3. DUST CONTAINMENT STRUCTURE

The equipment proposed for the fuel element size reduction system will undoubtedly produce dusts under normal operation; therefore, a dust containment structure is required. The primary objectives for this containment

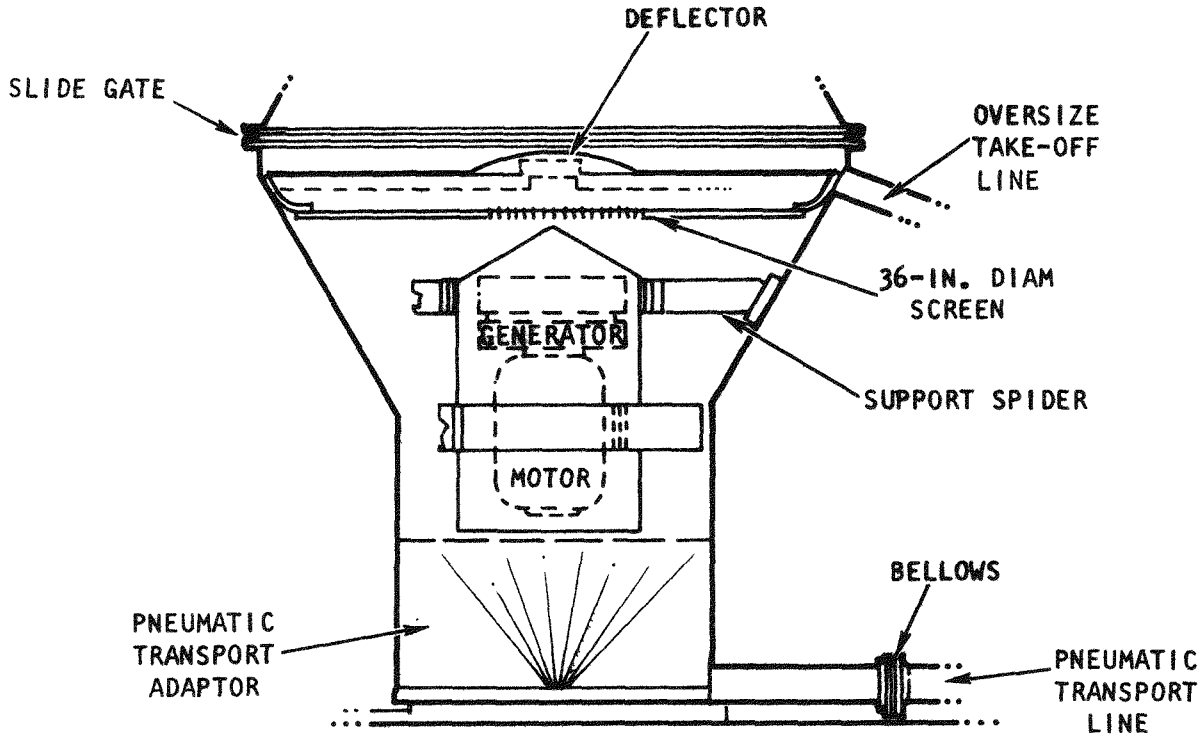

Fig. 4. Screener assembly

are to totally enclose all of the UNIFRAME dust-producing equipment while minimizing the surfaces that are exposed to the dust. Accomplishment of these objectives requires covering or "streamlining" equipment within the containment and making the containment no larger than required to produce the desired results without interfering with operations.

The dust containment design concepts, along with basic applicable ventilation calculations, will be included in the UNIFRAME design review report.

3. SOLIDS HANDLING

3.1. SOLIDS PROPERTIES

Due to the nature of the head-end processes of the Thorium Utilization Program, there are many applications of solids handling techniques. Handling of the types of solid materials peculiar to the head-end processes is an area lacking in specific information.

In order to better design solids handling equipment (e.g., bunkers, feeders, transporters, etc.), a literature search was initiated to determine the best available methods for prediction and measurement of the properties relating to the handling of particulate systems. From the literature it became apparent that there was little information that could be directly applied to our systems. However, one method that has enjoyed considerable success over the past few years was developed by A. W. Jenike (Ref. 6). This method combines a theoretical approach with empirical data gathered for support of the theory. Using this method a reliable design of bunkers and feed systems can be determined from the results of specific tests.

In order that these tests could be performed on the various particulate systems in the flowsheet, the actual type of testing equipment (flow factor tester and consolidating bench) perfected by Jenike was purchased (Figs. 5 and 6). Since many solids properties depend on humidity, a glove box and humidity control and monitoring equipment were also purchased and installed. Presently, preliminary tests are being conducted using primary burner fines to determine the optimum arrangement of the equipment and the adequacy of the humidity control equipment. Upon conclusion of these tests, scheduled for late November, extensive testing to find the relationship of the flow and storage properties for all of the particulate systems with time and humidity will be initiated.

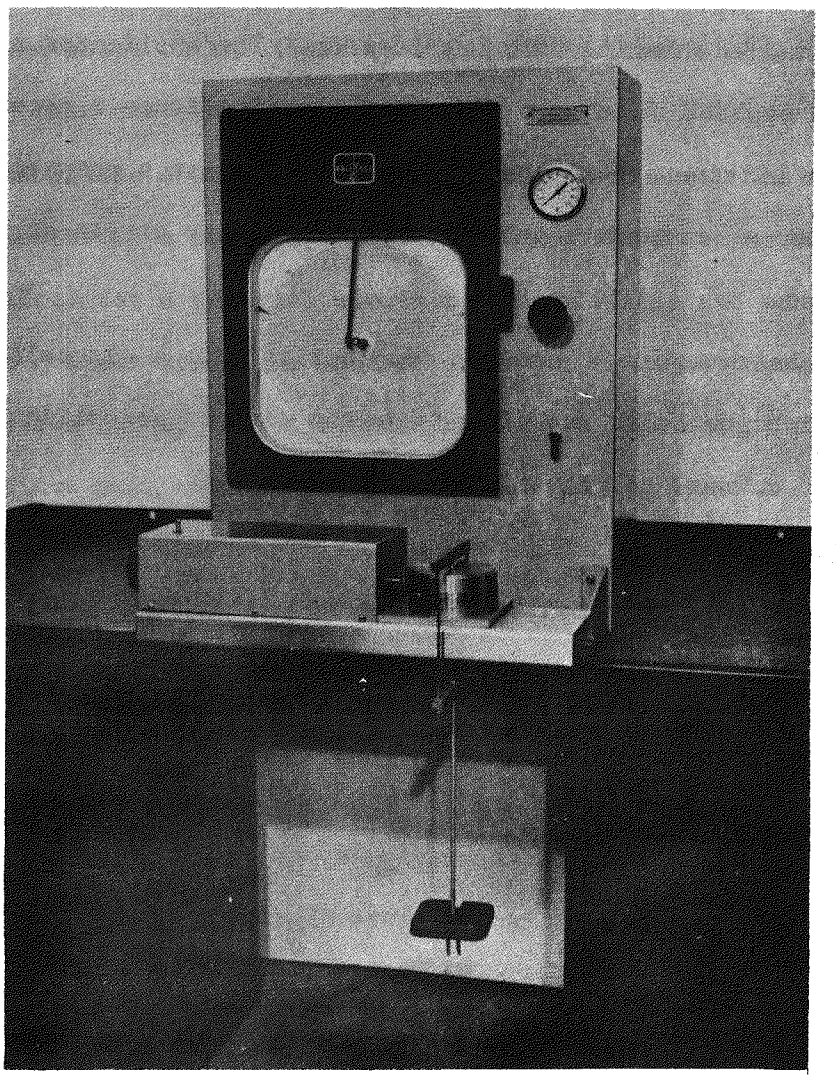

Fig. 5. Flow factor tester (from Ref. 6)

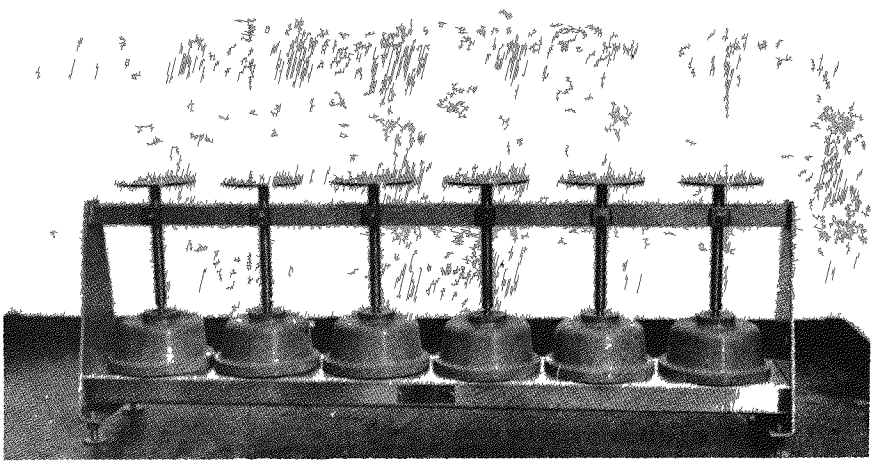

Fig. 6. Consolidating bench (from Ref. 6)

In parallel with these tests, a proposal is being submitted to ORNL requesting similar tests on these types of powder systems after irradiation. These tests would be performed in the ORNL hot cell using irradiated graphite and fuel from LHTGR fuel tests. Because of the hot cell constraints on manual dexterity, the flow factor tester and consolidating bench will be modified as shown in Fig. 7. The equipment list for these tests is given in Table 1. These modifications will allow faster and more accurate testing by eliminating many of the lifting and moving steps normally encountered in the course of performing the experiments. Also the addition of a movable catch bin will facilitate the accountability of the powders.

These tests will allow comparison of the flow and storage properties for the head-end particulate systems in both the unirradiated and irradiated state. This comparison will be invaluable in designing the handling equipment necessary for the transport and storage of the fuel between the various operations encountered in the flowsheet.

3.2. AIR CLASSIFICATION

A topical report on the experimental classification of TRISO/TRISO fuel blends is in preparation and is scheduled for publication in January. The report will document the efficiency of pneumatic classification and establish its relationship to: (1) air flow rates, (2) solids feed rates, (3) separation column height, (4) feed zone position, (5) the shape of the feed size distribution curves, and (6) the crossover between fissile and fertile streams. For comparison, the efficiency of separation by sieving and the effect of screen blinding will be included.

Experimentation using TRISO/BISO fuel blends is continuing.

For further demonstration of the pneumatic classification technique, a unit that is prototypical of the type equipment planned for "hot" demonstration is scheduled to be installed and tested at GA. A procurement schedule was completed and several purchase requisitions and requests for quote have been issued.

TABLE 1
PARTS LIST FOR SOLIDS PROPERTY TESTS AT OAK RIDGE HOT CELL[a]

Quantity	Description	Price ($)	Supplier
1	Flow factor tester with lead shielding	5,000	Jenike & Johanson
1	Consolidating bench	2,200	Jenike & Johanson
1	Change of overset of 2-1/2-in. cells	950	Jenike & Johanson
6	Cell bases	600	Jenike & Johanson
6	4-in. cell inserts	100	Machine shop
1	Tapping rod	50	Machine shop
1	Consolidating bridge	75	Sheet metal shop
1	1/4-in. base plate	300	Sheet metal shop
1	Schneeberger dovetail tract	1,500	Bendix Corp.
1	Lead screw with two bearings	300	Acme Tool and Supply
1	Electric motor (1/4 hp) with sprockets and chain	350	Sabina
7	Limit switches	200	General Electric
1	Catch pan with drainer	400	Sheet metal shop
1	Guide for pan	100	Sheet metal shop
1	Pulley assembly to drive pan	150	Sheet metal shop
1	Set of weights	500	American Balance Co.
1	Balance	1,300	Metler
1	Temperature/humidity recorder	1,000	Honeywell
		15,575	

[a]Assembly time - 80 hr.

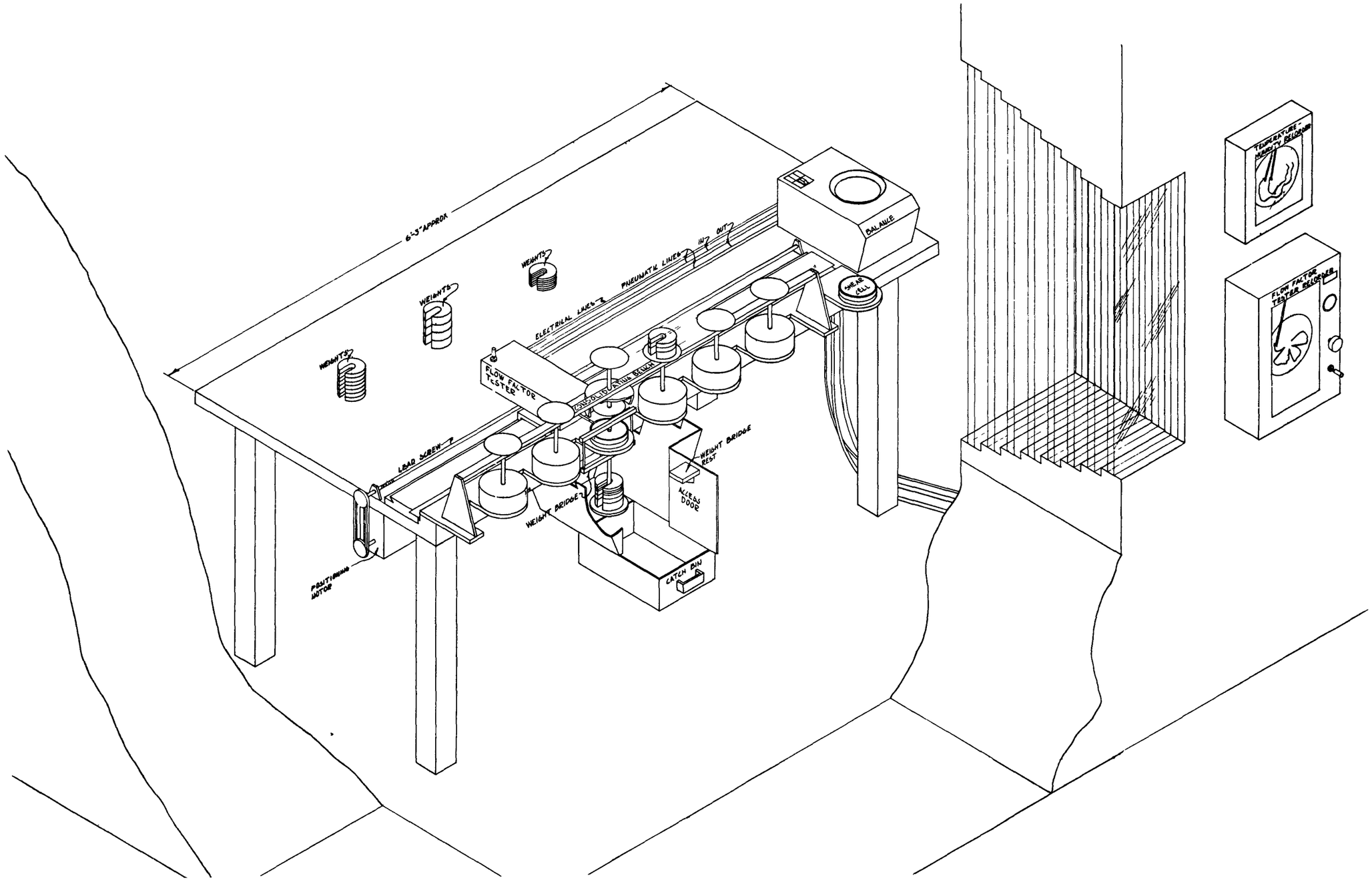

Fig. 7. ORNL hot cell arrangement

3.3. EXPERIMENTAL PNEUMATIC TRANSPORT SYSTEMS

Since there is a lack of data on the pneumatic transport of solids specific to the reprocessing of HTGR fuels, an experimental pneumatic transport system will be assembled for obtaining information to supplement known transport techniques. The system (described in Ref. 7) will be capable of testing a variety of parameters and equipment with the three major types of solids requiring transport in the proposed head-end process, i.e., crushed (-3/16 in. ring size) fuel element fragments, primary burner product, and secondary burner product.

Design of the system has been completed. Procurement requisitions for the necessary equipment have been written and some items have been received.

4. FLUIDIZED-BED COMBUSTION

4.1. PRIMARY FLUIDIZED-BED COMBUSTION

During this reporting period both the 10-cm and 20-cm primary fluidized-bed burners were operated to obtain development data for support of the prototype design. The 10-cm burner was utilized to determine the effect of the feed size distribution and the maximum feed size on burner operation. The burner was also operated with a bed height-to-diameter ratio approximating the conditions necessary to achieve the design burn rate of the prototype burner. The 20-cm burner is presently being used to study the effect of pneumatic fines injection as the technique for fines recycle. This is the reference technique for the prototype burner.

4.1.1. 10-cm Primary Fluidized-Bed Combustor

Seven runs were performed in the 10-cm primary burner during the last quarter. These runs are summarized in Table 2. Run 46 (Ref. 8) was performed to determine the effects on burner operation of operating with a large bed (6.5 to 8.0 kg, L/D of 7 to 9) and 100% oxygen in the inlet gas. Secondary oxygen (20% of total O_2) was used and experimental overall heat transfer coefficients were obtained. Results showed that operation with a larger bed resulted in more efficient utilization of the burner heat transfer area and a larger maximum burn rate. Larger fluctuations in bed ΔP were observed; cyclic variations of 5 to 10% of the total ΔP were noted every 15 to 60 sec. Slugging was evidently very severe and affected operation of the product take-off device (a rotary valve controlled by the bed ΔP). The severe slugging was consistent with the fact that the bubble diameter increases with bed depth and gas velocity and that the frequency with which bubbles are formed and rise through the bed is inversely dependent on bed depth and gas velocity. In addition, the bottom feed auger

TABLE 2
SUMMARY OF 10-CM PRIMARY BURNER RUNS

Run	Objectives	Fines Recycle	Fresh Feed Inlet	Results
46	Determine effects of operation with large bed and 100% oxygen inlet gas. Test new untapered recycle feed auger.	Yes	Bottom	The new auger provided improved operation of the recycle feed system A larger bed resulted in better heat transfer, a higher maximum burn rate, and increased slugging with cyclic variation of operating parameters.
47-48	Evaluate effects of feed size and feed size distribution on burner operation (-3/16-in. feed without additional fines mixed in).	No	Bottom	Both runs used feed with a higher than normal percentage of large material, which resulted in significant slugging and operating transients. Run 48 used larger feed and exhibited considerably more unstable operation.
49-50	Evaluate effects of feed size and feed size distribution on burner operation (-3/16-in. feed with additional fines mixed in).	No	Bottom	30 to 50% fines were added to -3/16-in. feed with the same size distribution as that of Run 48, which resulted in much smoother operation and control.

TABLE 2 (Continued)

Run	Objectives	Fines Recycle	Fresh Feed Inlet	Results
49-50				Material balances showed fines generation to exceed fines burning for Runs 47-50 and to be in direct proportion to the weight of large material (>1000 μm) in the feed.
51	Evaluate effects of feed size and feed size distribution on burner operation (-1/4-in. feed with additional fines mixed in).	No	Bottom	Extremely poor fluidization resulted in formation of large agglomerates and emergency shutdown. The -1/4-in. feed appears to be too large for use in the 10-cm primary burner.
52	Evaluate performance of new top fresh feed auger and compare operation with that of Run 47.	No	Top	Operation was again unstable due to large feed size and lack of fines. The new top feed auger performed adequately. Small agglomerates were formed which probably resulted from the existence of chemical impurities on the fuel particles.

(a two-section auger) was modified and tested. Use of an untapered lower auger resulted in improved operation of the recycle auger feed system (Ref. 9).

Runs 47 and 48 were performed to obtain data for evaluation of the effects of feed size and feed size distribution on burner operation. Both runs were performed without fines recycle and with the feed size distributions shown in Fig. 8. Run 47 utilized -3/16-in. feed with a size distribution having a greater amount of larger material than any previous run in the present burner. Since the run was performed without fines recycle, it can be considered to represent the worst case with respect to bed fluidization properties for the particular fresh feed size distribution used. Run 47 exhibited significant temperature and ΔP transients, which were the result of continuous internal phenomena. Slugging occurred such that the bed ΔP cycled by as much as 15 to 20% of the total ΔP at a frequency of 1 to 2 min.

Run 48 also utilized -3/16-in. feed but with an even greater amount of larger material than in Run 47. The results of Run 48 were similar to those of Run 47. During Run 48 the bed ΔP transients were only approximately 10% of the total ΔP but occurred at 2- to 6- min intervals. As a result, the temperature and CO off-gas transients were more severe. Typical cyclical variations were 900° to 1050°C and 22 to 30% CO, which indicated that the burning zone underwent continuous and drastic changes consistent with poor fluidization. Axial temperature gradients were extremely large, often varying by 200°C over an 8-in. length of the burning zone. When the gas velocity was increased during attempts to improve fluidization, a temporary improvement usually occurred; however, invariably the fluidization eventually worsened. Fines elutriation data for Runs 47 and 48 are shown in Tables 3 and 4.

Runs 49, 50, and 51 were also performed with bottom fresh feed and no fines recycle to further evaluate the effects of feed size and feed size distribution on burner operation. The fresh feed size distribution (-3/16 in.) for Runs 49 and 50 was the same as that used in Run 48 except that 30%

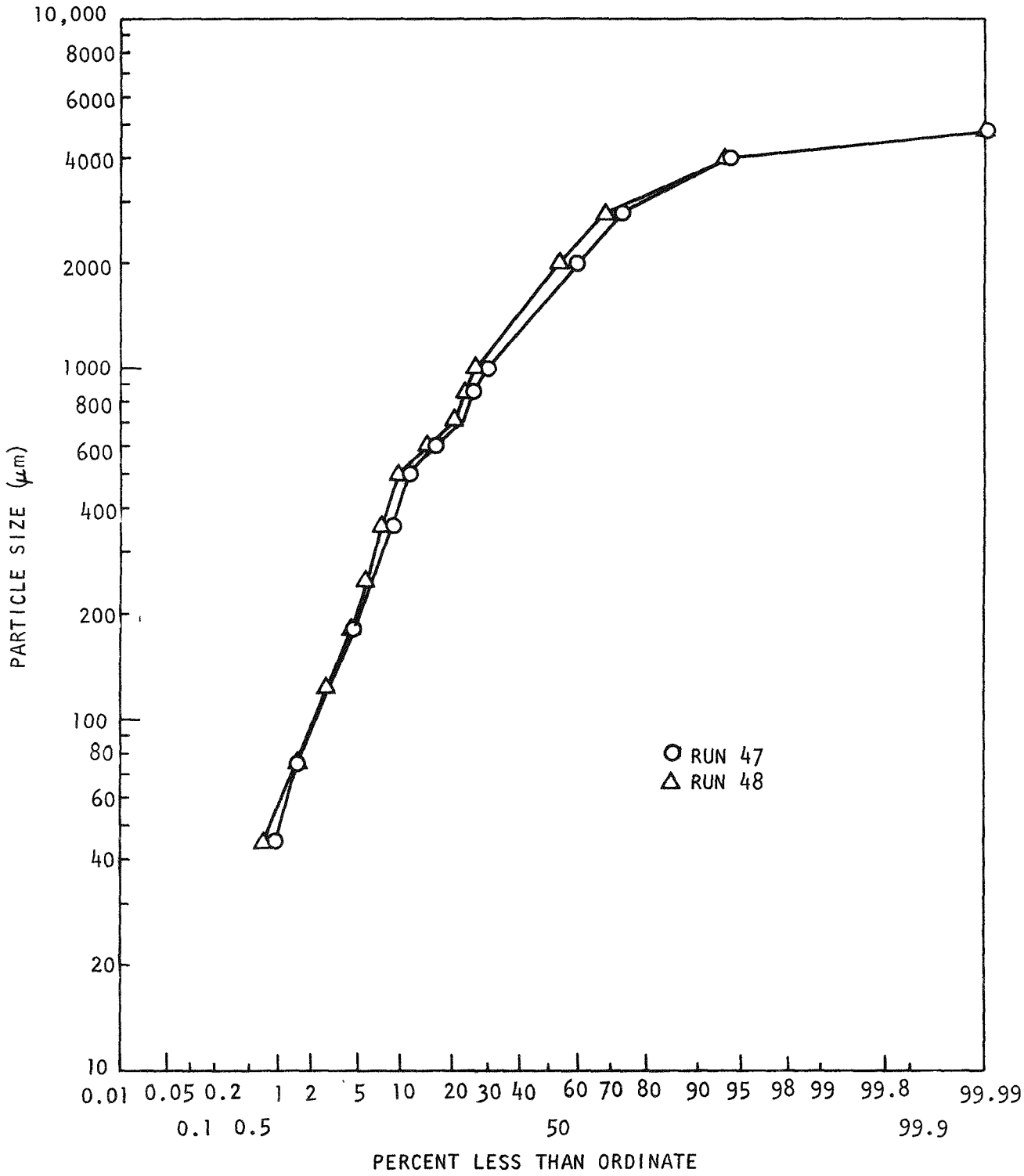

Fig. 8. Feed size distributions, Runs 47 and 48

TABLE 3
DATA FOR RUN 47

Time of Run (min)	Average Cone Gas Flows (SLPM)		Average Burn Rate (g C/min)	Average Bed Size (kg)	Average Top of Burner Superficial Velocity (cm/sec)	Total Fines (g)	Average Fines Rate (g/min)
	O_2	N_2					
60-106	65.8	16.2	38.2	4.3	45.2	1404	30.5
106-151	64.1	19.2	39.0	4.4	43.9	1114	24.8
151-196	63.9	19.7	39.2	4.4	44.6	1218	27.1
196-241	65.3	19.8	40.0	4.4	47.5	1420	31.6
241-276	64.0	20.9	39.1	4.5	46.3	977	27.9

TABLE 4
DATA FOR RUN 48

Time of Run (min)	Average Cone Gas Flows (SLPM)		Average Burn Rate (g C/min)	Average Bed Size (kg)	Average Top of Burner Superficial Velocity (cm/sec)	Total Fines (g)	Average Fine Rate (g/min)
	O_2	N_2					
60-105	64.2	18.9	37.9	4.0	48.0	1113	24.7
105-145	59.7	25.2	37.1	4.2	42.8	620	15.5
145-185	59.0	27.5	37.3	4.1	43.9	645	16.1
185-205	62.5	23.1	38.9	4.1	45.9	437	21.9
205-245	62.7	25.0	39.6	4.1	48.4	860	21.5
245-285	67.3	22.4	42.3	4.2	52.3	1136	28.4
285-313	65.0	27.0	41.9	4.1	51.1	574	20.5

and 50% fines, respectively, were added. Burner operation and control were much smoother as bed ΔP, off-gas, and temperature transients were much less severe. The difference in fines content of the feed between Runs 49 and 50 did not result in any appreciable difference in operation or burner control between these runs. The CO/CO_2 off-gas ratio was considerably smaller in Runs 49 and 50 then in Run 48, which can be attributed to the lack of the extremely high temperature at the bottom of the bed observed in Run 48. A cooler and longer burning zone is more conducive to CO_2 formation than to CO formation. Fines elutriation data for Runs 49 and 50 are shown in Tables 5 and 6.

Run 51 was performed with -1/4-in. feed mixed with 50% fines. This run was terminated by emergency shutdown prompted by the existence of two large agglomerates. Utilization of the -1/4-in. feed in Run 51 resulted in extremely erratic and unpredictable operating transients that occurred at no particular frequency. This represented a much more unstable situation than in the previous runs. During the final 20 min of the run, the off-gas transients increased drastically to a point where the CO concentration reached 40% shortly before shutdown. At that point, the cone exhibited large hot spots, which were caused by the agglomerates. Until the final 20 min of Run 51, there appeared to be no way of knowing from the burner controls and instrumentation that agglomeration was in the process. The reason for its occurrence was thought to be insufficient fluidization (mixing) in the bed caused by the use of the larger -1/4-in. feed. Because of the relatively small size of the burner (10-cm diameter) and because of the dependence of quality of mixing on the bed diameter, size distribution in the bed is probably affected more by feed size than by gas fluidization velocity. When mixing is poor, heat transfer from the system is considerably reduced. Static burning of this nature is particularly dangerous when one considers the potentially high local temperatures accompanying poor heat transfer through the bed. Due to the heat of combustion of carbon, the surface temperature of burning graphite can be as much as several hundred degrees Kelvin hotter than the surrounding

TABLE 5
DATA FOR RUN 49

Time of Run (min)	Average Cone Gas Flows (SLPM)		Average Burn Rate (g C/min)	Average Bed Size (kg)	Average Top of Burner Superficial Velocity (cm/sec)	Total Fines (g)	Average Fine Rate (g/min)
	O_2	N_2					
65-110	19.3	67.4	38.7	4.2	56.9	2661	59.1
110-145	24.7	64.2	38.2	4.2	54.7	1553	44.4
145-198	19.5	66.0	38.8	4.2	53.8	3178	60.0
198-230	19.5	66.0	38.9	4.4	53.8	1817	56.8
230-270	19.5	66.0	38.9	4.5	53.7	2392	59.8
270-303	19.5	66.0	38.9	4.3	53.8	1849	56.0

TABLE 6
DATA FOR RUN 50

Time of Run (min)	Average Cone Gas Flows (SLPM)		Average Burn Rate (g C/min)	Average Bed Size (kg)	Average Top of Burner Superficial Velocity (cm/sec)	Total Fines (g)	Average Fine Rate (g/min)
	O_2	N_2					
56-116	14.1	69.9	39.6	4.1	58.4	3592	59.9
116-149	20.9	67.0	38.3	4.2	58.2	2858	86.6
149-189	19.6	67.7	39.5	4.3	57.9	3487	87.2
189-224	21.2	67.1	39.7	4.1	56.5	2735	78.1
224-268	21.1	67.5	39.7	4.1	57.0	3610	82.0
268-311	19.7	68.7	40.2	4.0	58.2	4385	102.0

gas (Ref. 10). Static burning could very possibly cause local temperatures hot enough to initiate the agglomeration process in the bed.

Table 7 gives the fines elutriation data for Run 51. Table 8 shows a comparison of average fines data for various runs performed without fines recycle. For the purpose of definition, all graphite in each stream less than 355-μm ring size was considered to be fines. From size distribution analyses of elutriated fines, burner product, and feed, it was possible to perform average fines material balances for each run using the following equation:

Feed + generation = elutriation + product + burning.

In this way, a comparison of the relative generation and burning of fines was obtained for each run by calculating the quantity (fines generation - fines burning). In all cases it was found that fines generation exceeded fines burning. However, the difference between the quantity of fines generated and burned seemed to be directly proportional to the weight of material in the feed greater than 710 μm (or 1000 μm) for each run. This indicated that minimizing the weight of relatively large graphite in the feed would be desirable in order to achieve operation where fines burning exceeds fines generation in the bed. Also, it would seem that increasing the fines recycle rate would tend to have the same effect.

Run 52 was performed to test operation of a newly installed top fresh feed auger. The feed size and size distribution were equivalent to Run 47 so that differences in fines elutriation and overall burner operation could be determined between operation with top feed and with bottom feed. The top fresh feed auger was dimensionally identical to the tapered upper recycle auger (Ref. 9). The performance of the auger was entirely adequate during the run. A calibration is shown in Fig. 9. However, due to size of the exit duct (2-in. diameter) at the top of the burner, the fluidizing gas velocity was such that it prevented much of the fines in the fresh feed from entering the burner. Thus, fines elutriation

TABLE 7
DATA FOR RUN 51

Time of Run (min)	Average Cone Gas Flows (SLPM)		Average Burn Rate (g C/min)	Average Bed Size (kg)	Average Top of Burner Superficial Velocity (cm/sec)	Total Fines (g)	Average Fine Rate (g/min)
	O_2	N_2					
92-120	15.0	69.0	40.1	3.8	55.5	2089	74.6
120-157	12.8	68.8	39.2	4.1	50.1	2395	64.7
157-205	17.8	69.2	40.9	4.4	55.0	3823	79.6
205-250	17.8	69.2	41.4	4.2	56.2	3987	88.6

TABLE 8
COMPARISON OF FINES DATA FOR RUNS WITHOUT FINES RECYCLE

Run	Average Burn Rate (g C/min)	Average Fines in Feed (wt %)	Average Feed Rate (g/min)			Average Fines Elutriation (g/min)	Average Product Fines (g/min)	Average Fines in Feed (g/min)	Average Fines Rates (Generation - Burning) (g/min)
			>2000 μm	>1000 μm	>710 μm				
47	39.1	8.1	35	52	59	28.4	1.9	6.8	+23.5
48	39.2	7.3	38	52	57	21.3	2.5	5.9	+17.9
38	37.2	7.2	21	45	52	21.0	2.3	5.0	+18.3
39	36.6	7.8	18	39	47	19.0	1.8	5.5	+15.3
49	38.7	33.5	37	50	56	56.3	2.1	37.3	+21.1
50	39.5	56.5	27	36	40	80.8	2.2	72.0	+11.0
51[a]	40.5	57.0	25	33	38	77.6	2.3	73.0	+6.9

[a] Run terminated due to formation of massive agglomerates.

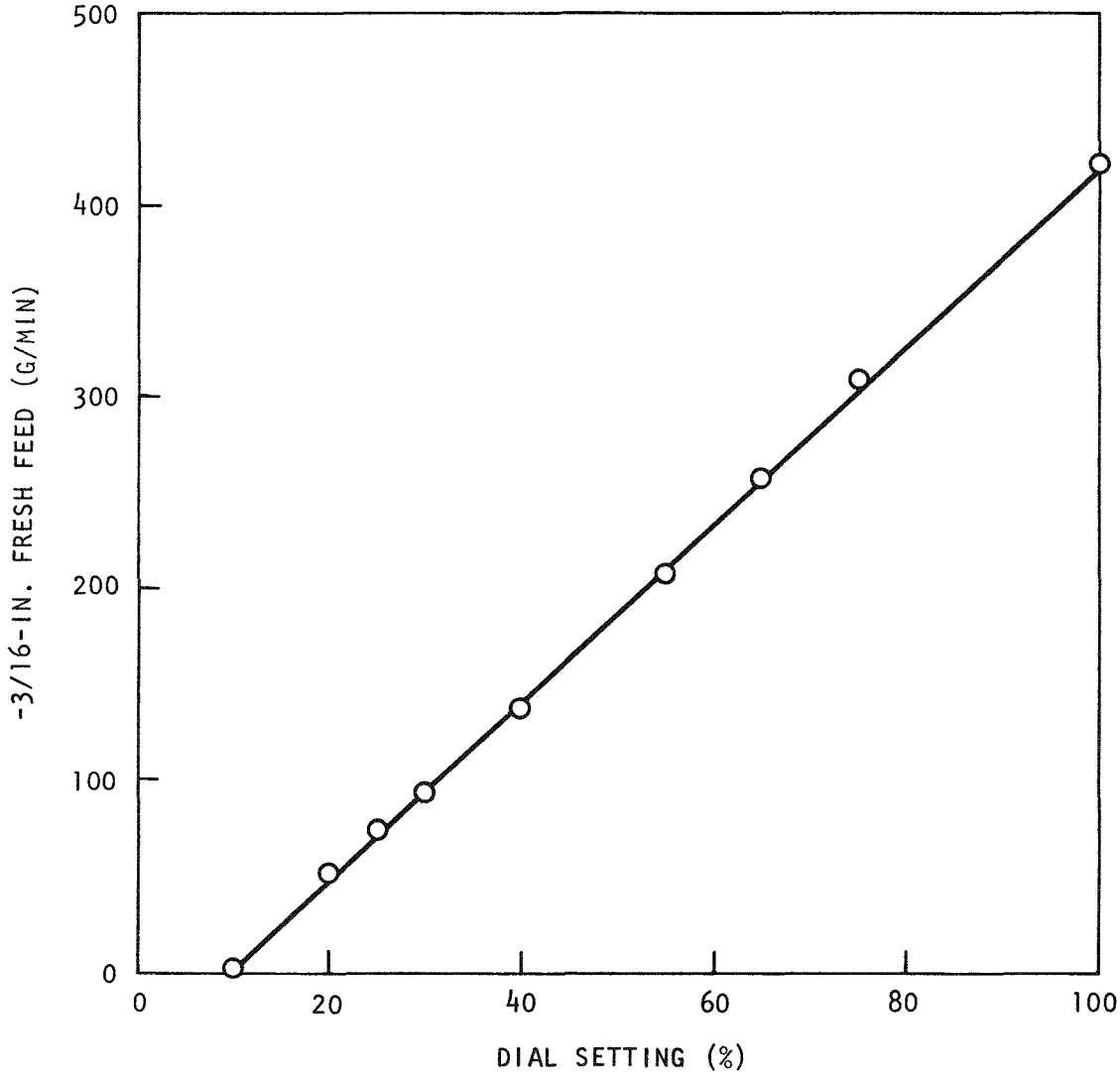

Fig. 9. Calibration for top fresh feed auger

data were not representative of the fresh feed size distribution, which turned out to be actually larger than that in Run 47. As a result, operation during Run 52 was considerably more unstable. After only 152 min of operation, operating transients became so severe that shutdown was necessitated. The final bed was found to contain an extremely large amount of small fuel particle agglomerates, all of which were in the 1000 to 2000 μm size range and were situated in the bottom half of the bed. In all probability, the small size of the agglomerates was due to the relatively short duration of the run. Previous experience has shown that agglomerates tend to grow as a function of time.

Several analytical tests were performed on the feed and product materials of Run 52 in an effort to determine a definite cause or mechanism for the observed agglomeration. Results showed that these materials contained significant amounts of surface impurities. Elements such as Ca, Cr, Ni, Fe, Cl, K, Al, and Cu were found in varying degrees. The magnitude of some of the detected impurities can be directly attributed to the fact that the feed particles used in Run 52 (and Run 51) had been used in previous runs and, therefore, could have accumulated certain amounts of impurities with each usage. The origin of the impurities, however, can be attributed to several possibilities. The stainless steel and Hastelloy-X burner vessel materials could account for several of the impurities. In addition, analysis of the coke used during startup for Run 52 showed the existence of significant amounts of Ca, Al, and Fe. Whatever the source of the impurities, their existence on the outer coatings of the fuel particles in significant amounts could lower surface melting points such that agglomeration becomes more possible at certain burner operating conditions. Future runs will use particles that have been analyzed for chemical impurities. The agglomeration problem that occasionally occurs may be eliminated by this preliminary analysis. Continued observation of the problem would indicate that the cause is attributable to burner operating conditions rather than to chemical impurities.

4.1.2. 20-cm Primary Fluidized-Bed Combustor

At present the 20-cm burner is being utilized for development and testing of pneumatic fines injection, which is the reference recycle technique for the prototype burner. As soon as the parts are available, the reference gas distributor design will also be tested. This design combines a perforated conical distributor with pneumatic fines injection, as described in Ref. 7. Pneumatic injection of fines to the bottom of the burner should provide better mixing of fines and oxygen than is possible utilizing a mechanical feeder; this should provide better fines combustion and lower elutriation rates than are obtained with mechanical feeders.

Two runs were made with pneumatic fines recycle premixed with cone gas and top feed of -3/16-in. graphite mixed with TRISO fertile particles, after prior runs with the new larger check ball had proved successful. Although the operational data are still being analyzed, preliminary calculations and observations specific to the last run (5 hr with fines recycle) indicate the following:

1. The average burn rate was approximately 200 g/min, with a maximum burn rate of about 250 g/min.

2. Operation with fines recycle was very stable, i.e., even temperature profiles.

3. Heat transfer was quite high as burner off-gas and clamshell cooling off-gas temperatures relative to the bed temperature were significantly higher than in past runs without fines recycle.

4. Continuous nitrogen purges in the fines recycle lines averted the cyclone and fines sample line bridging seen in the prior run with fines recycle, but fines line saltation requires resizing

and revamping of the fines circulation system before longer duration runs can be made with confidence.

5. Fines circulation/recycle/burn rates could not be measured due to saltation in the recycle line and failure of the nonmetallic seating surface on the fines sample diverter valve; however, total fines system clean-out at the end of the run revealed 18 kg of fines or 60 g/min buildup during the 5-hr run. This is compared to expected fines generation rates on the order of 130^{+} g/min. Thus, although fines generation exceeded fines burning, pneumatic injection of fines low in the burner shows promise.

The response of the eductor pneumatic fines ejector to the slugging bed was observed as pulsation of the fines feed. Calibration curves generated during bench tests of the fines eductor indicated recycle rates varying from 200 to 300 g/min at 40 and 60 psig supply gas pressure, respectively, with the bed backpressure between 2.5 and 4 psig. These values will remain qualitative until the fines transport system structural design and instrumentation are improved. A fines hopper load cell on-line weighing system is being evaluated, and design of the cyclone and fines lines is in review.

4.1.3. Prototype Primary Fluidized-Bed Combustor

The prototype design has progressed to the stage of detail design of auxiliary components. Current efforts have been concentrated on detail design of the cooling jacket, which will accommodate a susceptor in the lower section. The support for this susceptor must be sturdy enough to withstand the high-velocity air flow ($\sim$200 ft/sec) necessary for cooling and yet the susceptor should be remotely or semi-remotely replaceable. Centering and warping during thermal cycles of the susceptor in the annulus present another design constraint. Careful consideration of air velocity

in each portion of the jacket is exercised in the design to minimize the pressure drop across the cooling jacket, as well as to reduce noise and vibration. The design is further restricted in that the cooling jacket must be able to "swing away" or "retract" to allow removal of the burner vessel from the support platform to a work area for repair or maintenance.

4.1.3.1. Controls

The blower and associated cooling air system controls and instrumentation are being evaluated. The susceptor - induction heating system control method is being worked out with TOCCO and instrument vendors. Procurement of controls and instrumentation for the primary burner has been started.

4.1.3.2. External Air Cooling of Burner

4.1.3.2.1. Heat Balance. The heat generated by burning is removed by forced-air cooling in clamshell jackets surrounding the burner. At present, the cooling system will be sized for a maximum burn rate of 800 g C/min. Based on fluidized-bed calculations for the 16-in. burner (Ref. 11), the slugging fluid bed will provide a 10-ft surface for uniform heat transfer. Two cooling jackets will be used. The lower 6-ft jacket will also house the induction heating coil and the susceptor used during startup. The upper jacket measures approximately 4 ft.

Based on experiences with the 4-in. and 8-in. primary burners, fines recycle is expected to improve uniform heat transfer by maintaining a constant bed temperature over the entire length of the bed. Fines tend to provide better mixing. Further improvement in uniform bed temperature can be achieved with a secondary oxygen line, which extends the combustion zone further up from the distributor area. It is, therefore, assumed that the heat removal rate for each cooling jacket will be proportional to the burner surface area it covers.

Figure 10 is a steady-state heat balance for the 16-in. primary burner at the design burn rate of 800 g C/min or 104 kcal/sec. Axial conduction and radiation losses to burner flanges and plenums, top and bottom, are neglected. Heat removal by off-gas and elutriated fines is estimated at 14%. Fines elutriation is expected to be much higher than estimated; the present estimate therefore provides a conservative air cooling requirement.

4.1.3.2.2. Internal Film Coefficient. The inner film coefficient, bed-to-wall, was estimated using the Wender and Cooper correlation (Ref. 12). A film coefficient of 58 Btu/hr-ft^2-°F or 7.83 x 10^{-3} cal/sec-cm^2-°C was calculated with the bed at 900°C and a fluidizing velocity of 79.6 cm/sec. Average bed characteristics and properties are taken from the conceptual design basis document (Ref. 11). Conduction by radiation accounts for additional heat transfer bed-to-wall. The addition brings the overall internal heat transfer coefficient to 106 Btu/hr-ft^2-°F or 1.44 x 10^{-2} cal/sec-cm^2-°C. The overall internal coefficient obtained from experimental measurements was around 90 to 100 Btu/hr-ft^2-°F (Refs. 13, 14).

4.1.3.2.3. Heat Transfer to Cooling Air. Several assumptions are made prior to calculating vessel wall temperatures:

1. Heat transfer through the inner film by conduction and radiation.

2. Uniform heat flux across the 10-ft burner cooling section.

3. Isothermal inner and outer vessel wall temperatures.

4. Negligible heat loss through outer insulation.

Cooling air is forced through the 1/2-in. annular gap formed by the cooling jacket. The external convective film coefficient between the outer vessel wall and the cooling air is calculated using the Nusselt-type turbulent heat transfer equation for concentric annuli (Refs. 15, 16):

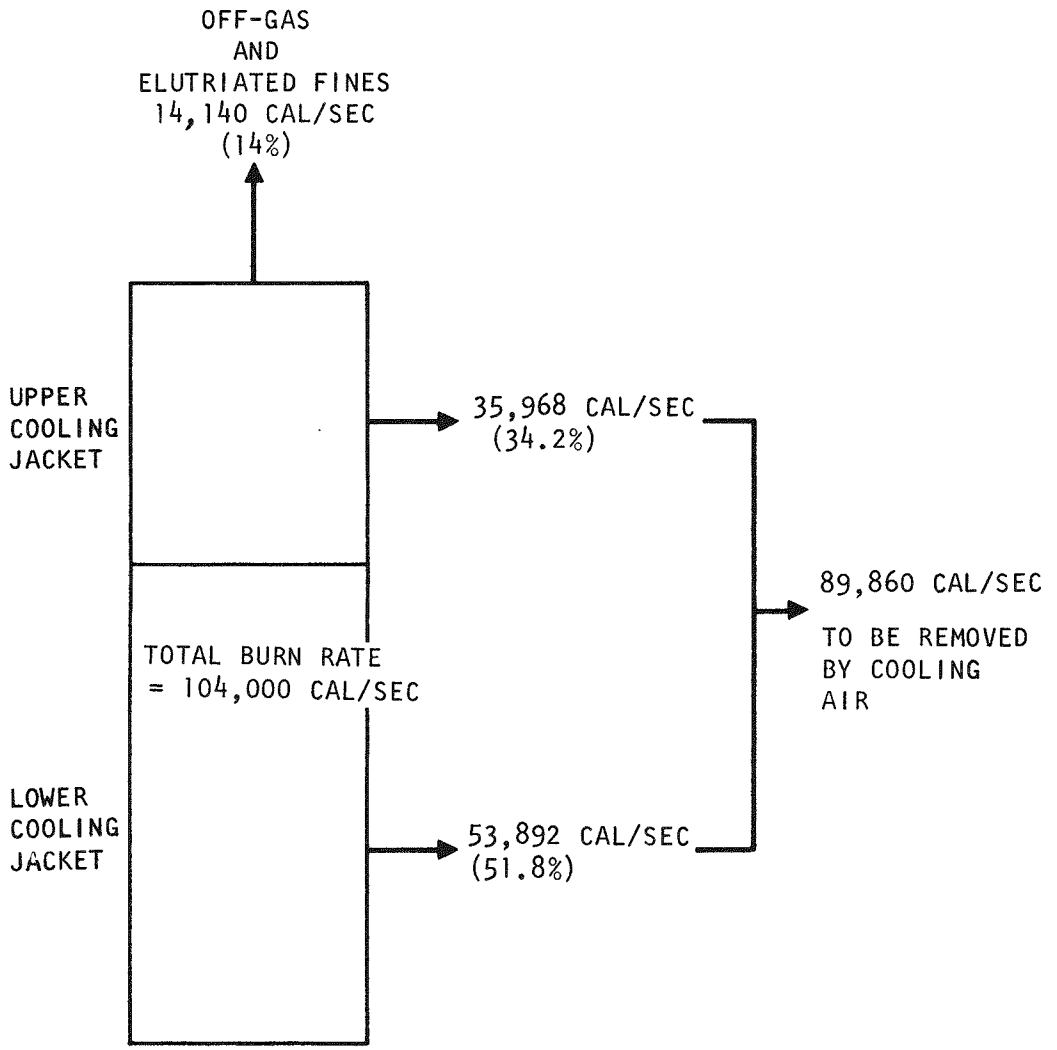

Fig. 10. 16-in. prototype primary burner heat balance

$$h_o \propto G^{0.8},$$

where h_o is the external film coefficient and G is the air mass flux.

The susceptor, which forms the outer surface of the annulus, also serves as a heat transfer area by absorbing radiation heat from the vessel wall and subsequently releasing the heat through forced-air convection.

Tables 9 and 10 summarize the cooling air system requirements for the lower and upper cooling jackets at three bed operating temperatures. Case I represents the nominal burner operating temperature of 900°C, which has a range 900 ±50°C (Ref. 17). Case II is a 50°C increase in bed operating temperature. This case serves as a sensitivity check on the cooling requirement change (for the same burn rate) due to bed temperature fluctuation. Case III represents the maximum bed operating temperature, which corresponds to a burner wall temperature of 900°C (the maximum allowable for the cooled vessel).

The conditions of case II require 20% less cooling air than those of case I. This is due to a higher temperature driving force in case II for the same heat flux across the vessel wall. From Tables 9 and 10 it can be realized that there is an advantage in operating at higher bed temperature insofar as the cooling requirement is concerned. For the same cooling air flow, more heat can be removed from the burner if the bed operating temperature is higher. However, the maximum bed operating temperature is limited by the ASME Boiler and Pressure Vessel Code, Section VIII, Division 1.

For the purpose of sizing the blower, and control valve and instrument evaluations, the cooling requirement at 900°C bed temperature will be adopted as the reference design. A schematic of the air cooling system is shown in Fig. 11.

TABLE 9
SUMMARY OF LOWER JACKET AIR COOLING REQUIREMENTS[a]

	Case I	Case II	Case III
Bed temperature, °C	900	950	1030
ΔT bed-to-wall, °C	160	150	130
Inner wall temperature, °C	740	800	900
ΔT across vessel wall, °C	43	43	43
Outer wall temperature, °C	697	757	857
Inlet air flow (inlet at 50°C and 1 atm), ft^3/min	1428	1209	960
Inlet air velocity, ft/sec	125	105	83
Air outlet temperature, °C	351	405	499
Susceptor temperature, °C	420	507	657
External film coefficient (averaged), $Btu/hr\text{-}ft^2\text{-}°F$	23.3	20.6	17.3

[a] Co-current flow, overall internal coefficient = 106 $Btu/hr\text{-}ft^2\text{-}°F$, and air inlet at 50°C.

TABLE 10
SUMMARY OF UPPER JACKET AIR COOLING REQUIREMENTS[a]

	Case I	Case II	Case III
Bed temperature, °C	900	950	1030
ΔT bed-to-wall, °C	160	150	130
Inner wall temperature, °C	740	800	900
ΔT across vessel wall, °C	43	43	43
Outer wall temperature, °C	697	757	857
Inlet air flow (inlet at 50°C and 1 atm), ft^3/min	1127	962	768
Inlet air velocity, ft/sec	98	84	67
Air outlet temperature, °C	304	350	423
Susceptor temperature, °C	479	570	716
External film coefficient (averaged), $Btu/hr\text{-}ft^2\text{-}°F$	19	17	14

[a] Co-current flow, overall internal coefficient = 106 $Btu/hr\text{-}ft^2\text{-}°F$, and air inlet at 50°C.

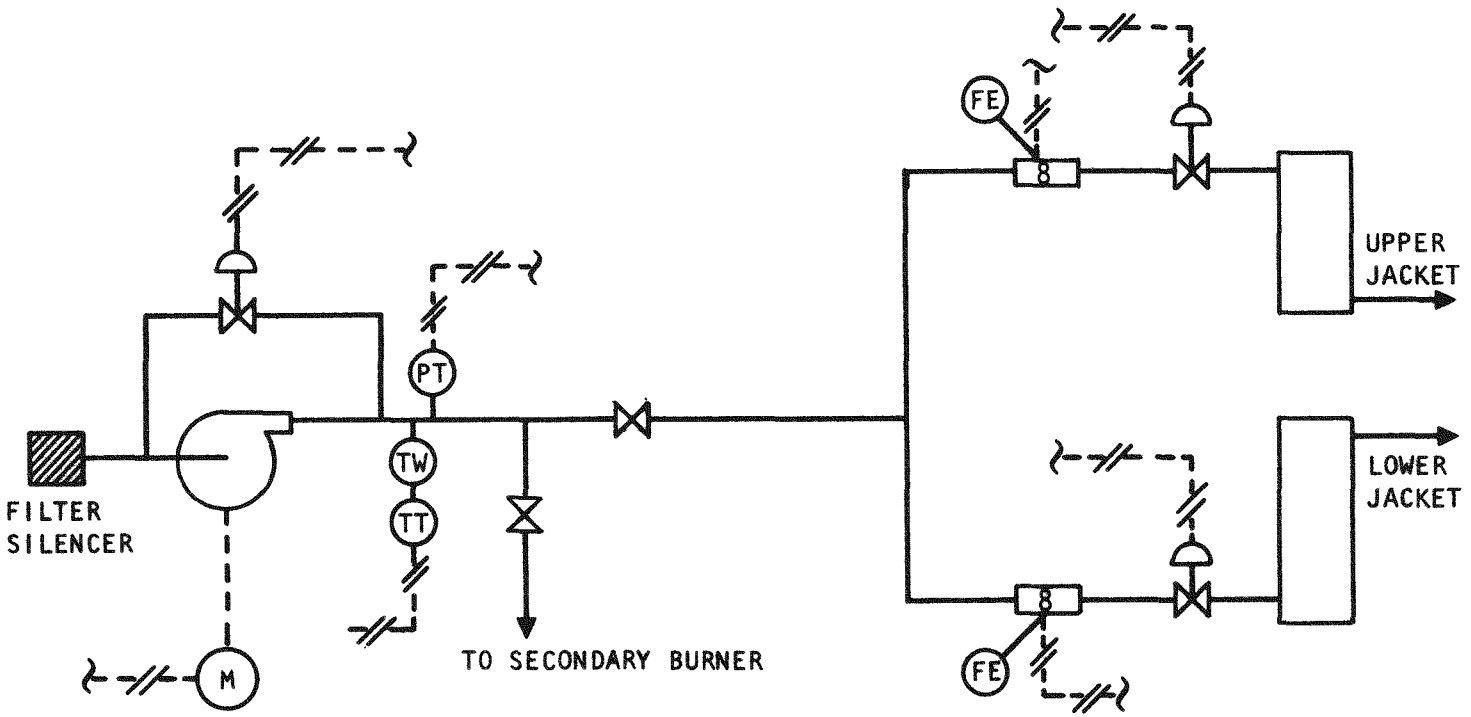

Fig. 11. Schematic of external air cooling system for 16-in. prototype burner

4.2. SECONDARY FLUIDIZED-BED COMBUSTION

The 10-cm secondary fluidized-bed burner presently incorporates all of the process considerations that are included in the reference prototype design: pneumatic feed and product removal, induction heating, and a perforated flat distributor plate. The maximum burner capacity (bed size and fluidizing velocity) were established. Currently, an automatic control system for the burner is being installed for testing. The prototype secondary burner design was reviewed; modifications to the design will be made to incorporate several mechanical design considerations.

4.2.1. 10-cm Secondary Fluidized-Bed Combustor

Five experimental runs (40 through 44) were carried out in the induction-heated Hastelloy-X burner tube. Problems with a recycle pump failure and use of very finely crushed feed caused two filter failures. These problems indicate areas for consideration, namely, backup equipment in the prototype design and the necessity of preventing the feed material from being overcrushed. Pneumatic transport of product was successfully used in all runs except one, where a clogged filter bag lowered the transport flow which caused choking of solids in the vertical line. Improved filter cleaning methods have eliminated this problem. The runs are summarized in Table 11.

4.2.1.1. Run 40

In Run 40, 18 kg of crushed TRISO fertile particles were burned to 0.7% carbon content in the secondary burner. Insufficient product transport air flow resulted in choking flow in the vertical transport section.

The burner feed size distribution is shown in Fig. 12.

The Secondary Burner Operating Procedures were followed during the run. After the tube was preheated to 850°C, approximately 9 kg of feed were added. This partial bed equilibrated at 600°C and was then ignited by

TABLE 11
SUMMARY OF 10-CM SECONDARY BURNER RUNS

Run No.	Objectives	Feeding and Ignition	Filter Blow-Back	Miscellaneous Run Conditions	Results
40	Continue test of the induction heating system and the pneumatic transport.	850°C - 9 kg 600°C - ignition 900°C - 9 kg	54 psig recycled off-gas Δp = 50 in. H_2O	Product valve opening = 3/8 in.	Smooth operation with startup by induction heating. No burner idling with induction heating was attempted. Insufficient product transport air flow resulted in choking flow in the vertical transport section.
41	Test the pneumatic transport with an improved filter cleaning. Try an alternative burner cooling method with a fixed fluidizing gas supply. (Standard method is to control the burner temperature by the oxygen supply with a fixed air cooling.)	Same as Run 40 except: 700°C - ignition	56 psig recycled off-gas	Product valve opening = 3/16 in.	3/16-in. valve opening resulted in bridging of product material at the valve. A further opening effected a complete burner cleanout. With a fixed fluidizing velocity the burner operation was smoother and the burner temperature was successfully controlled by the cooling air.
42	Same as above, except with a larger product valve opening.	Same as Run 41	Same as Run 41	Product valve opening = 1/4 in.	The run was terminated when one of the blow-back gas pumps failed, resulting in the collapse of one filter. The filter collapsed along the weld seam. More studies on the filter strength at high temperature and on alternative filters are planned. Product removal with a larger valve opening was smooth.
43	Simulate an automatic startup. Test the effect of very fine feed particles.	Same as Run 42	60 psig N_2, Δp = 20 in. H_2O	O_2 flow was increased from 40 to 140 SLPM in a 10-min ramping operation	Startup successfully simulated an automatic startup. Use of too fine feed particles resulted in a filter failure due to stagnant burning of carbon fines at the filter chamber.
44	Simulate an automatic startup with a full charge. Batch size was reduced from 18 kg to 14 kg to prevent clogging of the filters by the bed materials.	875°C - 14 kg 650°C - ignition 900°C - bed	40 psig recycled off-gas. Blow-back cycle was increased from once per min to once per 40 sec, Δp = 15 in. H_2O	O_2 flow from 40 to 100 SLPM in 6 min. Total flow was reduced from 140 to 100 SLPM. Normal feed size was used.	Startup was smooth with a ramping oxygen flow. Reduced batch size, fluidizing velocity, and more frequent blow-back resulted in a low filter Δp.

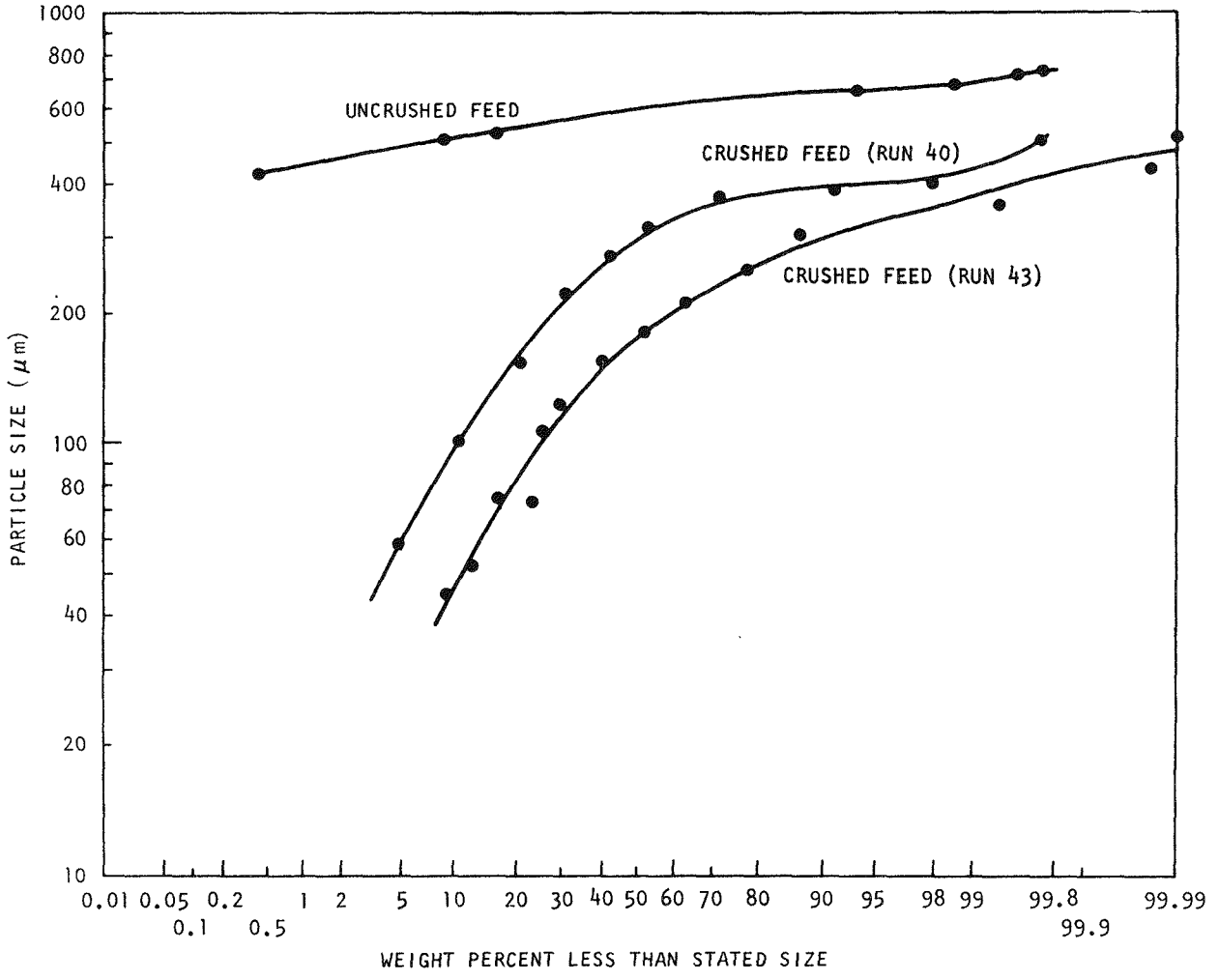

Fig. 12. Feed size distribution, Runs 40 and 43

introducing the oxygen. After the bed temperature was brought to 900°C, the remainder of the bed was added. The combustion period lasted 95 min, with peak burn rates of over 85 g/min.

The filters were blown-back with 12% of the process flow. (Each filter was blown-back once a minute for 3 sec at 54 psig initial blow-back pressure.) The peak filter pressure drop was ∿50 in. H_2O.

The bed was cooled to 500°C after shutdown and the product valve was then opened 3/8 in. A choking flow occurred in the vertical section of the pneumatic transport line. The filters at the transport pump were found to have excessive drops due to buildup of material from the air classifier system and the secondary burner system, which probably prevented sufficient flow rates for transport of the product. These filters were changed before the next run and will eventually be replaced with sintered metal filters representative of those to be used in the commercial plant.

The product contained 0.7% burnable carbon and had an angle of repose of 37°, a bulk density of 2.5 g/cm^3, and a tap density of 3.1 g/cm^3. The size distribution of the product is shown in Fig. 13.

4.2.1.2. Run 41

In Run 41, 18 kg of crushed TRISO fertile particles were burned to 0.6% carbon content in the secondary burner. Product transport was effected by opening the product valve fully.

The burner feed was the same as in Run 40.

The Secondary Burner Operating Procedures were used throughout the run. After preheating the tube to 875°C, approximately 9 kg of feed were added. This bed was brought to 700°C and ignited. The temperature was increased to 900°C and the remainder of the bed was added. The gas inlet flows were then fixed at 20 liters/min N_2 and 140 liters/min O_2, with the temperature

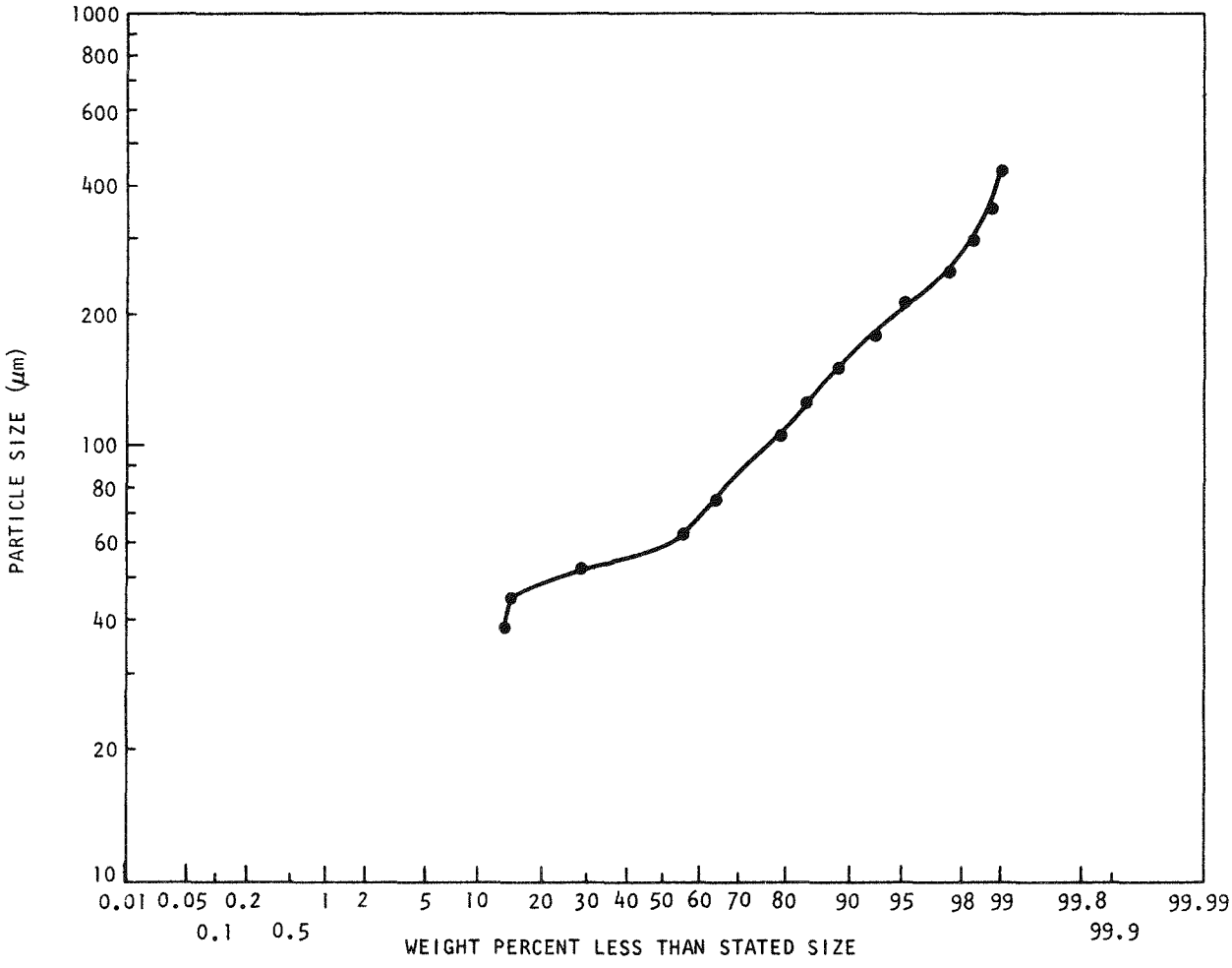

Fig. 13. Product size distribution, Run 40

kept at 900°C by varying the air cooling rate. This temperature control method has the advantage of a constant fluidizing velocity that is unaffected by temperature fluctuation. The total combustion time was 62 min for an average burn rate of ∿75 g/min.

The filters were blown-back for 2 sec every minute at 56 psig initial pressure for a total blow-back flow of ∿10% of the process flow. The peak filter pressure drop was 45 in. H_2O.

After cooling the bed to 400°C, the product valve was opened 3/16 in., which gave no flow of product through the valve. The valve was then opened fully with subsequent complete burner cleanout. The 3/16-in. opening was evidently not sufficient to preclude bridging at the valve. A larger opening of 1/4 in. was therefore used in the next run.

The product contained 0.6% burnable carbon and had an angle of repose of 38°, a bulk density of 2.4 g/cm^3, and a tap density of 3.2 g/cm^3. The size distribution is shown in Fig. 14.

4.2.1.3. Run 42

In Run 42, 18 kg of crushed TRISO fertile particles were burned to yield ash with a high carbon content (4.6%) due to loss of a blow-back pump that caused trapping of fine carbon in the filter chamber. The product was pneumatically transported using a 1/4-in. product valve initial opening.

The feed consisted of 18 kg of crushed TRISO fertile particles with a size distribution as shown in Fig. 15. The crushed material had a bulk density of 1.7 g/cm^3, a tap density of 2.0 g/cm^3, and an angle of respose of 24°.

The run was carried out according to the Secondary Burner Operating Procedures. The tube was induction heated to 875°C, followed by addition

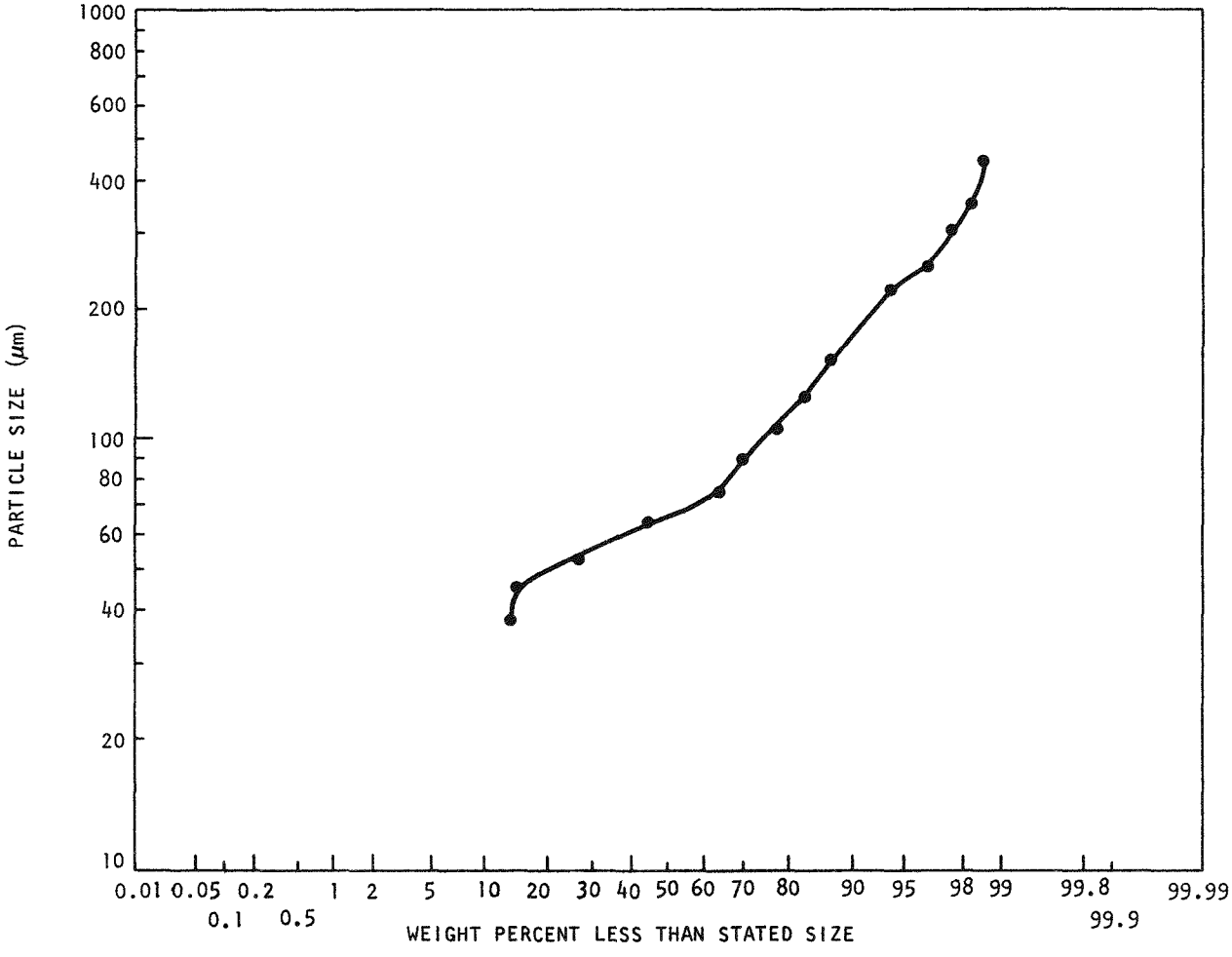

Fig. 14. Product size distribution, Run 41

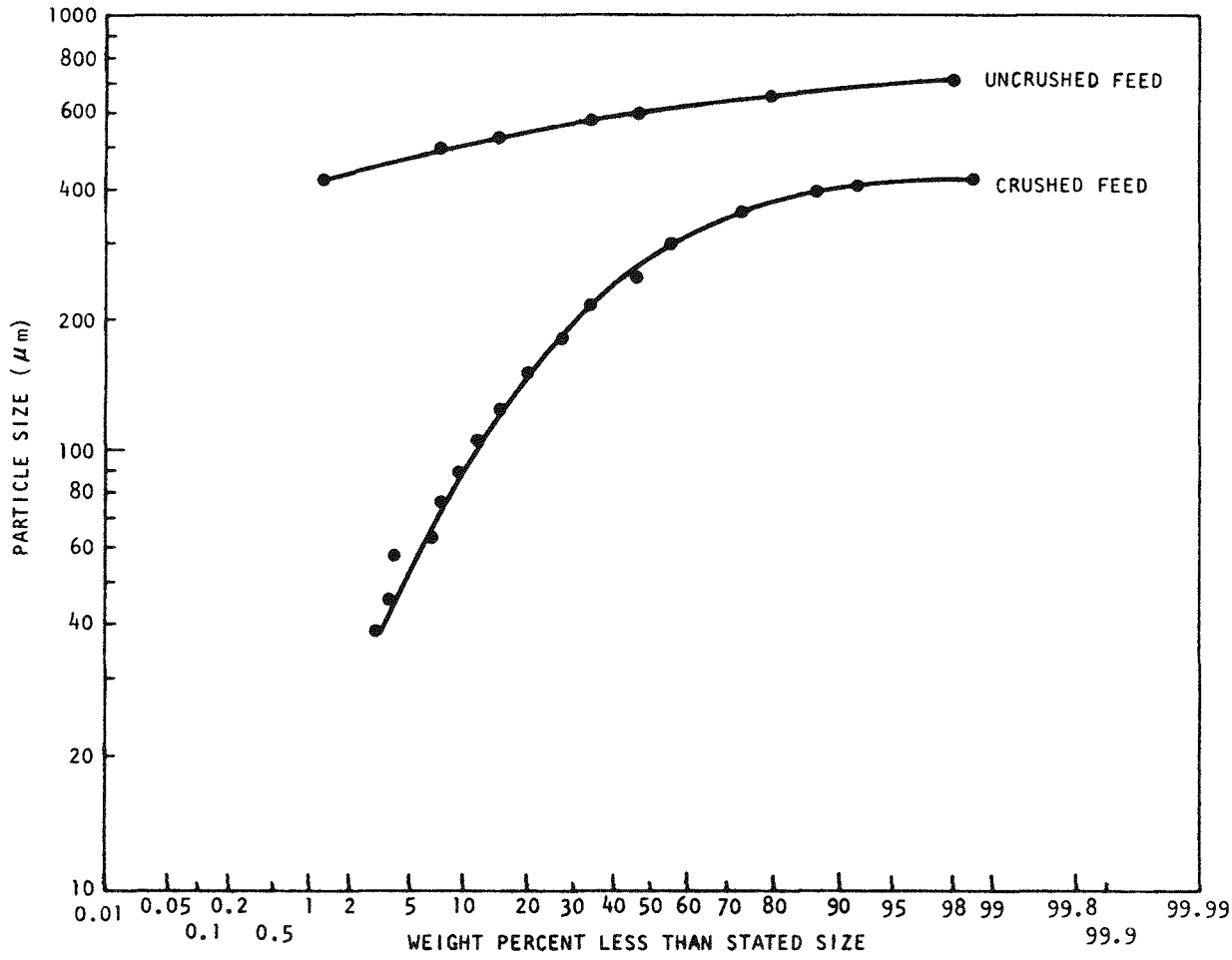

Fig. 15. Feed size distribution, Run 42

of 9 kg of particles that were heated to 700°C and ignited. The remaining 9 kg were then added as the bed was brought to 900°C.

During the run, the filter ΔP increased past the range of the ΔP cell. This was attributed to failure of the blow-back pump, which resulted in excessive fines buildup in the filter chamber.

The run was terminated when high temperatures (925°C) were noted in the filter chamber, while the bed temperature was only 700°C. The high temperatures are believed to be caused by the carbon depletion of the fluidized bed allowing O_2 to enter the filter chamber and to oxidize the large amount of fines contained therein. Local temperatures may have been much higher than 925°C because the carbon fines were essentially a cake surrounding the filters, with resulting poor heat transfer capabilities.

At the same time that the high temperatures were noted, the filter pressure drop decreased to about 10 in. H_2O, which is somewhat less than normal when fines are in the filter chamber. The burner was shut down, emptied, and later dismantled.

The upper portion of one of the filters was deformed as if flattened by a hammer. The longitudinal weld seam formed one of the flattened edges and was cracked open as shown in Fig. 16. This opening explains the sudden reduction in filter pressure drop.

The most probable cause of the filter failure is as follows:

1. The blow-back system became inoperative allowing large amounts of fines to build up around the filter, which caused high ($\sim$4 to 5 psig) filter pressure drops.

2. When the fluid bed burned down to a low carbon content, oxygen was allowed to pass through unreacted and enter the filter chamber.

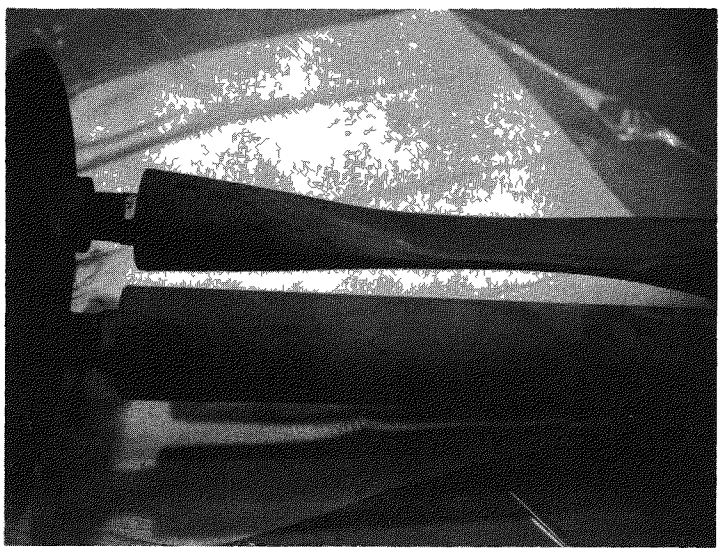

Fig. 16. 10-cm secondary burner off-gas filter following Run 42

3. The fines packed around the filters began reacting with the oxygen and generating significant amounts of heat, thus causing localized hot spots due to the static nature of the fines.

4. One of the filters developed a local hot spot that reduced the filter strength sufficiently to allow collapse of the filter due to the pressure drop across the filter. When the filter collapsed, the weld seam was put in severe stress and cracked, producing an opening in the filter that rapidly reduced the pressure drop to a low value.

Following actuation of the pneumatic transport system, the product valve was opened 1/4 in. for 10 min., and then fully opened for 10 additional minutes along with use of the distribution plate sweep. Complete cleanoff of the distribution plate was achieved; the only material remaining in the vessel was the filter precoat (which must be left in for filter performance).

The product contained 4.6% burnable carbon with a size distribution as shown in Fig. 17. The bulk density was 2.2 g/cm^3, the tap density was 2.7 g/cm^3, and the angle of repose was measured as 38°.

4.2.1.4. Run 43

Run 43 was made after the blow-back recycle pump system had been repaired (and enlarged 50% to allow more frequent flow-backs). The startup successfully simulated automatic operation. A filter failure occurred just before shutdown.

Feed for this run was 18 kg of finely crushed TRISO fertile particles. (Size distribution is given in Fig. 12 for comparison.) This feed was much finer than that used in the previous runs. The <100-μm fraction was 25 wt % and the <50-μm fraction was 10 wt % as compared to values of 11 wt % and

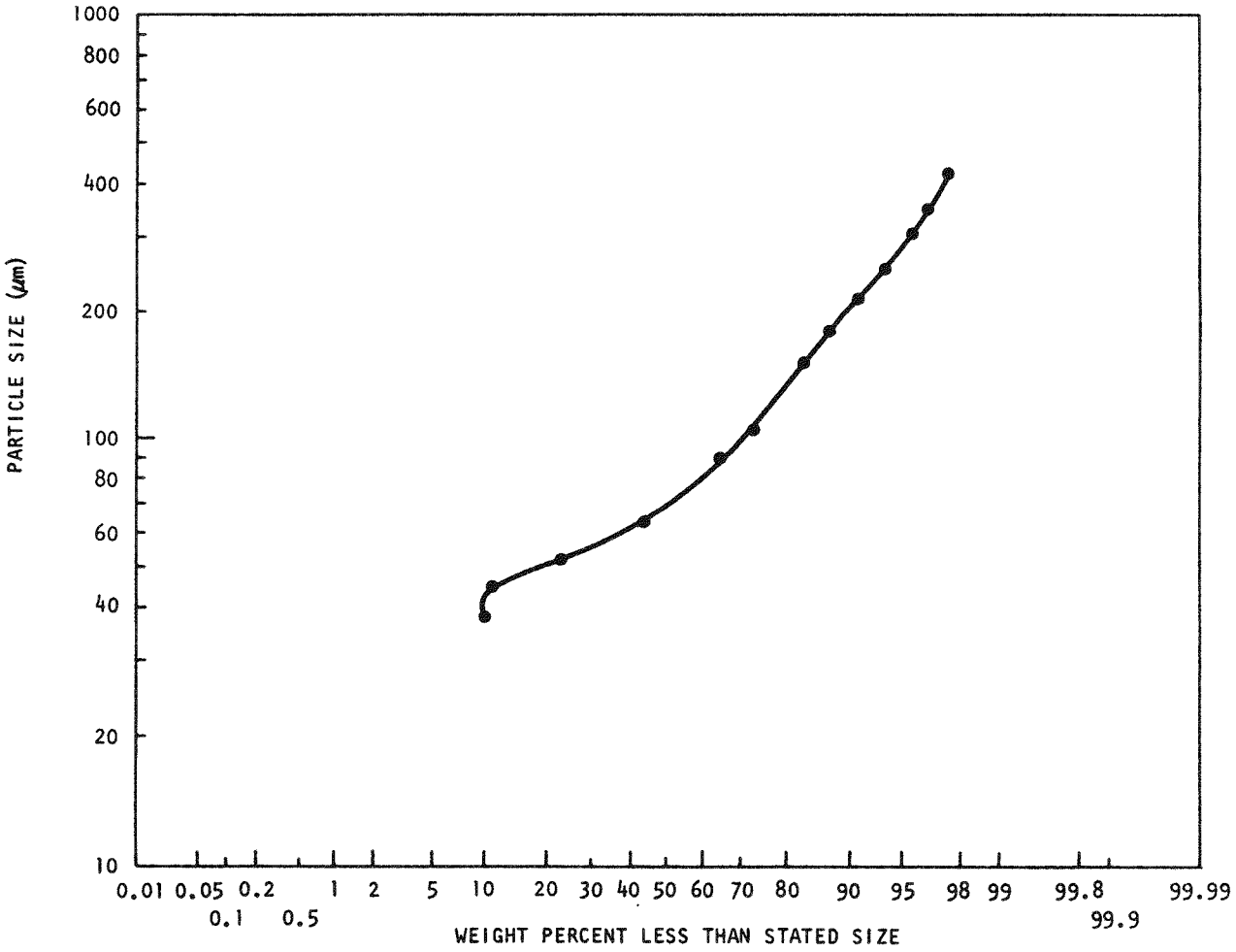

Fig. 17. Product size distribution, Run 42

4 wt %, respectively, in previous feeds. The bulk density was 1.8 g/cm^3 and the tap density was 2.2 g/cm^3.

A close gap crusher was used to generate the feed for this run. An objective of the run was to test the feasibility of using such finely divided material. Earlier runs (Runs 16 and 17) with finer material had been unsuccessful, and no data were available in the intermediate region.

The burning procedure followed the Secondary Burner Operating Procedures. Starting O_2 flow was increased from 40 to 140 SLPM in a 10-min ramping operation to simulate automatic startup techniques. The startup went smoothly with no O_2 in the off-gas and a smooth temperature increase.

The run proceeded uneventfully with a 20-in. H_2O filter ΔP (using 60 psi N_2 for blow-back). When the bed began to burn out, as evidenced by the presence of O_2 in the off-gas, the filter ΔP dropped suddenly to a very low value, indicating an opening in one of the filters.

At this point the run was terminated by switching to N_2 flow and emptying the bed into the pneumatic transport system, which carried it to the upper deck receiver-hopper.

Subsequent disassembly of the burner revealed that the lower end of one filter had been burned off.

Using the finely crushed feed resulted in a higher portion of unburned material on the hot filter surfaces throughout the run. When the O_2 front reached the filters, in situ combustion occurred and melted the filter. This has never been a problem with coarsely crushed feed.

A solution to prevent further filter failures is to eliminate both the large fines buildup and the presence of O_2 in the filter chamber when filter temperatures are high. The first problem is handled by reducing

bed size to 14 kg and reducing total flow 15%. This would reduce the fines loading in the filter area. The second problem is handled by reducing flow to bring fines down from the filter chamber when the off-gas CO gets below 5% (indicating the O_2 front is nearing the filter chamber). This would lower the filter temperature caused by the expanded hot bed before the O_2 enters the chamber. Another control is to not use finely crushed feed.

4.2.1.5. Run 44

In Run 44, 14 kg of coarsely crushed TRISO fertile particles were combusted to yield product containing 1.1 wt % burnable carbon. The start-up again successfully simulated automatic operation. Filter pressure drops were significantly reduced by using a smaller bed size and a lower superficial velocity. Pneumatic product removal was routine with complete burner cleanout achieved.

Feed for this run was 14 kg of crushed TRISO fertile particles. The size distribution is the same as that shown in Fig. 12. The feed contained 60.8% ThC_2, 17.4% C, and 21.8% SiC.

The run was made using modified operating procedures. These included reduced bed size, reduced total flow, filter cooling before the oxygen front enters the filter chamber, and the use of feed that is crushed just enough to expose the fuel kernels.

After preheating the tube to 875°C, the 14 kg bed was added batchwise and heated to 650°C, followed by ramping the O_2 inlet flow from 40 to 100 SLPM over a 6-min period for startup. The startup went well with the bed temperature reaching the 900°C setpoint within 10 min.

Filter cooling was left on throughout the run. For the main burning portion of the run, the inlet O_2 flow was 100 SLPM and the N_2 flow was 40 SLPM.

Filter blow-back was effected every 20 sec at 40 psig for 2 sec. The maximum filter pressure drop was 15 in. H_2O. This was a considerable reduction from previous runs, as expected, due to the smaller bed size and lower superficial velocity.

When the off-gas CO concentration went below 3%, indicating that the O_2 front was nearing the filter chamber, the inlet flow was changed to 60 SLPM of O_2 and 40 SLPM of N_2. The induction heater was then actuated, holding the bed temperature above 700°C during the burnout portion of the run.

When the burn rate dropped below 1 g/min, the bed was fluidized with 100 SLPM of N_2. The product valve was actuated with the bed at 650°C. Pneumatic transport of the product was rapid, with 93% of the bed removed in 5 min and the remainder in 15 min. This time could be significantly reduced by introducing the sweep after 5 min of bed removal instead of waiting 10 min as is presently done.

The product size distribution is shown in Fig. 18. The angle of repose was 32°, the bulk density was 2.3 g/cm^3, and the tap density was 3.0 g/cm^3. The product burnable carbon content was 1.1 wt %.

The next run will utilize an automatic ramp generator for O_2 inlet flow, based on the success demonstrated to date with manual ramping operations. To speed up crushed feed preparation, a matched set of hardened crushers will be installed and used in tandem.

4.2.2. 20-cm Prototype Secondary Fluidized-Bed Combustor

The conceptual design of the 20-cm prototype secondary burner is completed and is progressing well into a detailed design stage. The

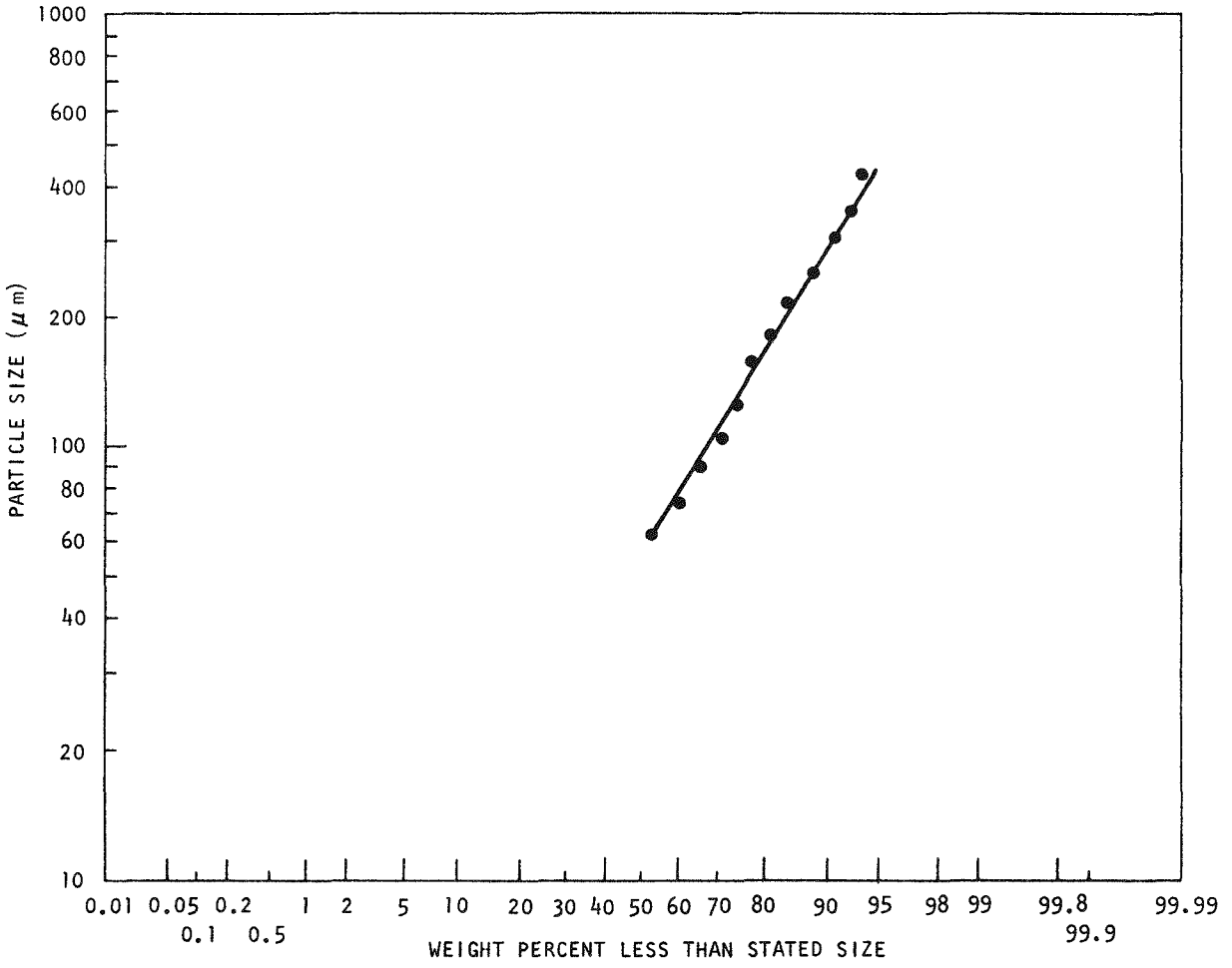

Fig. 18. Product size distribution, Run 44

burner vessel design, including the product removal valve, was reviewed at a design review meeting. The analysis was focused on three major aspects of the design:

1. Process.
2. Mechanical design (including stress analysis).
3. Remote operation.

The process and the remote operation aspects were generally well understood and incorporated into the design. The mechanical design analysis, however, revealed several possible weak points of the design. The most serious problem arises from a steep temperature gradient in various burner parts during the startup (induction heating), ignition, and transient cooling cycle, as well as from the introduction of cold fluidizing gases into the distributor plenum. A lack of design data for Hastelloy-X material compounds the difficulty of analysis.

Areas affected by the mechanical stress analysis are:

1. Product withdrawal valve - distributor plate assembly.
2. Filter blow-back assembly.
3. Top cap assembly.

Design modifications for the above items are under way and are described in a later section.

The detailed design of the burner parts requires in-depth analysis of the process in addition to the mechanical design considerations. As a continuation of the previous Quarterly Progress Report (Ref. 7), some of the process and system parameters are summarized in the following sections.

4.2.2.1. Fluidization Velocity, u

In determining an optimum fluidization velocity, the following should be taken into consideration: (1) fluidization characteristics,

(2) elutriation of bed materials, (3) heat transfer characteristics, and (4) burn rate.

4.2.2.1.1. Fluidization Characteristics. The minimum fluidization velocity, U_{mf}, for the burner feed and product components is given in Table 12. For mixed particles, however, the minimum fluidization velocity is very difficult to predict. The change of particle size and size distribution with time further complicates the problem. With small particles the bed easily defluidizes, especially at the bottom corners (Ref. 18), due to a large channeling tendency. The minimum safe operating velocity, at which bed stagnation does not occur, is usually much higher than the minimum fluidization velocity and is determined experimentally. At present, 15 cm/sec is considered to be a safe minimum for the 10-cm secondary burner. Considering the tapered bottom section, the same value may be conservatively used for the 20-cm secondary burner.

The bed slugging characteristics at higher fluidizing velocities are given in the previous Quarterly Progress Report (Table 31, Ref. 7). In general, the quality of fluidization deteriorates rapidly with increasing fluidizing velocity in a slugging bed. However, 10-cm secondary burner experience shows that the bed slugging is tolerable up to a velocity of 120 cm/sec for a bed having an L/D greater than 10.

4.2.2.1.2. Elutriation of Bed Materials. The elutriation in the secondary burner is not a critical problem since the fine materials are retained in the vessel by the use of in-vessel filters. Too much elutriation of fine particles, nevertheless, causes a high filter pressure drop and difficulty in completing burning of the graphite. The amount of particle elutriation depends largely on the fluidizing velocity and the fines concentration.

The amount of elutriation per unit area per unit time, elutriation rate constant K, is given by Wen and Hashinger (Ref. 19):

TABLE 12
U_{mf} AND U_t FOR FEED AND PRODUCT

	d_p (μm)	ρ_s (g/cm^3)	U_{mf} (cm/sec)	U_t (cm/sec)
Feed				
Average	228	3.79	4.8	177
ThC_2	333	8.4	22.7	837
SiC	140	3.18	1.52	56
C	127	1.57[a]	0.62	23
Product				
Average	56	6.79	0.97	26
ThO_2	52	9.1[a]	1.13	22
SiC	85	3.18	1.05	21

[a]Estimated apparent densities.

$$\frac{K}{\rho_g (U - U_t)} = 1.7 \times 10^{-5} \left[\frac{(U - U_t)^2}{gd}\right]^{0.5} \left[\frac{dU_t\rho_g}{\mu}\right]^{0.725} \times \left[\frac{\rho_s - \rho_g}{\rho_g}\right]^{1.15} \left[\frac{U - U_t}{U_t}\right]^{0.10}, \quad (1)$$

where K = elutriation rate constant, $g/cm^2/sec$

U = fluidizing velocity, cm/sec

U_t = terminal velocity of particle, cm/sec

d = particle diameter, cm

g = acceleration of gravity, 980 dynes

ρ_g = density of fluidizing gas, g/cm^3

ρ_s = density of solid particle, g/cm^3

μ = viscosity of fluidizing gas, g/cm/sec.

Equation 1 assumes that particles which have a larger terminal velocity than the fluidizing velocity will not be elutriated. This applies only when the disengaging section is larger than the TDH (transport disengaging height). The height of the disengaging section in the 20-cm secondary burner is kept short (30 to 50 cm) to facilitate the return of back-blown fine particles into the bed, as compared to the TDH of 100 to 150 cm (order of magnitude estimate from Ref. 20). The amount of elutriation, therefore, will be higher than that predicted by Eq. 1.

If the fines concentration is arbitrarily defined as the fraction of particles having a terminal velocity less than the fluidizing velocity, the fines content increases with increasing fluidizing velocity, as shown in Fig. 19. Equation 1 also shows that a drastically higher fraction of particles having a terminal velocity less than the fluidizing velocity will be elutriated with increasing velocity. From Fig. 19, it is evident that a lower fluidizing velocity is preferable in order to decrease the elutriation rate, especially for the carbon fines. In the 20-cm secondary burner design, a further attempt was made to decrease the elutriation rate by expanding the top of the fluidized bed section. The effect of this

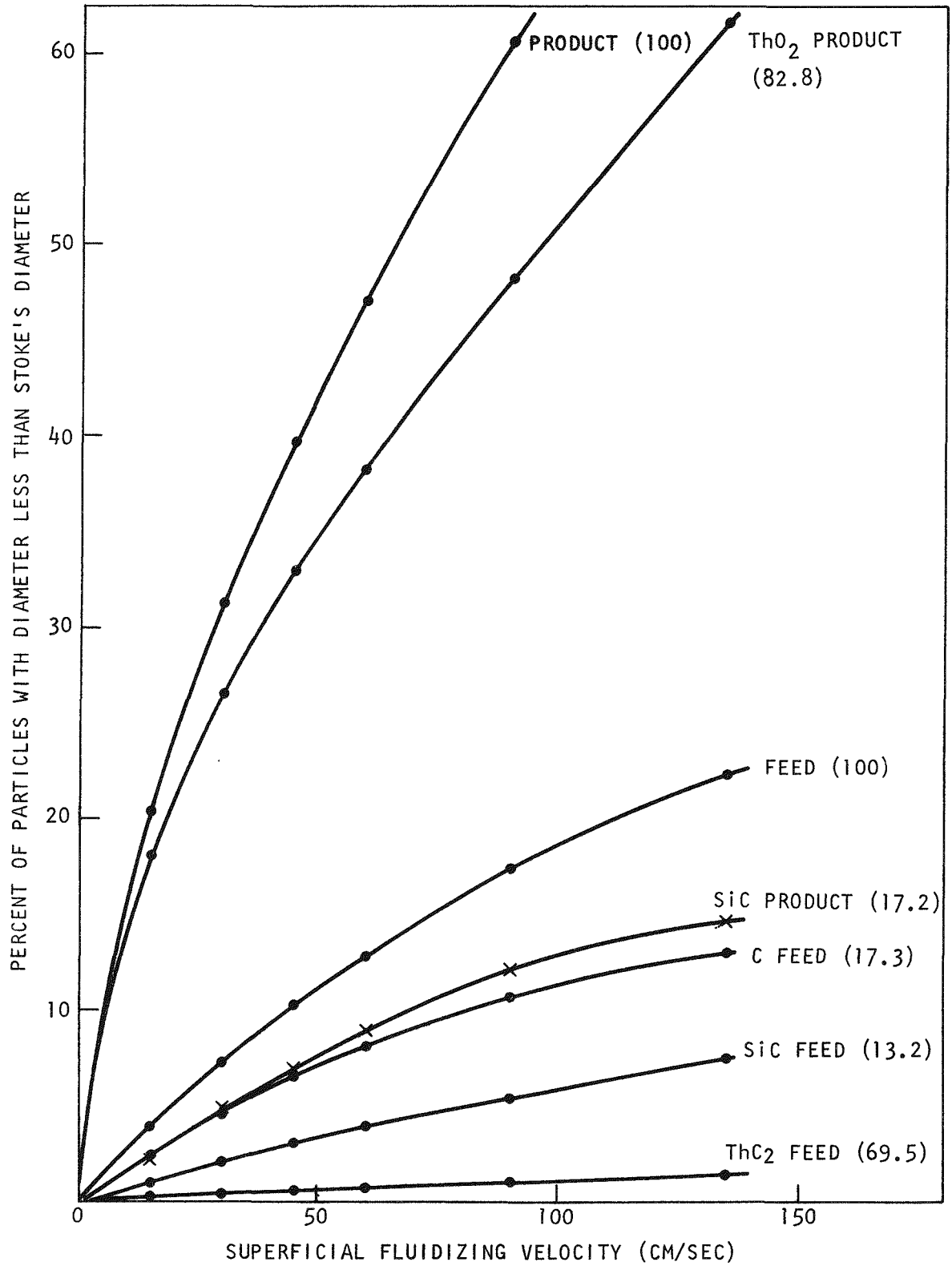

Fig. 19. Fines content as a function of superficial fluidizing velocity

reduced superficial velocity at the top of the bed is shown in Fig. 20. The size distributions of the feed and the product are given in Figs. 21 and 22 as a reference. A further quantitative study of particle elutriation will be made.

4.2.2.1.3. Heat Transfer Characteristics. A typical dependence of the heat transfer coefficient on the fluidizing velocity is shown in Fig. 23. The heat transfer coefficient drastically increases as the bed begins to fluidize, reaches a maximum, and then decreases at higher velocity due to a larger voidage and low heat conductivity of the gas. The velocity at which the heat transfer coefficient reaches a maximum is defined as an optimum velocity for heat transfer, U_{opt}.

The rising branch 1 of Fig. 23 changes with the percent of open area on the distributor plate near the onset of fluidization. However, the influence gradually diminishes with an increase in U, and close to U_{opt} it is negligibly small.

The optimum velocity, U_{opt}, can be obtained from the following equation (Ref. 21):

$$Re_{opt} = \frac{Ar}{18 + 5.22\sqrt{Ar}} \quad , \tag{2}$$

where $Re_{opt} = U_{opt}\, d_e/\nu_f$, Reynolds number at h_{max}

$$Ar = \frac{g d_e^3}{\nu_f^2} \cdot \frac{\rho_s - \rho_g}{\rho_g} \quad , \text{ Archimedes number}$$

d_e = equivalent diameter of solid particle

ν_f = kinematic viscosity of fluidizing gas

In this connection it is appropriate to give universal formulae for calculating Re_{mf} (Ref. 22) and Re_t (Ref. 23), which are valid over a wide range of Ar:

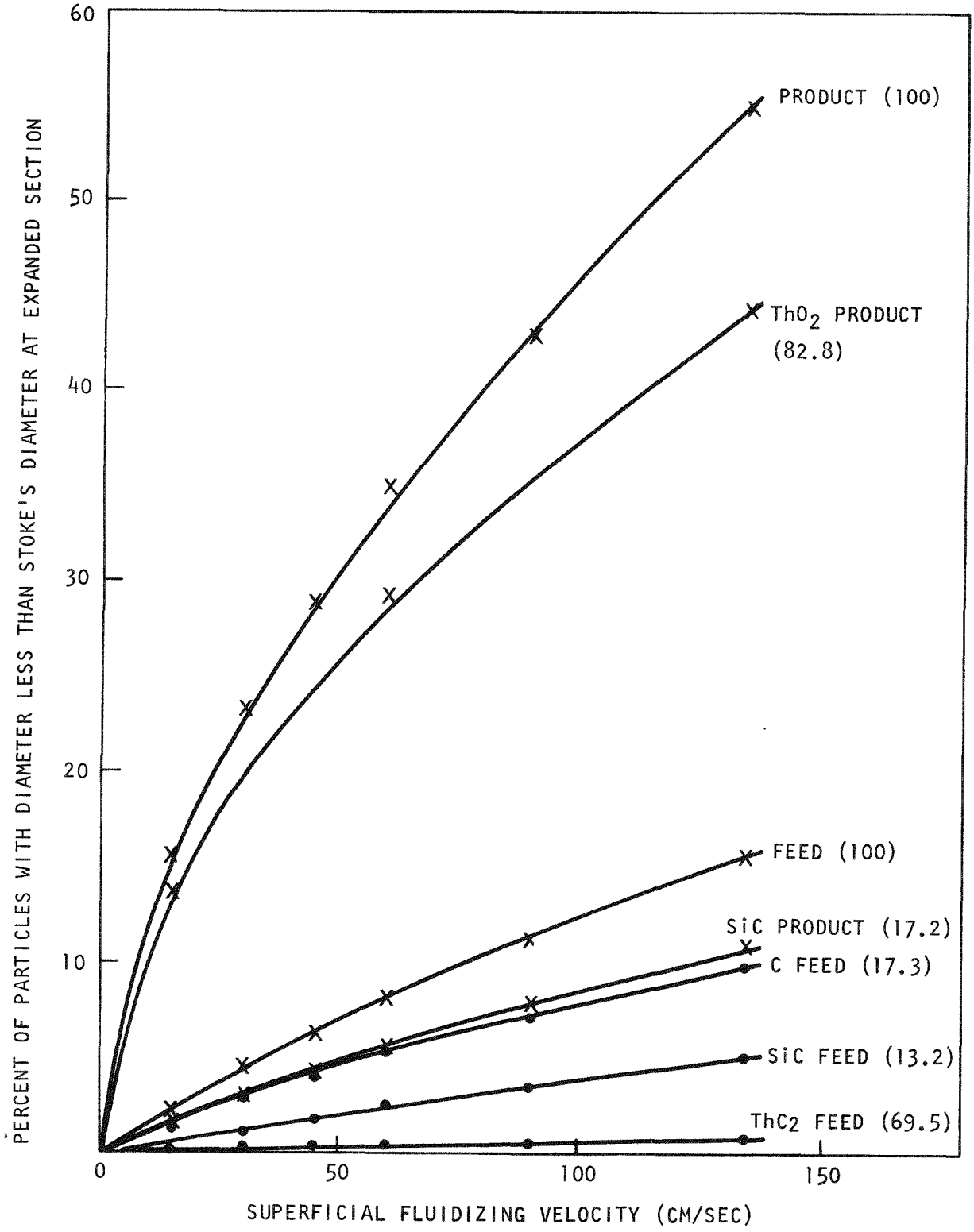

Fig. 20. Fines content as a function of superficial fluidizing velocity with top of fluidized bed expanded

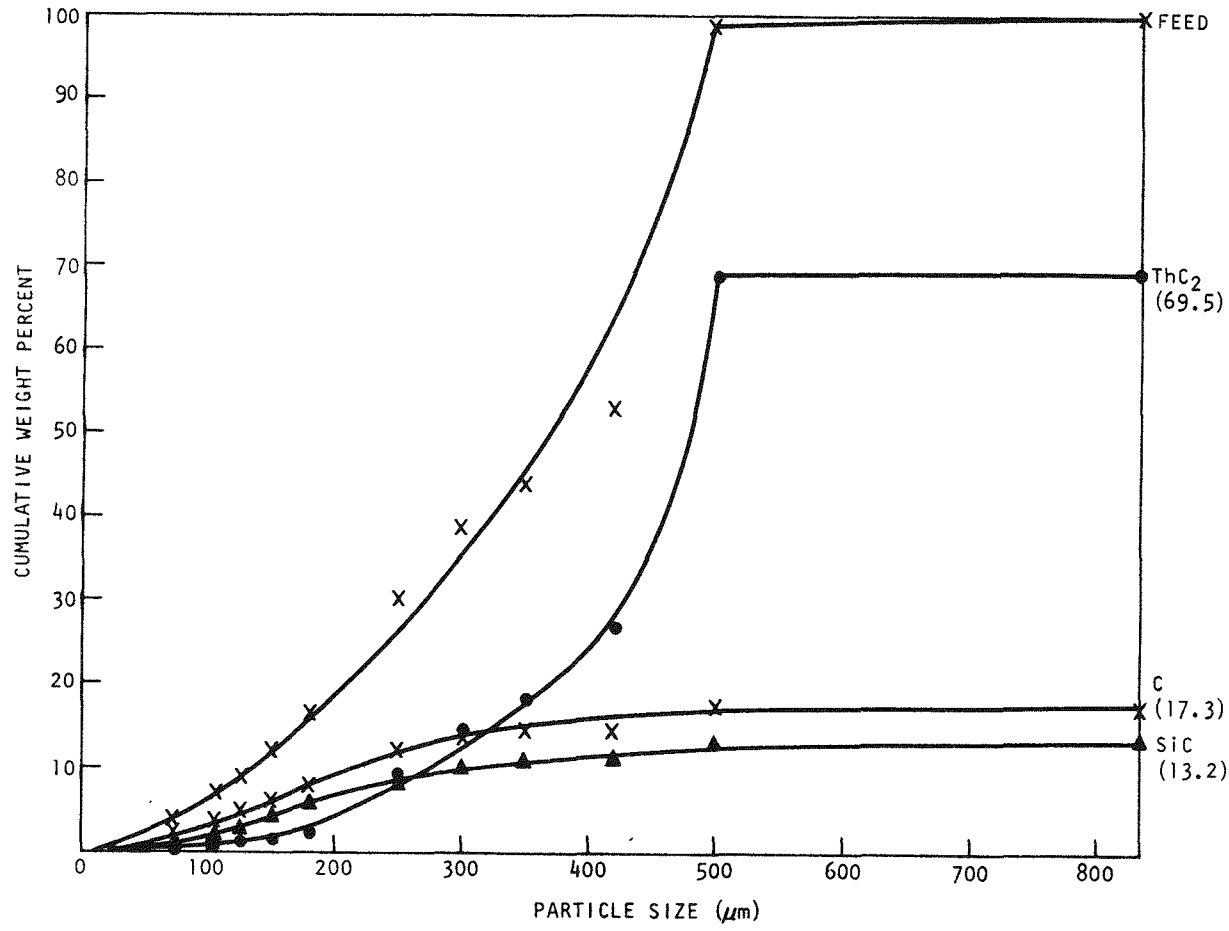

Fig. 21. Feed percent of total weight

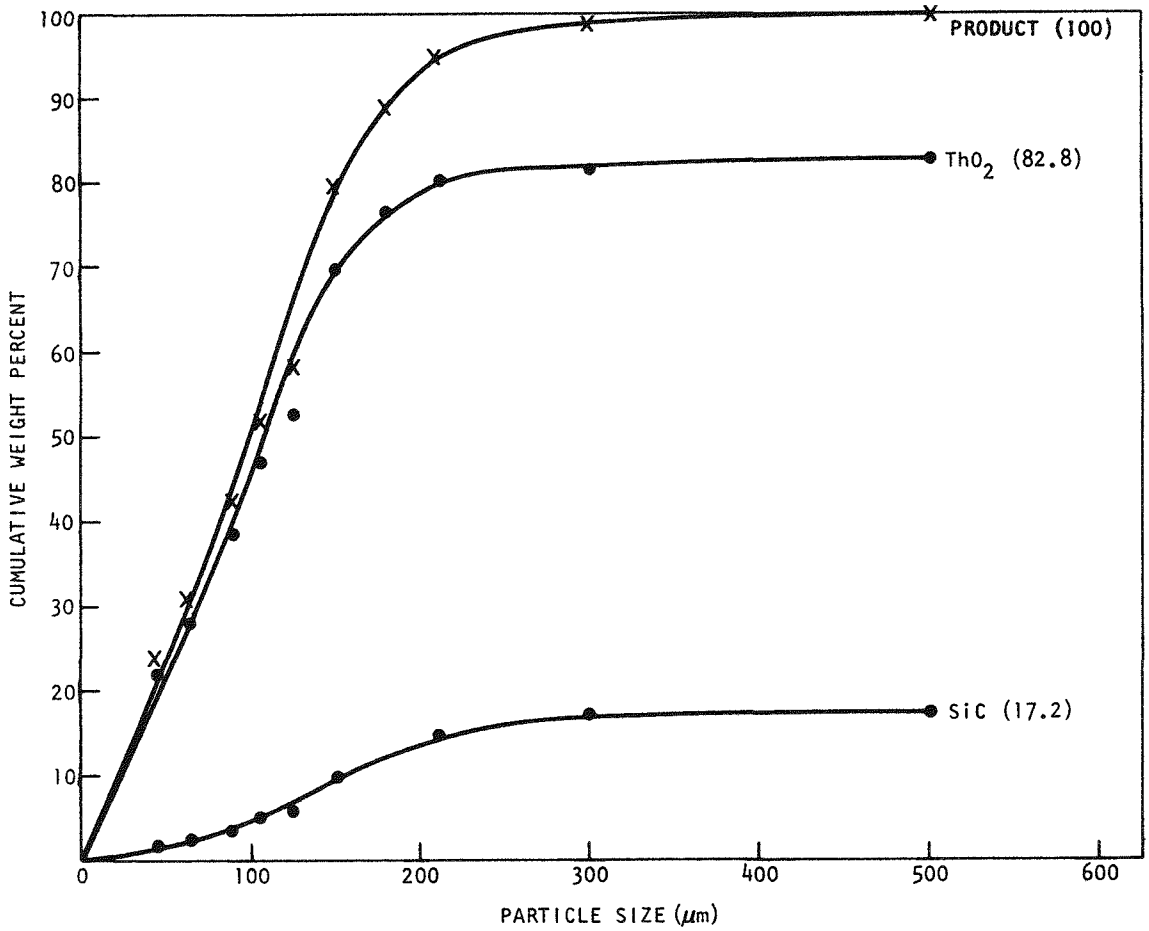

Fig. 22. Product percent of total weight

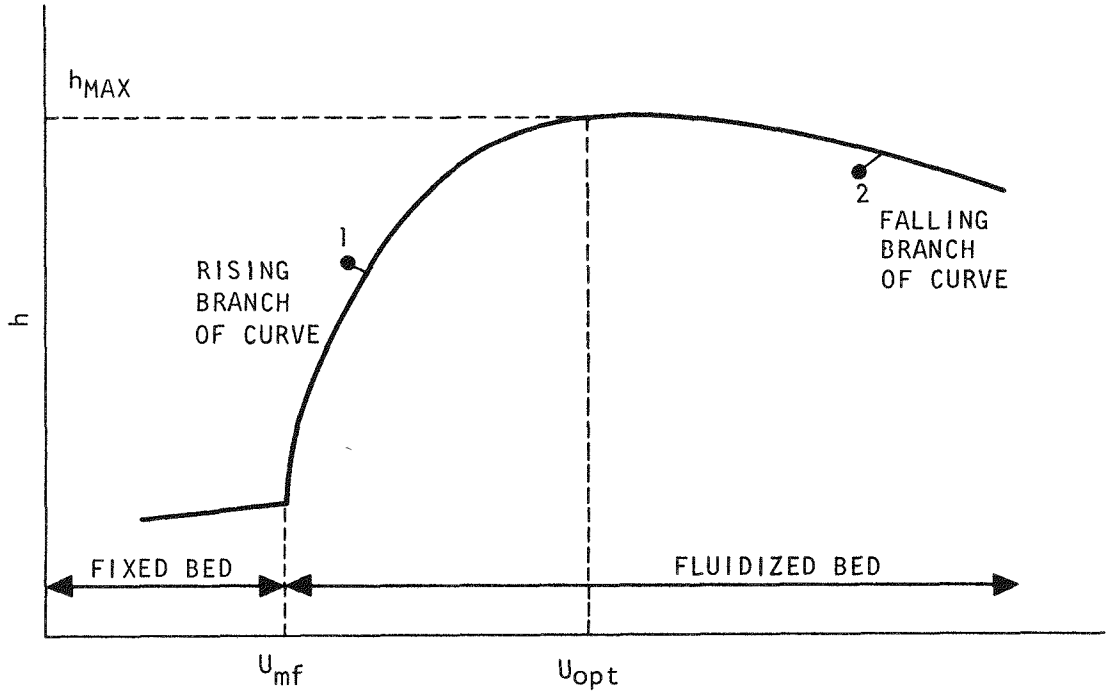

Fig. 23. Typical dependence of heat transfer coefficient on fluid velocity

$$Re_{mf} = \frac{Ar}{150 \frac{1-\varepsilon_{mf}}{\varepsilon_{mf}^3} + \sqrt{\frac{1.75\ Ar}{\varepsilon_{mf}^3}}} \quad (3)$$

$$Re_t = \frac{Ar}{18 + 5.22\sqrt{Ar}} \quad (4)$$

where $Re_{mf} = U_{mf}\ d_e/\nu_f$

$Re_t = U_t\ d_e/\nu_f$

ε_{mf} = minimum voidage fraction

The calculated values for the feed and the product are given in Table 13. The values given in Table 13 are in good agreement with the more rigorous values of U_{mf} and U_t in Table 12.

TABLE 13
OPTIMUM VELOCITY FOR HEAT TRANSFER

	Feed	Product
Ar	54.1	1.43
U_{mf}, cm/sec	8.7	2.0
U_t, cm/sec	165	21
U_{opt}, cm/sec	66	17

4.2.2.1.4. Burn Rate. The differential pressure across the bed and the filter in the 10-cm secondary burner run is shown in Fig. 24. (Ref. 24). The two curves show interesting combustion characteristics in the bed.

At the beginning of the run, the bed ΔP drops slightly and the filter ΔP increases. This is probably due to the elutriation of fine particles

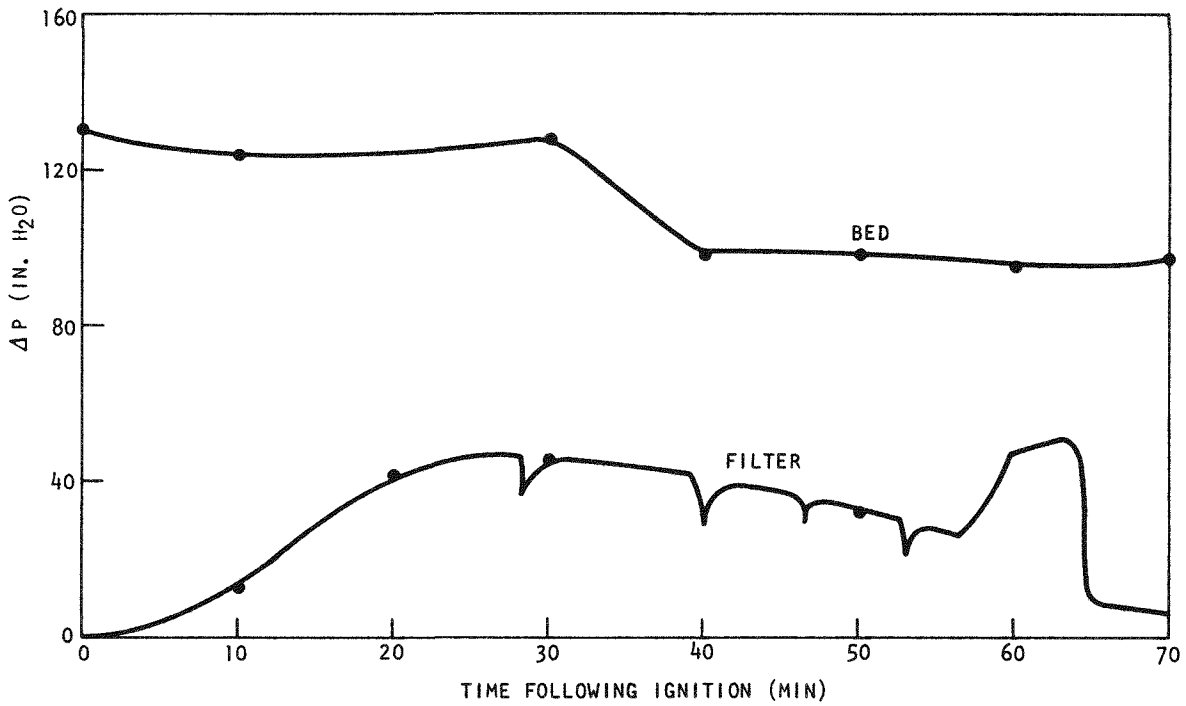

Fig. 24. Differential pressures across bed and filter, Run F4RHB-M36

into the filter section. Ten minutes after ignition, the bed weight increases slightly, while the filter ΔP increases rapidly. When ThC_2 kernels react with oxygen, they rapidly crack into fine powders (Ref. 25) and plug the filter, which increases the filter ΔP. At the same time the bed weight increases slightly according to the reaction (Ref. 26):

$$ThC_2 + 3O_2 \rightarrow ThO_2 + 2CO_2 - 435.1 \text{ kcal} \quad . \tag{5}$$

Compared to the carbon-oxygen reaction, in which there is no oxygen loss, one mole of oxygen is lost into the solid product (ThO_2) for every two moles of CO_2 off-gas. Therefore, by checking the off-gas composition with reference to the inert nitrogen, the rate of reaction of ThC_2 can be obtained. A point check during an earlier part of a run confirms that the reaction is almost entirely $ThC_2 - O_2$ reaction.

As the $ThC_2 - O_2$ reaction nears completion the bed and filter ΔP both reach their maximum, followed by a rapid drop in the bed ΔP. This is an indication of a second reaction between the carbon and oxygen. As the carbon in the bed is depleted, the bed and filter ΔP both decrease. Although qualitative, this analysis confirms that most of the ThC_2 reacts with oxygen during the earlier part of the process. This is important because the $ThC_2 - O_2$ reaction produces 54% more heat than the carbon-oxygen reaction with the same oxygen supply. A preliminary calculation indicates that the 20-cm secondary burner capacity is limited by the heat transfer through the wall. A maximum allowable fluidizing velocity (when 100% O_2) for adequate burner cooling appears to be around 70 to 80 cm/sec, which supplies enough O_2 to achieve the design burn rate of 1 fuel element/hr.

From the above analysis, an allowable burner operating velocity ranges from 15 to 80 cm/sec. Changing the velocity as the process proceeds would be most ideal. However, a velocity in the range of 40 to 60 cm/sec appears to be optimum except at the end of the run.

4.2.2.2. Induction Heating for Startup

An induction heating coil was designed to heat the bed to 900°C during the startup and the tail-burn period. Different cases, with and without a susceptor plate and with different coil-workpiece couplings, were studied.

The coil electrical efficiency is substantially lower for the case without a susceptor plate, as shown in Fig. 25. In addition, the conduction loss to the coil is four times higher without a susceptor plate due to the use of stronger silica insulation material which is a poor insulator. The total useful power input to the burner is less than 65% of the total power even with 3 in. insulation. It was therefore decided to use a susceptor plate. The use of a susceptor plate adds an additional safety measure to the system. The susceptor acts as a secondary containment for the bed materials in the event of a vessel wall burn-through. Susceptor heating provides more uniform heating of the vessel even with a miscentering of the vessel around the coil and also reduces the thermal shock and the resulting material fatigue of the tube caused by a rapid heatup. The coil electrical efficiency, the number of coil turns, and the total useful power input are plotted in Fig. 25.

The final coil design was determined so as to maximize the overall useful power input into the burner (see Table 14). The final coil dimensions and design parameters are summarized in Tables 15 and 16.

In order to prevent the suscepting on the support plates, magnetic field cutting coils will be used at both ends of the coil (see Ref. 27).

4.2.2.3. Heat Transfer Coefficient

Heat transfer between solid particles and fluid in a fluidized bed includes the following stages (Ref. 28):

1. Supply of heat to (or take-off from) the system by fluid flows or solid particles (the "thermal balance" problem).

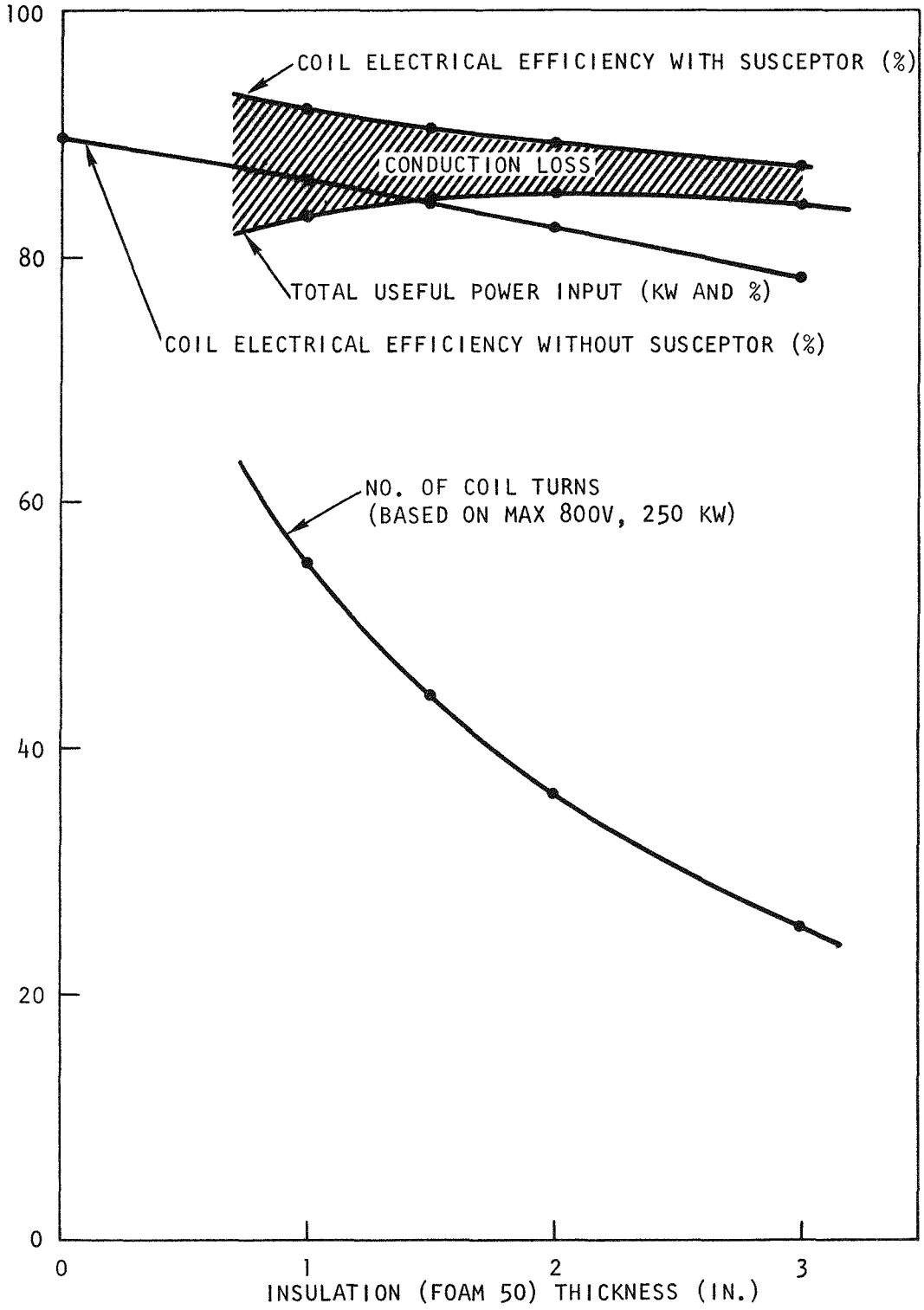

Fig. 25. Induction coil efficiencies

TABLE 14
OPTIMIZATION OF INSULATION THICKNESS

	1 in.[a]	1.5 in.	2 in.[b]	3 in.
Coil electrical efficiency, %	92.07	90.85	89.63	87.62
Coil electrical loss, kW	7.93	9.15	10.37	12.38
Coil conduction loss, kW	8.72	6.06	4.72	3.38
Total coil heat loss, kW	16.65	15.21	15.09	15.76
Number of coil turns	55	44	32	25

[a] Insulation thickness.

[b] Optimum insulation thickness with a minimum total coil heat loss.

TABLE 15
INDUCTION COIL DIMENSIONS

Coil turn inside diameter	4-7/16 in.
Total projected length	36 in.
Coil size	3/4-in.-o.d. copper tubing
Number of coil turns	33
Coil electrical efficiency	89.1%
Maximum coil capacity	250 kW at 800 V
Maximum coil current	1220 amp at 800 V
Capacitor	1010 KVAR at 800 V
Coil cooling water capacity	3 gpm
Coil cooling water line pressure drop	20 psi

TABLE 16
INDUCTION COIL DESIGN PARAMETERS

Motor-generator set frequency.	1000 Hz
Coil voltage	800 V
Hastelloy-X magnetic permeability. . .	1.002
Hastelloy-X electric resistivity . . .	1.183×10^5 abohm
Insulation (Foam-50) thermal conductivity	0.15 Btu/hr/ft/°F at 1000°F
Maximum susceptor plate temperature	1100°C
Maximum coil temperature rise.	40°F

2. Heat transfer from the fluid flow to the surface of the solid particles, or conversely (the "external" problem).

3. Propagation of heat within the solid particle (the "internal" problem).

The heat transfer rate as a whole depends on the slowest stage. The criteria for the dominating stage are as follows:

1. If $\phi_1 \to 0$, stage (1) governs (Ref. 29),

$$\text{where } \phi_1 = UC_g\rho_g\, d/h_p\, H(1-\varepsilon) \tag{6}$$

C_g = heat capacity of gas, 0.28 cal/g-°C
h_p = particle heat transfer coefficient
H = height of bed
ε = bed voidage

This expression is satisfied with an error $\nmid$ 2% when $\phi_1 \leq 1.5$, $\nmid$ 5% when $\phi_1 \leq 2$, and $\nmid$ 10% when $\phi_1 \leq 2.6$. In the converse relation, stage (2) governs.

2. If $B_i < 0.25$, stage (2) governs
   $B_i > 20$, stage (3) governs,

$$\text{where } B_i = h_p\, R_p/k_s, \text{ Biot's number} \tag{7}$$

R_p = radius of solid particle
k_s = thermal conductivity of solid particles

3. If $\phi_2 < 0.5$, stage (1) governs,

$$\text{where } \phi_2 = UC_g\rho_g\, d^2/k_s\, H(1-\varepsilon) \tag{8}$$

The value of h_p can be obtained from the relation

$$Nu_p = 0.4\ (Re/\varepsilon)^{2/3}\ Pr^{1/3},$$

where Nu_p = particle Nusselt number, $\dfrac{h_p\, d_e}{k_g}$

$$Re = \text{Reynolds number, } Ud_e/\nu_g$$
$$Pr = \text{Prandtl number, } C_g\mu_g/k_g$$

By substituting proper values for U, μ_g, C_g, etc., we obtain:

$$\phi_1 \approx 10^{-3}$$
$$B_i \approx 10^{-4}$$
$$\phi_2 \approx 10^{-7}$$

Therefore, the heat transfer between the solid particles and fluid is governed by the "thermal balance" problem, which means that the solid particles are at the same temperature as the fluid. The overall heat transfer is controlled by the bed-to-wall heat transfer coefficient under the circumstances.

For small particles, the bed-to-wall heat transfer rate due to convection of fluid is usually very small (Ref. 28):

$$Nu_{conv} = 0.0175\ Ar^{0.46}\ Pr \qquad (9)$$
$$h_{conv} = \frac{(Nu_{conv})(k_g)}{d_e}.$$

Below 1000°C the heat transfer due to radiation is not more than 5% of the total h (Refs. 28, 30). Under these conditions the maximum bed-to-wall heat transfer coefficient can be obtained from the following equations (Refs. 28, 31):

$$Nu_{max} = \frac{h_{max}\, d_e}{k_g} = 0.86\ Ar^{0.2}\left(\frac{k_g}{k_{air}}\right)^{0.6} \qquad (10)$$

$$\text{for } 30 < Ar < 2 \times 10^5$$

or

$$h_{max} = 33.7\ \rho_s^{0.2}\ k_g^{0.6}\ d_e^{-0.36} \qquad (11)$$

The values for the feed and product are given in Table 17.

TABLE 17
HEAT TRANSFER COEFFICIENT
($Btu/hr-ft^2-°F$)

	Feed	Product
h_{max}	108.9 (Eq. 10) 102.4 (Eq. 11)	190.7 (Eq. 11)
h_{conv}	5.2	4.5

Many correlations for the bed-to-wall heat transfer coefficient have been developed. The scatter of data is very large, as shown in Table 18. However, the correlations by Wen and Leva (Ref. 32) and Wender and Cooper (Ref. 33) are believed to be the most reliable.

TABLE 18
HEAT TRANSFER COEFFICIENTS
BY VARIOUS CORRELATIONS
($Btu/hr-ft^2-°F$)

Dow and Jakob (Ref. 34)	127.4
Van Heerden (Refs. 35, 36)	74.7
Toomey and Johnstone (Ref. 37)	44.2
Levenspiel and Walton (Ref. 38)	18.7
Wen and Leva (Ref. 32)	60.1
Wender and Cooper (Ref. 33)	100.2

From the last two correlations, the bed-to-wall heat transfer coefficient in the 20-cm secondary burner is assumed to have a value of 80 $Btu/hr-ft^2-°F$. When crushed ThC_2 fuels were burned in an alumina bed at ORNL (Ref. 39), a bed-to-wall heat transfer coefficient of 85 $Btu/hr-ft^2-°F$ was obtained. A detailed heat balance and transient responses will be reported at a later date.

4.2.2.4. High-Temperature Product Withdrawal Valve

The high-temperature product withdrawal valve/distributor plate assembly reported in the previous Quarterly Progress Report (Ref. 7) was

reviewed. Thermal stress analysis showed that the proximity of the distributor plate to the Gray-Loc metal seal is undesirable and that a possible warpage of the distributor plate might hamper valve operation. An alternative design that alleviates this problem was proposed (Fig. 26). However, with this design there is the possibility of stagnation of particles at the bottom corner and particle segregation caused by a tapered neck in the middle of the burner. Further studies of this design and possible modifications are under way.

4.2.2.5. Filter Blow-Back Assembly

The presently designed filter blow-back assembly (Ref. 7) uses too many welds. These weld points might crack under a severe thermal stress or repeated thermal shocks caused by the cold blow-back gas. A design modification is under way.

4.2.2.6. Top Cap

If a sintered metal filter fails, fine radioactive materials can get into the top filter chamber plenum. In order to clean the plenum should this happen, the top cap must be separable from the top Gray-Loc hub. This creates a mechanical seal problem between the top cap of the burner and the thermowell. A design using a metal bellows to absorb the stress (including the stress caused by thermal expansion of the thermowell) and a completely new design without a metal bellows are under study.

4.2.2.7. In-Vessel Filters

The in-vessel filter design was reevaluated in view of the recent filter failures in the 10-cm secondary burner. A conservative estimate predicts a higher filter pressure drop in the 20-cm secondary burner. The filter area was doubled by increasing the length from 18 in. to 36 in. and also increasing the diameter of the filter element from 2-3/4 in. to 3 in. This will reduce the maximum forward linear velocity at the surface from 8 to 4 ft/min. All other dimensions remain the same.

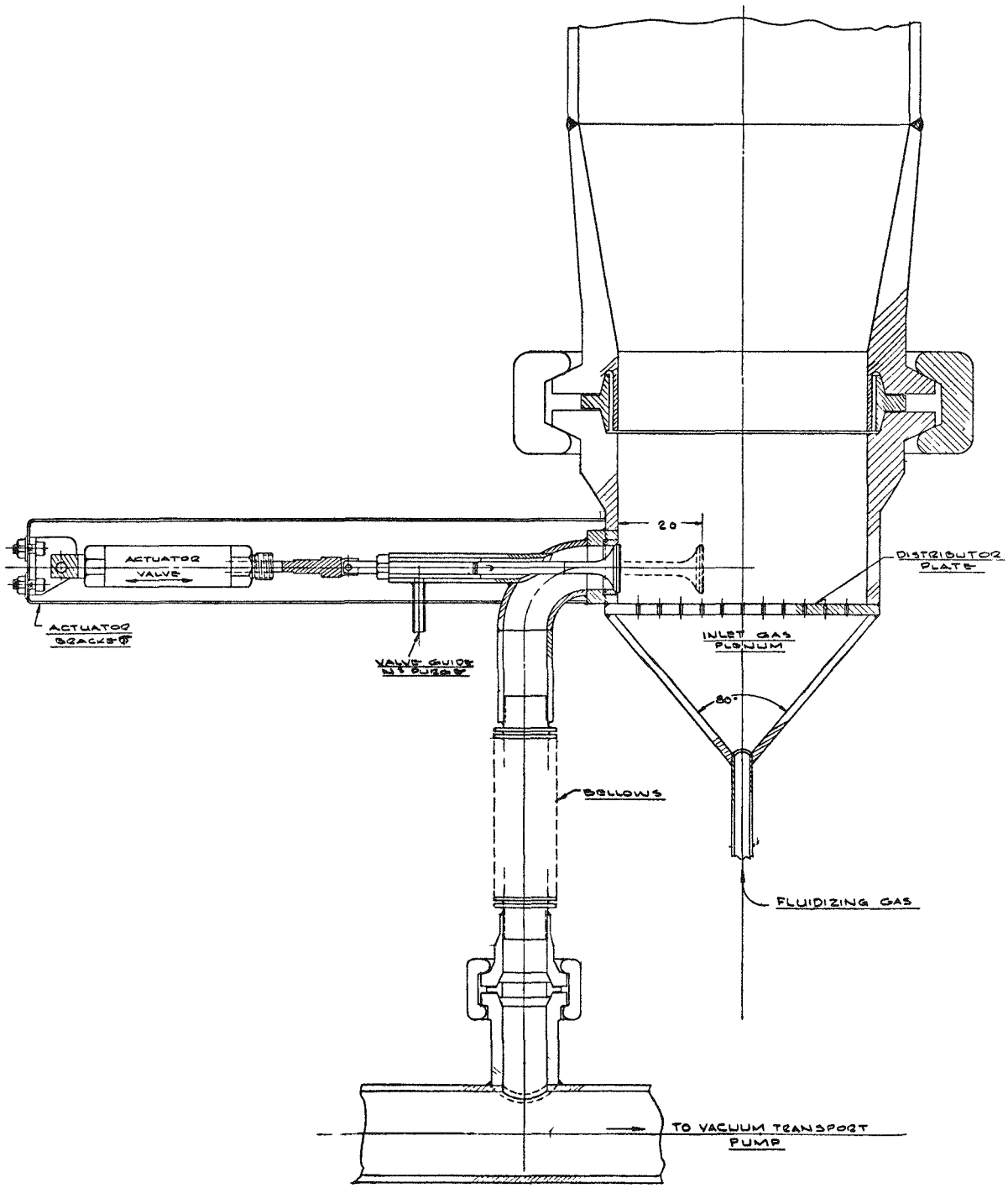

Fig. 26. Alternate design of high-temperature product withdrawal value

4.2.2.8. Burner Outer Clamshell Insulation

Assuming that the induction coil will maintain its maximum temperature at 130°F, the lower cooling jacket does not need any additional insulation outside of the coil. In order to protect the coil assembly, however, a minimal (1 in.) insulation will be used at the bottom cooling section.

Above the induction coil, the inside temperature of the cooling jacket will reach a high temperature (~400°C) due to radiation from the hot burner wall. The outside insulation temperature should be maintained below 140°F in the hot cell. Assuming heat transfer to the ventilating air by natural convection, a 3-in. Foam-50 insulation will keep the outside temperature below 140°F. Less than 1% of the total heat generation in the burner vessel is expected to be released into the hot cell through the insulation.

5. AQUEOUS SEPARATIONS

5.1. DESIGN OF INSOLS DRYER FOR PILOT PLANT STUDIES

A fluidized-bed drying system has been designed for drying the insoluble silicon carbide hulls from the centrifuge separation. The capacity of the pilot-scale unit is approximately 15 kg/day. This capacity is close to full scale of that required to process the fertile portion of twelve Fort St. Vrain fuel blocks per day, as called for in the ICPP hot demonstration.

5.1.1. Design Criteria

The insoluble silicon carbide hulls, unburned carbon, and any uncrushed particles from the TRISO/TRISO processing flowsheet will be discharged from the leacher in a slurry form with the mother liquor. The slurry is then centrifuged for solid-liquid separation and rinsed with water to remove residual acid. At this point the solids must be dried and the whole particles separated.

5.1.1.1. Functional Requirements

Criteria for the design of an insols dryer to be used in pilot-plant operations are basically those of versatility. The unit should have the following capabilities: (1) batch or semicontinuous remote operation, ability to accept a fairly wide range in feed moisture content (2 to 25 wt %), and production of sufficiently dry product. There should also be a minimum of mechanical devices.

The unit should be capable of drying approximately 15 kg of feed per day. This capacity is close to 100% of that expected in processing the fertile portion of twelve Fort St. Vrain Fuel blocks per day.

Typical solids that will be fed to the insols dryer will be the perforate bowl centrifuge product. It has been reported (Refs. 40,41) that these solids will contain from 2 to 10 wt % water and will have a particle size distribution from 10 to 250 μm.

The bulk density of the dried product will be about 1.2 g/cm^3.

5.1.1.2. Performance Parameters

Design of the insols dryer is based on the following performance parameters:

1. An adequate source of heat is supplied to vaporize the contained moisture in a 10-kg batch of feed containing 10% moisture.

2. Sufficient fluidizing medium (air or nitrogen) is available to achieve fluidization and elutriation of the solids.

3. The unit is capable of batchwise and semicontinuous operation.

4. Provisions are made for distribution of the fluidizing media to ensure adequate mixing and minimum clump formation while drying the solids.

5. Provisions are made for operating the unit at less than 15 psig.

5.1.1.3. System Orientation

The physical location of the insols drying system will be within the leaching room of the Experimental Building. The system will be installed on the west wall of the room.

5.1.2. Proposed Design

5.1.2.1. General Flow

A fluidized-bed drying system was chosen to process the wet silicon carbide hulls. An overall flow diagram is presented in Fig. 27.

The washed centrifuge cake is loaded into the fluidized-bed vessel through a Y-transition at the top. Heated nitrogen is passed through each batch of solids to drive off the contained moisture. Nitrogen enters the system from a pressure-regulated existing supply and, after being metered, is routed through a bank of variable resistance heaters. After the desired temperature is reached, the nitrogen is routed to the base cone of the fluidized bed and up through the bed of insols.

At the completion of each drying cycle, the dried solids are elutriated from the fluid bed and collected via a high-efficiency cyclone separator. Fine solids are removed from the off-gas by a 5-μm porous sintered metal filter that is equipped for blow-back. The moisture-laden off-gas is routed through an acid solution to rid the stream of any residual nitric acid vapors and then to a bank of absolute filters.

Elutriation of the silicon carbide hulls will be carried out such that separation of any uncrushed particles can be accomplished in the fluidized-bed vessel. Any remaining uncrushed particles will be discharged through the base cone.

5.1.2.2. Equipment Description

Detailed construction drawings for the assembly of the insols drying system are included as Appendix A. A short description of each essential part follows.

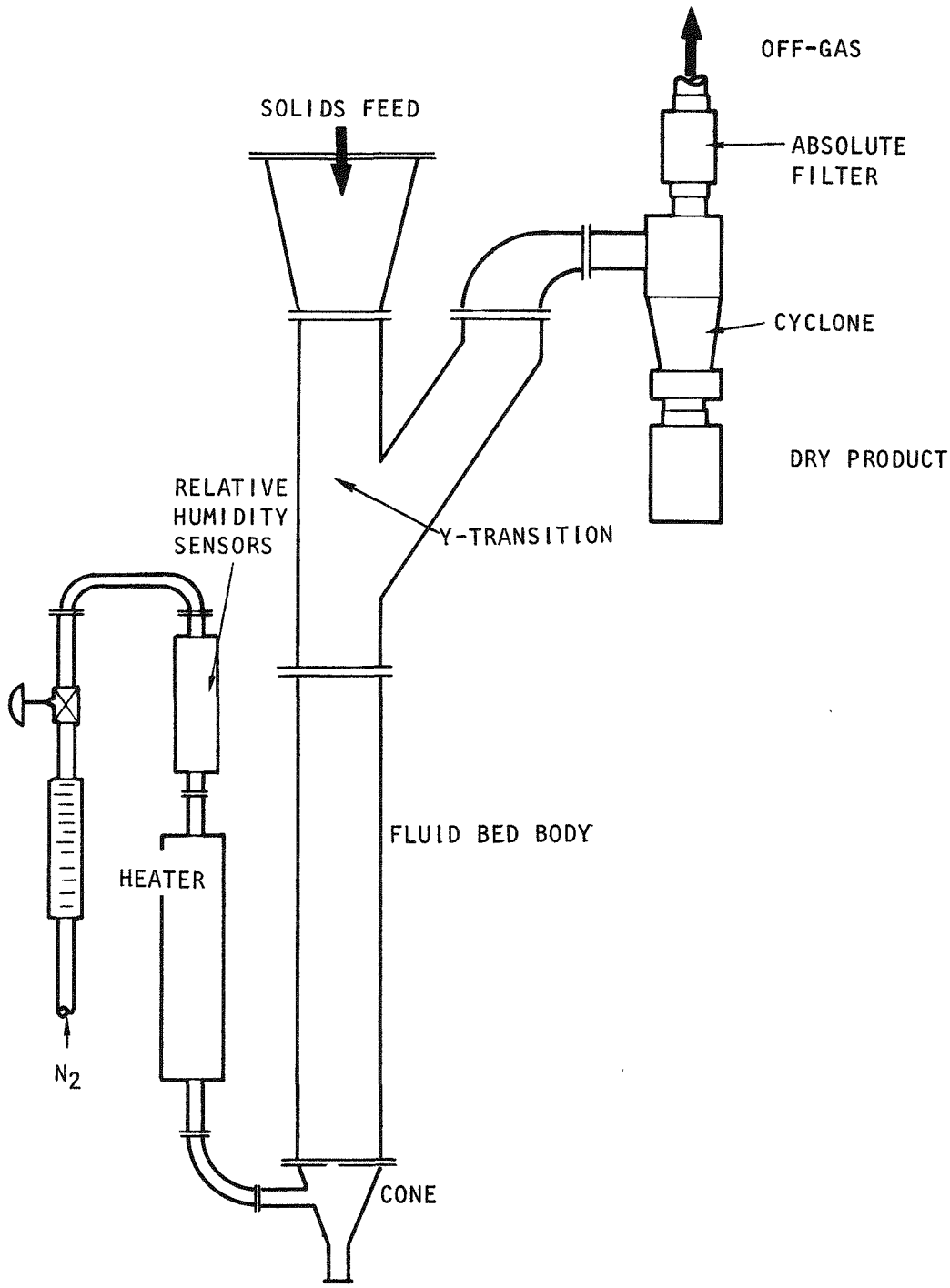

Fig. 27. General flow diagram for insols dryer

All parts within the system that will come in contact with moisture-laden gas or wetted solids will be constructed of 304 stainless steel when practicable. Connections will be accomplished with Tri Clamp fittings when possible.

The nitrogen heater is constructed to house five General Electric Calrod finned strip heaters, each of which has a heating capacity of 500 W. The heater passes pressurized nitrogen from a metered source and raises its temperature to the desired range. The hot nitrogen is vented to the base cone of the fluizided-bed vessel.

The base cone consists of a 60° included angle cone with an outside jacket. The inner wall of the cone is fabricated from a wire mesh laminate screen which acts as a distributing device for the drying nitrogen. The cone is equipped with a discharge port to allow dumping of whole particles or unelutriated clumps. The cone is connected with Tri Clamp connectors to the bottom of the fluidized-bed main vessel.

The main vessel for the fluidized-bed drying system is simply a length of 4-in. tubing. The vessel is equipped with couplings to accept temperature and/or pressure sensors. The main body is, in turn, connected to a transition piece via Tri Clamp fittings.

The Y-transition serves two purposes, a feed port for solids and a connection to the cyclone separator. The transition is equipped with Tri Clamp fittings for coupling to the main vessel, the cyclone transition piece through a 90° elbow, and the centrifuge transition piece.

The cyclone transition is a round-to-rectangular piece that allows connection of the Y-transition and 90° reducing elbow to the purchased Fischer-Klesterman cyclone separator.

The cyclone separator is a vendor-supplied item from Fischer Klesterman [Model XQ3(S)]. The dimensions of the separator are consistent with those published by the manufacturer (Bulletin 217C). The separator is connected to a collection vessel and a filter housing via appropriate transitions and Tri Clamp fittings. This cyclone transition is merely a rectangular-to-round transition to allow use of Tri Clamp fittings for the filter housing and product collection vessel.

The filter housing contains one 3-in-o.d. porous sintered metal filter with a mean pore opening of 5 μm. The housing is coupled to the gas exit port of the cyclone separator and the existing off-gas system. The housing is equipped with a filter blow-back mechanism.

The product collection vessel consists of a blinded straight piece of tube connected to the bottom port of the cyclone separator. Connection is made with the use of Tri Clamp fittings to allow ease of removal.

Two humidity sensor ducts are used to house the Honeywell sensing units. These ducts are located before the heater and after the filter assemblies.

5.1.3. Instrumentation

Control and instrumentation of the fluidized-bed dryer consists of temperature monitoring, pressure monitoring, drying gas analysis, and measurement of gas flow.

Flow of the nitrogen gas into the heater is monitored with a Brooks variable-area rotameter (see Fig. 28). Nitrogen is received from an existing supply source and is pressure regulated prior to its entrance into the flowmeter. The rotameter is equipped with a transmitter to convey the rate data to recording instruments in the control room.

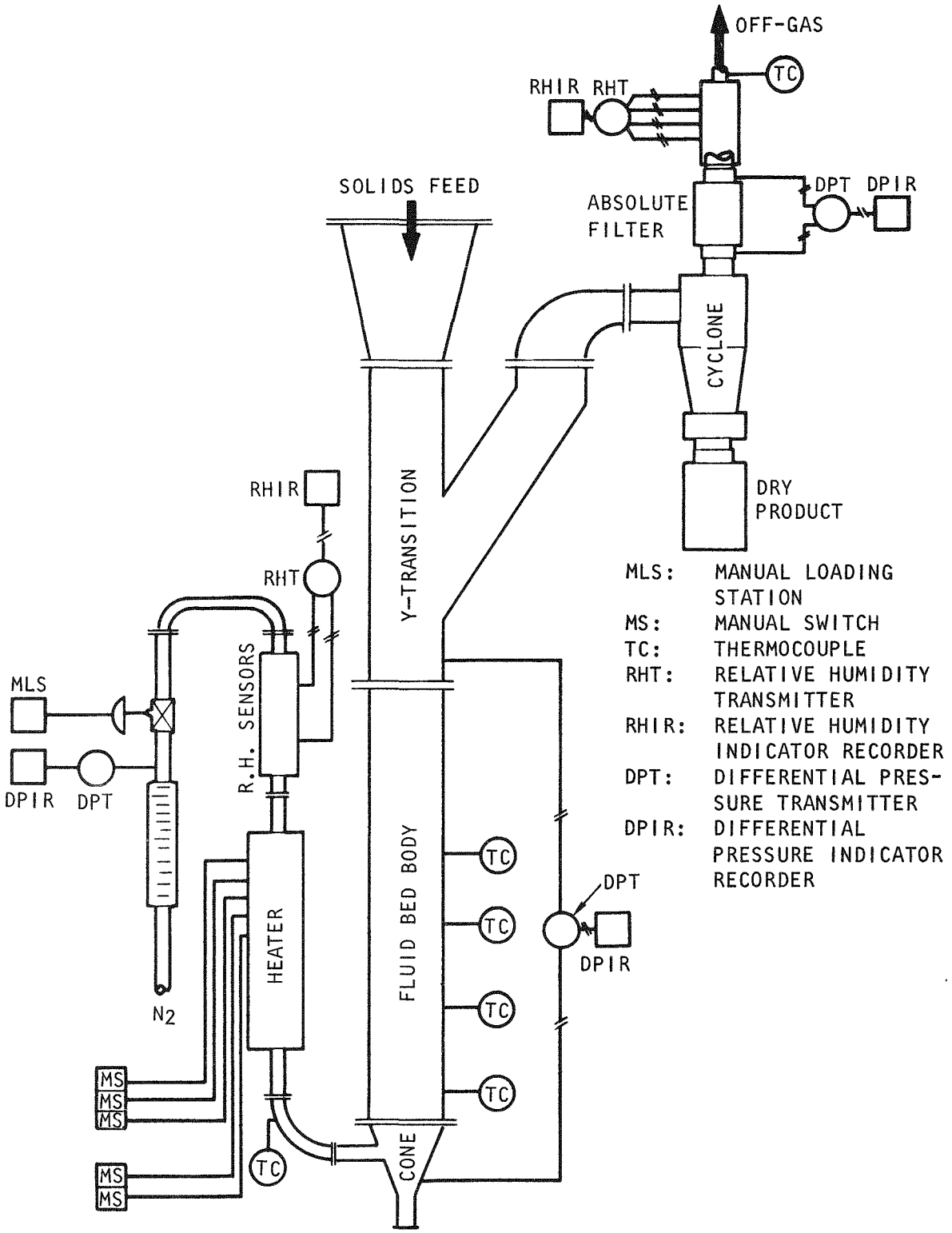

Fig. 28. Instrumentation for insols dryer

The flow rate of the nitrogen gas is controlled via an air-actuated bellows control valve from Badger Meter.

Honeywell humidity sensors are used to analyze the drying gas. Two composite sensors (SSP144) are located before the heater and four are located downstream of the filters. The sensors are coupled to transmitters which in turn relay the data to the control room recorders.

Pressure monitoring consists of measuring the differential bed pressure, absolute bed pressure, and differential filter pressure. Pressure monitoring is accomplished via ITT-Barter differential pressure cells coupled to transmitters for transferring the data to appropriate recorders in the control room.

Continuous monitoring of gas inlet and outlet temperatures, as well as measurement of temperatures at various locations within the fluidized bed, is accomplished with type-K thermocouples. The thermocouples are connected to a multipoint recorder, a digital readout, and any control loops that use temperature as the primary control.

5.1.4. Hazards Analysis

The hazards associated with the cold pilot plant operation of a fluidized-bed insols dryer are primarily those of handling acid vapors and any radioactive thorium that might be present.

Since the unit will be installed in a specially fabricated acid cell, which incorporates adequate precautions for the handling of acid solutions and vapors, the hazard presented by the acid vapors is minimal. However, all required procedures as outlined by the GA safety manual and all procedures necessary to ensure minimal safety and health hazards will be followed.

Handling of the small amounts of thorium that will be present in the insols feed is of no major consequence. Compliance to the stringent requirements set forth by 10 CFR 20, Title 17, California Administrative Code Chapter 5, Subchapter 4, Group 3, and the GA Radiological Safety Guide is all that is necessary.

6. SOLVENT EXTRACTION

Six solvent extraction run summaries were completed during the quarter. The flowsheets under investigation are related to HTGR reprocessing and fuel materials recycle. Results indicate no problems have been encountered that cannot be solved by changes in either flowsheet design or column design.

6.1. RUNS 9 and 10

Runs 9 and 10 consisted of uranium and thorium extractions, partitioning, partition-scrub, and uranium stripping. These runs were conducted in the pilot plant two-column system to obtain efficiency and capacity data. The resulting data are applicable to solvent extraction in the Idaho HTGR reprocessing plant and the Target Recycle Plant.

The flowsheet tested was the first cycle of Fig. 29 (from Ref. 42) with the exception that in Run 9 the acid was added to the solvent rather than directly to the column. Table 19 shows the stream analyses and flow for each type operation.

Table 20 gives the flooding data and height equivalent to a theoretical stage (HETS) when operating at the observed percentage of flooding frequency. Additional aluminum added to the Run 10 feed (Al/F ratio of 3.64 versus 2.0 in Run 9) apparently improved the extraction of thorium. It is assumed that this improvement is due more to lowering of thorium complexing by flouride than to additional salting by aluminum nitrate. Additional data are needed on the effects of the Al/F ratio on thorium distribution at the raffinate end of the column. Currently, the thorium waste loss, rather than HETS for a given length of extraction column, is being reported.

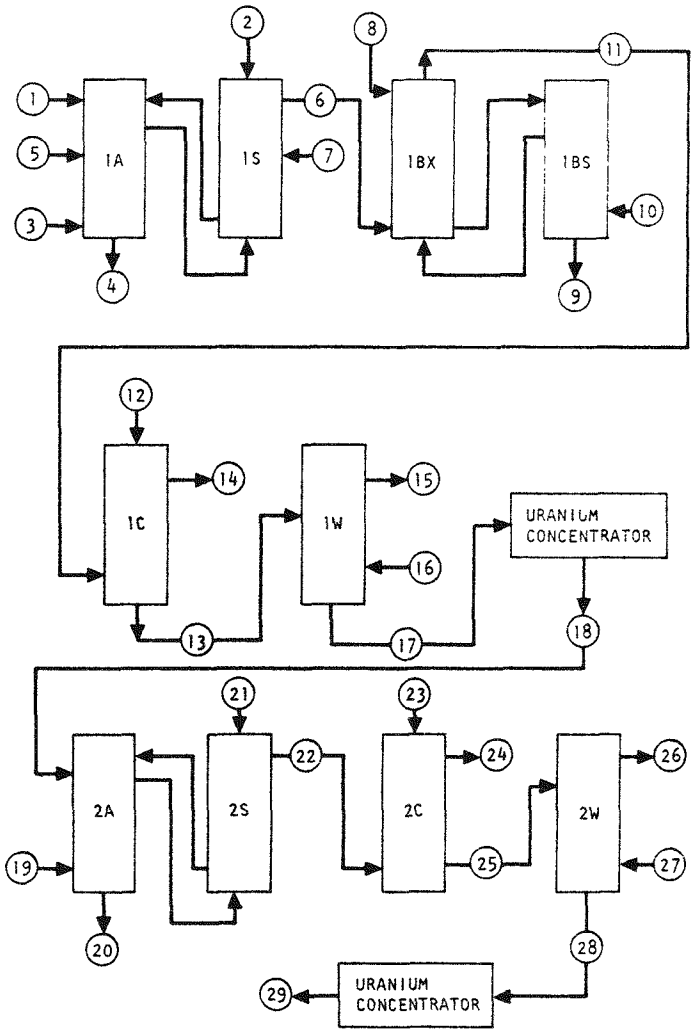

STREAM NO.	FLOW (L/DAY)	COMPOSITION U (G/L)	Th (G/L)	HNO_3 (M)
1	725	14	348	<1.0
2	754			0.01
3	7250		(30% TBP)	
4	1903		(FISSION PRODUCTS)	
5	234			13.0
6	7250	1.4	35	
7	190			5.0
8	4350			0.2
9	4350	Trace	102	
10	1300		(30% TBP)	
11	8550	1.19		
12	4300			0.01
13	4300	2.37		
14	8550		(30% TBP)	
15	430		(NPH)	
16	430		(NPH)	
17	4300	2.37		
18	43.6	233		
19	858		(5% TBP)	
20	294		(WASTE)	
21	243			2.0
22	858	11.8		
23	430			0.01
24	858		(ORGANIC)	
25	430	23.6		
26	43		(NPH)	
27	43		(NPH)	
28	430	27.5		
29	43.6	233		

Fig. 29. Partition flowsheet

TABLE 19
ANALYTICAL DATA AND STREAM FLOWS, RUNS 9 AND 10

Stream	Stream No.(a)	Run 9 Analyses and Flow				Run 10 Analyses and Flow			
		Th (g/l)	U (g/l)	HNO_3 (M)	Flow (ml/min)	Th (g/l)	U (g/l)	HNO_3 (M)	Flow (ml/min)
1AF	1	352	33.8	1.03	68	331	7.2	0.28	105
1AS	2	-	-	~1.0	115	-	-	1.1	130
1AA	5	Added to 1AX			-	-	-	15	18
1AX	3	36% TBP			740	32% TBP			1080
1AP	6	31	2.97	0.23	-	27.2	0.7	0.2	-
1AW	4	1.9	0.0002	0.9	180	0.040	<0.00008	0.7	245
1BX	8	-	-	0.2	450	-	-	0.23	600
1BXT	-	54	0.5	0.55	-	55	0.1	0.7	-
1BU	11	0.003	3.0	0.02	740	0.001	0.65	0.013	-
1BXT (avg)	-	55.8	1.35	0.56	977	58(b)	0.27(b)	0.6(b)	970
1BS	10	36% TBP			328	32% TBP			320
1BT	9	44	0.0025	0.52	-	48	0.006	0.58	-
1BSU	-	32.5	3.4	0.11	-	30	0.8	0.1	-
1BU (avg)	11	-	2.63	0.033	1200	-	0.58	0.017	800 (1500)
1CX	12	-	-	0.01	600	-	-	0.009	400 (780)
1CU	13	-	5.0	0.07	-	-	1.0	-	-
1CW	14	-	0.0015	0.0001	-	-	0.0004	-	-

(a) From Fig. 3, Ref. 42.

(b) Calculated by material balance.

TABLE 20
COLUMN HETS AND FLOODING DATA, RUNS 9 AND 10[a]

Column	Purpose	Volume Velocity (gal/hr/ft^2)	Flooding Frequency (cycles/min)	Continuous Phase	Loss (%) or HETS (ft)	Percent of Flooding Frequency
			RUN 9			
1A	Extraction	670	>140	Organic	1.4%(Th)[b]	<80
1BX	Partition	865	40	Aqueous	2.5 ft (Th)	80
1BX	Partition scrub	950	58	Aqueous	2.1 ft (U)	83
1C	Strip	1310	60	Aqueous	3.2 ft (U)	90
			RUN 10			
1A	Extraction	952	143	Organic	0.03%Th[b]	80
1BX	Partition	1220	36	Aqueous	2.1 ft (Th)	83
1BS	Partition scrub	940	60	Aqueous	2.1 ft (U)[c]	80
1C	Strip	870	98	Aqueous	4.7 ft (U)	∿100
		1650	50	Aqueous	<4.7 ft (U)	80

[a]Extraction column: 23% free area, 1/8-in.-diameter-hole nozzle plates; nozzles down; 2-in. plate spacing, 18-ft length (extraction 15 ft and scrub 3 ft); ambient temperature; 1-in. amplitude.

Other columns: 23% free area, 1/8-in.-diameter-hole nozzle plates; nozzles up; 2-in. plate spacing, upper column (15-ft length); 1-in. amplitude; 1BX and 1BS temperature ambient, 1C temperature 48°C (Run 9) and 43°C (Run 10); (plate spacing, lower column: Run 9, 4 ft, 5-in. plate spacing; Run 10, 8-1/2 ft, 4-in. plate spacing and 1-1/2 ft, 3-in. plate spacing).

[b]Al/F ratio in feed was 2 in Run 9 and 3.6 in Run 10.

[c]Poor column operation HETS for upper 10 ft of 15-ft column.

The two-column system was used for these runs. Coextraction and partitioning were run through the two-column system in 1 day, followed by partition scrub and uranium stripping in the second column on successive days. Thus, loaded solvent aging is no longer a variable in the retention of thorium during partitioning. However, the much lower HETS for aqueous continuous versus organic continuous operation in the 1BX column may be a result of 1BU sample aging causing thorium to be unstrippable. Tests will be made to confirm these 1BX column HETS values.

The HETS were calculated from McCabe-Thiele diagrams using the best estimate available for equilibrium lines. The HETS data are average numbers for the length of column used; additional column length will change the average HETS.

6.2. RUNS 13 AND 14

Runs 13 and 14 consisted of uranium-thorium concentration and costripping. These runs were conducted in the pilot plant two-column system to provide efficiency and capacity data. The resulting data are applicable to solvent extraction in the Idaho HTGR reprocessing plant and the Target Recycle Plant.

The flowsheet tested was the first cycle of Fig. 30 (from Ref. 42) with some modifications. Modifications in Run 13 included consolidation of the scrub streams (streams 2 and 7 in Fig. 30) into a 1M HNO_3 stream at the inlet point for stream 2. Aluminum nitrate was added via inlet point 7. In Run 14, stream 5 was 14M HNO_3 versus the 13M shown in Fig. 30. Table 21 shows the stream analyses and flow rates for each run.

Table 22 gives the flooding data and percentage losses via the 1AW stream when operating at the observed percentage of flooding frequency. Table 22 also shows the HETS for stripping operations.

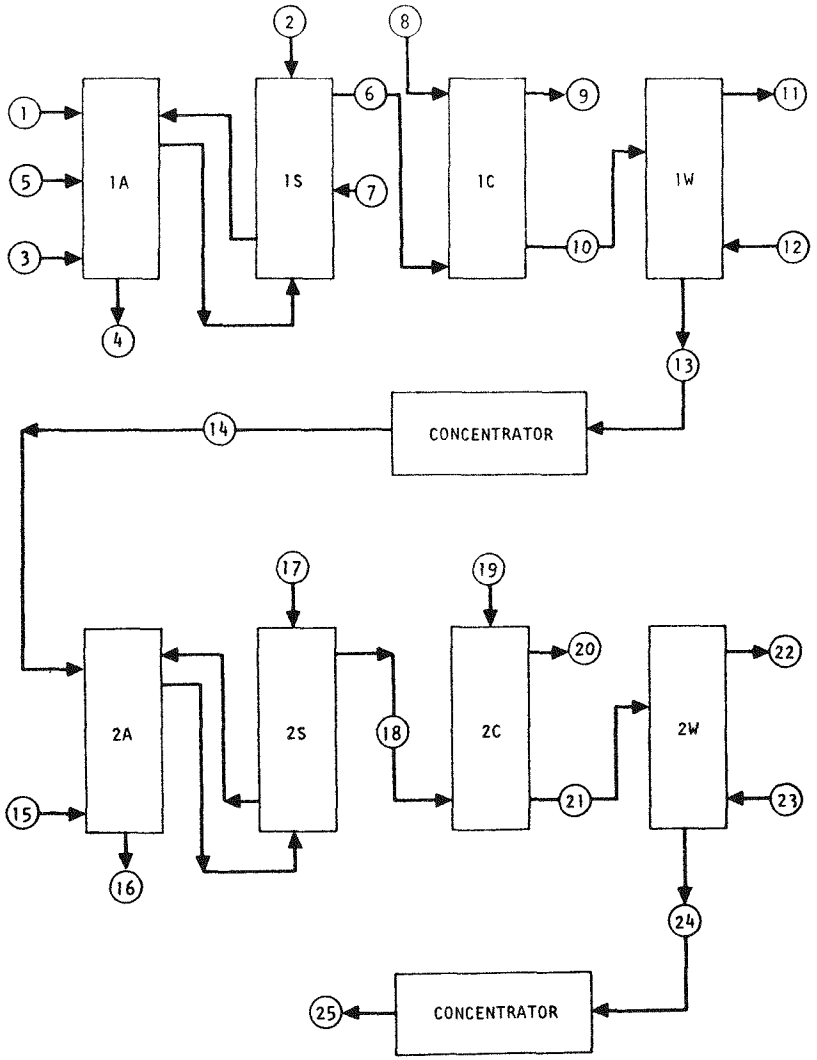

STREAM NO.	FLOW (L/DAY)	COMPOSITION U (G/L)	Th (G/L)	HNO_3 (M)
1	725	14	348	<1.0
2	754			0.01
3	7250		(30% TBP)	
4	1903		(FISSION PRODUCTS)	
5	234			13.0
6	7250	1.4	35	
7	190			5.0
8	7250			0.01
9	7250		(ORGANIC)	
10	7250	1.4	35	
11	725		(NPH)	
12	725		(NPH)	
13	7250	1.4	35	
14	725	14	348	
15	940		(5% TBP)	
16	1007		255	
17	282			2.0
18	940	10.8		
19	470			0.01
20	940		(ORGANIC)	
21	470	21.6		
22	47		(NPH)	
23	47		(NPH)	
24	470	21.6		
25	43.6	233		

Fig. 30. Co-strip flowsheet

TABLE 21
ANALYTICAL DATA AND STREAM FLOWS, RUNS 13 AND 14

Stream	Stream No.	Run 13 Analyses and Flow				Run 14 Analyses and Flow			
		Th (g/liter)	U (g/liter)	HNO_3 (M)	Flow (ml/min)	Th (g/liter)	U (g/liter)	HNO_3 (M)	Flow (ml/min)
1AF	1	362	34	0.608	110	380	36	1.285	107
1AS	2			1	130			0.008	110
1AA	5			13	23			14	31.6
1AIS	7				7.5			4.79	21.8
1AX	3			(31.9% TBP)	910			(30% TBP)	863 (1070)
1AP	6	36.65	3.62	0.075	-	36 (32.7)	3.12 (2.58)	0.07 (0.14)	-
1AW	4	3.23	$2x10^{-4}$	0.470	-	0.18 (0.011)	$9.2x10^{-5}$ ($4.6x10^{-5}$)	2.55 (2.16)	-
1CX	8			0.01	980			0.008	1000
1CP	10	33.16	3.37	0.080	-	34.03	2.71	0.071	-
1CW	9	$<4x10^{-5}$	$3.4x10^{-3}$	$9x10^{-4}$	-	$2.15x10^{-3}$	$0.24x10^{-3}$	$4x10^{-4}$	-

TABLE 22
COLUMN HETS AND FLOODING DATA, RUNS 13 AND 14[a]

Column	Purpose	Volume Velocity (gal/hr/ft^2)	Continuous Phase	Flooding Frequency (cycles/min)	Temperature (°F)	Loss (%) or HETS (ft)	Percent of Flooding Frequency
			RUN 13				
1A	Extraction	854	Organic	147	97	4.21% (Th)	80
1C	Strip	1373	Aqueous	38	121	4 ft (Th) 3 ft (U)	100
			RUN 14				
1A	Extraction	847 (975)	Organic (Organic)	145 (b)	94 (94)	0.12% (Th) (0.007%)(Th)	78 (85 est)
1C	Strip	1385	Aqueous	53	120	4 ft (Th) 2 ft (U)	80

[a]Extraction column: 23% free area, 1/8-in.-diameter-hole nozzle plates; nozzles down; 2-in. plate spacing, 18-ft length in Run 13 and 22-ft length in Run 14); 1-in. amplitude; scrub section, 9 ft and extraction - remainder, 9-ft in Run 13 and 13 ft in Run 14.

Stripping column: 23% free area, nozzle plates; nozzles up; plate spacings from top; 2-in. spacing for 5 ft, 3 in. for 1-1/2 ft, and 4 in. for 8-1/2 ft; 1-in. amplitude; 1/8-in.-diameter holes for Run 13 and 3/16-in.-diameter holes for Run 14.

[b]No flooding point was determined at higher rates.

The relatively high thorium losses and low nitric acid content in the Run 13 1AW stream resulted from flow difficulties with the 14M acid stream. This problem has been corrected by a better rate checking technique on the low-flow acid stream.

Samples from the extraction column scrub section in Run 13 produced three phases after a short settling period. The third phase (second organic phase) was recognized in the column as a cloudy emulsive zone. An apparent third phase was also observed during Run 14 operation. This cloudy emulsion in the extraction column was very sensitive to flow fluctuations. The column contents cleared substantially when the 14M acid stream flow was interrupted for a short period during the run. The reduction of the aqueous-to-organic ratio in the latter part of Run 14 also reduced the third phase.

The data in parentheses for Run 14 in Tables 21 and 22 resulted from the increased AX flow. The increased solvent flow produced a significant reduction in the thorium loss.

Column flooding in both runs occurred near the uranium color line for both columns. The flooding frequency of the extraction column compared closely with previous and subsequent runs. However, the stripping column with 3/16-in. holes in the nozzle plates in Run 14 would handle a much higher pulse frequency before flooding than the plates with 1/8-in. holes used in Run 13.

6.3. RUNS 15 AND 16

Runs 15 and 16 were made to obtain efficiency and capacity data for the Interim-23 flowsheet as a possible production mode in the HTGR Idaho reprocessing plant if such processing is requested by the AEC. The runs consisted of uranium extractions from a thorium-uranium nitrate mixture using 5% TBP in the kerosene-like diluent(NPH).

The flowsheet tested was the first cycle of Fig. 31 (from Ref. 42) with the exception that the scrub section aqueous-to-organic flow ratio was reduced from 0.3 to 0.18 and the solvent loading was reduced to lower uranium reflux. Table 23 shows the stream analyses and flow for each run.

The two-column cold pilot plant solvent extraction system was used for these runs. The extraction-scrub column was lengthened prior to these runs to a 22 ft cartridge height from the 18 ft available earlier. The column configurations and cartridges used are described in Table 24. Table 24 also gives capacity data obtained from these runs and some limited efficiency data.

It was determined in Run 15 that a 1.5M thorium feed concentration could not be used without forming a third phase at the bottom interface (organic continuous operation with the Southampton normal paraffin hydrocarbon diluent). In Run 16 the thorium feed concentration was reduced to 1M and no interface third phase was observed.

Throughout these runs, using 5% TBP, problems in phase dispersion and flooding were noted. In coextraction of uranium and thorium with 30% TBP, as in Runs 6, 7, 9, and 10, the scrub and extraction sections had similar dispersions and capacities, making a unidiameter column easy to design for [illegible] system. In the Interim-23 type flowsheet under investigation in [illegible] 15 and 16, the scrub section floods before the extraction section can [illegible] sufficiently dispersed for adequate efficiency. Also, dispersion in the scrub section was poor up to the point of flooding. For the ACC demonstration, the scrub and extraction sections may be separated into two columns. This split may be mandatory if both coextraction and Interim-23 flowsheets are to be run in the same solvent extraction battery.

The scrub section efficiency for thorium was poor in the organic continuous 9-ft section. This was anticipated from the poor discontinuous phase dispersion. An aqueous continuous scrub section could be used with split extraction and scrub columns.

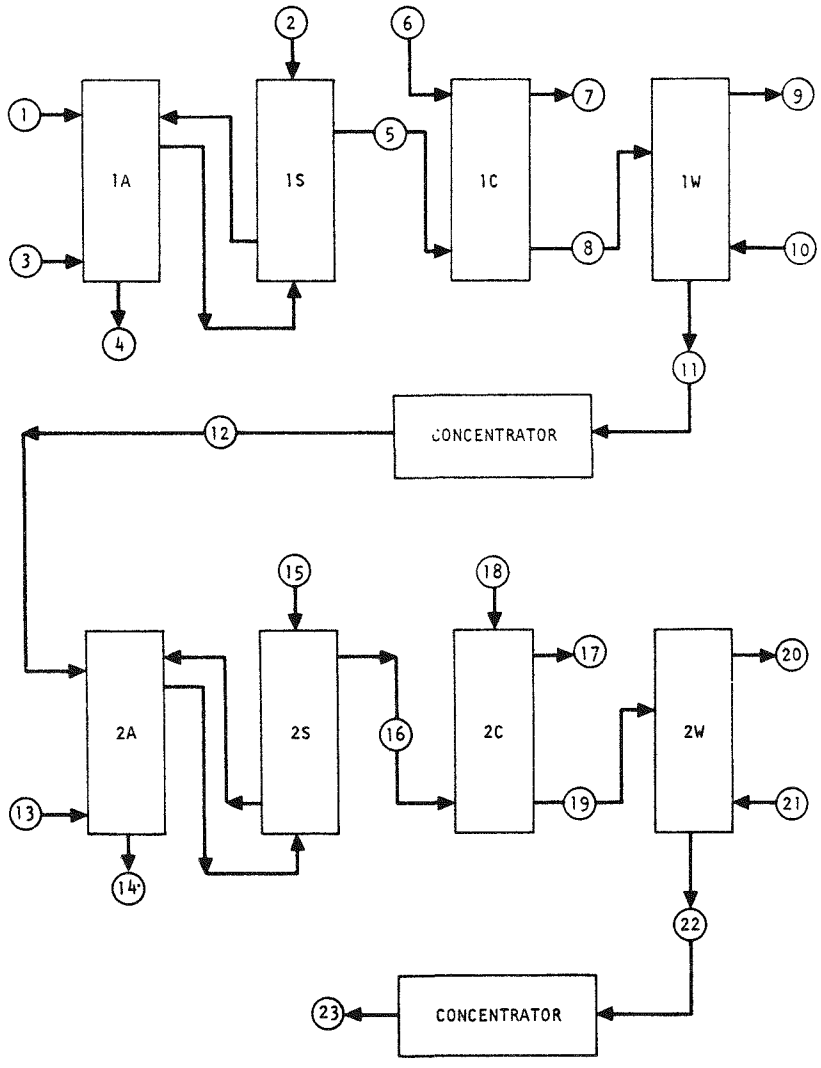

STREAM NO.	FLOW (L/DAY)	COMPOSITION U (G/L)	Th (G/L)	HNO_3 (M)
1	725	14	348	<1.0
2	282			2.0
3	940		(5% TBP)	
4	1007		255 (PLUS FISSION PRODUCTS)	
5	940	10.8		
6	470			0.01
7	940		(ORGANIC)	
8	470	21.6		
9	47		(NPH)	
10	47		(NPH)	
11	470	21.6		
12	43.6	233		2.0
13	858		(5% TBP)	
14	294		(WASTE)	
15	243			2.0
16	858	11.8		
17	858		(ORGANIC)	
18	430			0.01
19	430	23.6		
20	43		(NPH)	
21	43		(NPH)	
22	430	27.5		
23	43.6	233		

Fig. 31. Low TBP process

TABLE 23
ANALYTICAL DATA AND STREAM FLOWS, RUNS 15 AND 16[a]

Stream	Stream No.[a]	Run 15 Analyses and Flow				Run 16 Analyses and Flow			
		Th (g/l)	U (g/l)	HNO_3 (M)	Flow (ml/min)	Th (g/l)	U (g/l)	HNO_3 (M)	Flow (ml/min)
1AF	1	354	14.2	1.29	560	221	11.1	1.17	560
1AS	2	-	-	1.98	165	-	-	1.84	150
1AX	3		5.01% TBP		920		5.14% TBP		825
1AW	4	278	1.84	1.30	-	178	0.2	1.16	-
1AP	5	0.34	6.78	0.03	-	1.4×10^{-3}	6.1	0.037	-
1AP (avg)	5	-	-	-	-	-	4.47	0.032	795
ICX	6	-	-	0.01	390	-	-	0.01	410
ICW	7	9.8×10^{-4}	6.4×10^{-4}	1.4×10^{-3}	-	-	1.5×10^{-3}	0.001	-
ICU	8	0.83	13.3	0.11	-	-	9.52	0.12	-

[a]From Fig. 5 of Ref. 42.

TABLE 24
COLUMN DATA, RUNS 15 AND 16

Column	Purpose	Continuous Phase	Volume Velocity ($gal/hr/ft^2$)	Flooding Frequency (cycles/min)	U Loss (%)	HETS (ft)	Thorium Separation Factor	Temp. (°C)
			RUN 15[a]					
1A	Extraction	Organic	1200	76 (scrub)	16.7	7 (Th scrub)	500	32
1C	Strip	Aqueous	950	>37	0.009	<7	-	35
			RUN 16[b]					
1A	Extraction	Organic	1115	84[c]	2.3	-	8.6×10^4	27
1S	Scrub	Aqueous	710	>37	-	3.3 (Th scrub)		29
1C	Strip	Aqueous	870	71	0.03	<8	-	42

[a] Extraction Column: 23% free area, 1/8-in.-diameter-hole nozzle plates; nozzles down; 2-in. plate spacing, 22-ft length (extraction - 13 ft, scrub - 9 ft); 1-in. amplitude.

Strip Column: 23% free area, 1/8-in.-diameter-hole nozzle plates; nozzles up; 2-in. plate spacing, upper column; lower column plate spacing: 8-1/2 ft, 4-in. spacing; 1-1/2 ft, 3-in. spacing; 1-in. amplitude.

[b] Extraction column - same column as (a) extraction column, 22-ft extraction section. Scrub - same column as (a) strip column. Strip - same column as (a) strip column.

[c] This flooding point variable flow from poor control on aqueous return from scrub section. Actual flood point estimated at <125 cycles/min.

The strip column HETS values of <7 and <8 ft calculated for Runs 15 and 16, respectively, are undoubtedly limited by "unstrippable" uranium in the overhead solvent. A lowering of aqueous flow in future stripping runs will not only demonstrate a higher uranium product concentration, but will also provide a more meaningful HETS number.

Additional runs for Interim-23 type flowsheets will be scheduled in the run plan for the first half of CY-75. The data from Runs 15 and 16 can only be considered preliminary. With better column operation and flowsheet modification, the uranium loss can be less than 0.1% in a 22-ft extraction section.

Future Interim-23 runs will be made in equipment optimized for coextraction, and the relative uranium capacity will be determined. Extraction column length will be the only compromise from coextraction column optimization; allowance can easily be made for this in the ACC plant by having two alternate feed points in their design. Also, the ACC scrub column could be operated aqueous continuous if a second top interface controller is added.

6.4. SOLVENT EXTRACTION FACILITY EXPANSION

The planned expansion of the two-column solvent extraction system in the pilot plant to a five-column system is in progress. The platform and basic structure have been completed. Installation of the columns, tanks, and associated piping remains to be completed. The system is scheduled to be complete and ready for testing and solvent extraction development runs in January 1975.

7. SYSTEMS DESIGN

7.1. PROTOTYPE SIZE REDUCTION SYSTEM

A meeting between ACC and GA on October 9, 1974 resulted in a re-evaluation of directed effort on the crushing system and incorporation of remote handling techniques. The constraint of cell No. 2 installation was indicated as no longer a mandatory requirement.

Efforts toward incorporation of these tenets are in progress. An attempt is being made to finalize all of the concepts prior to a January meeting with ACC. A series of keyed isometric drawings depicting the requested techniques has been prepared for a conceptual presentation at the December meeting.

7.2. PROTOTYPE PRIMARY BURNER

Conceptual studies of related components of the burner were undertaken during this quarter. A design review meeting during November pointed out a number of areas wherein design simplification could accomplish considerable cost reduction. These concepts are being developed toward incorporation of the best design.

The design review also brought out the fact that thermal stresses are a more significant problem then it was thought. As a direct result, a more intensive investigation of heat transfer techniques and vessel insulation has been initiated. Details of the induction heating coil are nearing completion, with special emphasis on remote techniques. A remotely operated cooling water disconnect valve incorporating electrical connection capabilities is being developed jointly with a vendor. Preliminary efforts show considerable promise.

Detail drawings of components used in support of burner operation are progressing at a rate commensurate with overall system design.

7.3. PROTOTYPE SECONDARY BURNER

Progress on the secondary burner parallels that for the primary burner since the basic concepts have a degree of similarity. This makes it possible to order material and parts with long lead times earlier than might normally be the case.

7.4. AQUEOUS SEPARATION

Drawings of the insols dryer, which will be part of the leaching and solvent extraction system expansion, were completed and are being reviewed by the responsible engineers prior to final release. The drawings necessary to accomplish the expansion of the leaching and solvent extraction systems have been completed and are ready for review.

7.5. PROTOTYPE PLANT SYSTEMS, GENERAL

The designs for the control room/office complex and the burner support structure are complete.

8. ALTERNATE REPROCESSING TECHNIQUES

Current studies concerning alternate reprocessing techniques are aimed at a graphite/fuel separation method in which the majority of the graphite is mechanically removed. A cooperative experimental program is being conducted with HFH Systems, Inc., manufacturers of electrohydraulic equipment. These experiments are designed to (1) evaluate the capability of a high-frequency electric discharge to produce a controlled fracture of H-327 graphite, and (2) measure the effect of such a discharge or series of discharges on the integrity of both fertile and fissile particles.

8.1. INITIAL FEASIBILITY TEST

A right circular cylinder will be loaded with "reject" FSV fuel. The arrangement of the fuel holes (open at one end) and the coolant holes (open at both ends) will be the same as in a standard fuel element. A single probe (shown in Fig. 32) will be inserted in the central coolant hole and will initially be located at or near the bottom of the hole. The probe will be discharged in this position and also at, for example, 1/2-in. increments along the length of the coolant hole.

The extra aluminum rods in the other coolant holes (Fig. 33) are provided to prevent the fractured cylinder from collapsing (i.e., particles falling into coolant holes). The thick outer cylinder should behave as a "sink" for acoustic stress waves which, hopefully, will make contact at right angles and allow some degree of reflection. It is expected that such reflected stress waves would be of opposite sign (probably tension). In this way, the graphite could be separated from the fuel.

8.2. FUTURE TESTS

If this method of fracture looks promising from the standpoint of minimum particle breakage (at least comparable to a crusher) and the possibility of separating the fuel from the moderator material, then a portion of a fuel element (e.g., a half-length) will be tested in a similar manner. The hexagonal shape of the fuel element offers certain geometrical advantages over a cylindrical shape (principally, the corner edges); an attempt will be made to capitalize on these advantages.

8.3. TEST MATERIAL

Initial tests will be performed using "reject" FSV fuel rods from batch number CR-14-K30152-6 with the properties shown in Table 25.

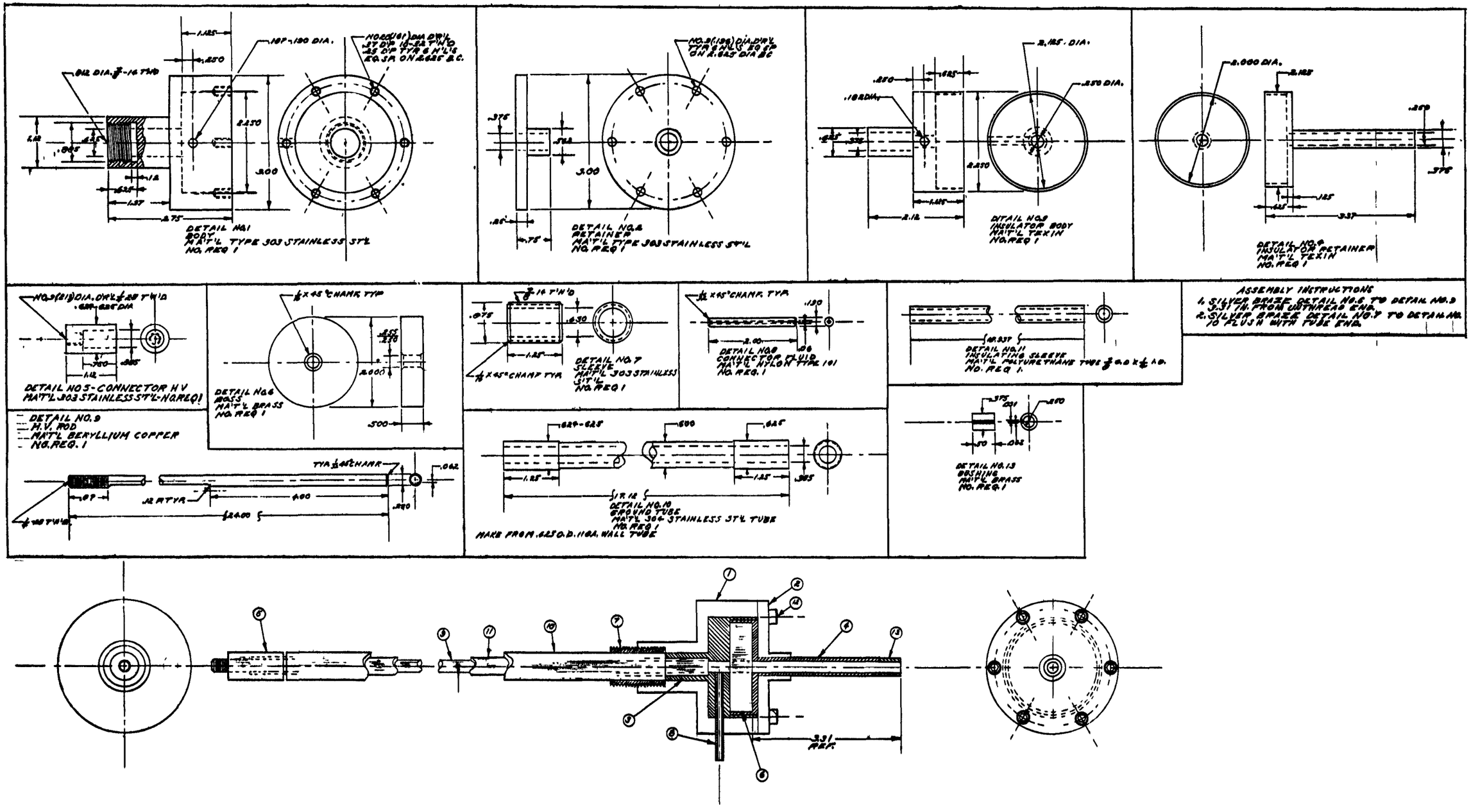

Fig. 32. Inverted pinch electrode assembly

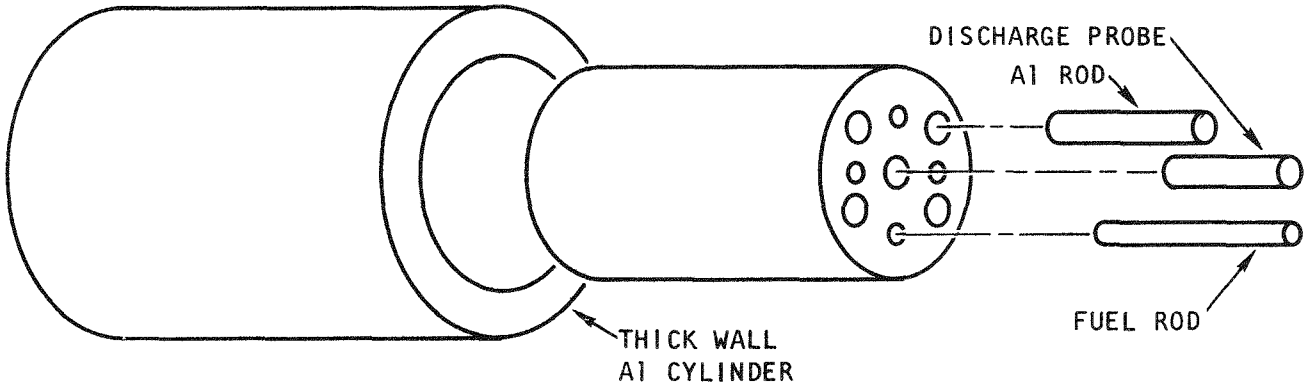

Fig. 33. Experimental apparatus for graphite-fuel separation

TABLE 25
ROD PROPERTIES (FROM BATCH NO. CR-14-K30152-6)

Fissile A		
Batch No.	CU6A3198C	CU6A6196C
Weight, g/rod	2.82	2.38
Fissile B		
Batch No.	-	
Weight, g/rod	-	
Fertile A		
Batch No.	CT6A3087C	
Weight, g/rod	2.37	
Fertile B		
Batch No.	CT6B3016C	
Weight, g/rod	2.45	
Estimated crossover (wt %)	9	
Packing fraction	61.5	
Electrical resistivity, % < 0.5	100.0	
Matrix Uniformity		
Minimum	21	
Maximum	32	
Macroporosity, vol %	24	
Diameter, in.	0.488	
Length, in.	1.940	
End cap, in.	0.13	
Fuel homogeneity		
Mean	1.060	
Standard deviation	0.060	
Uranium weight, g/rod		
Mean	0.1786	
Standard deviation	0.007	
Thorium weight, g/rod		
Mean	3.154	
Standard deviation	0.07	
Carbon weight, g/rod	6.71	
Silicon weight, g/rod	1.46	
Surface contamination		
Fission gas release (R/B)	3.3×10^{-5}	
Thorium, g/g	2.4×10^{-4}	
Broken SiC		
Uranium, g/g	0	
Thorium, g/g	0	
Impurities (ppm)		
Boron equivalent	2	
Iron	40	
Sulfur	100	
Titanium	40	
Vanadium	40	
Hydrogen	1	
Ash	2300	
Water	1	
Production status	3	
Weight percent broken particles (based on U, Th analysis)	2.90	

9. CONCEPTUAL DESIGN OF A TARGET RECYCLE PLANT FOR HTGR FUEL

9.1. INTRODUCTION

Work continued with the Ralph M. Parsons Company of Pasadena on the conceptual design of a Target Recycle Plant (TRP) for the reprocessing and refabrication of HTGR fuel. This work is jointly funded by the Thorium Utilization Program and General Atomic Company. The conceptual design effort is about 75% complete.

The general approach followed in implementing the conceptual design effort was to prepare design criteria and system description documents. A total of 43 such documents (see Table 26) has been issued for use in the conceptual design effort. In the system description, the major process steps are described and are also portrayed in block flow diagrams. On the basis of the design criteria and system descriptions, material balances were prepared. For some systems the material balances and the block flow diagrams were combined on a drawing which was issued as a process flow diagram. Based on the process flow diagram (or the block flow diagram plus material balance), piping and instrument diagrams were prepared. Next, specifications were prepared for the individual equipment items. These specifications included equipment sizing as well as materials of construction, wall thicknesses, supports, internals, and unusual design features. Based on the above, equipment arrangement drawings are made for the individual systems, which are then combined to form the plant arrangement. The number of various drawings issued to date for use on the conceptual design effort is listed in Table 27. Drawings referred to in the following sections are listed in Appendix B.

TABLE 26
DESIGN CRITERIA AND SYSTEM DESCRIPTIONS

DC-202001	Design Criteria--Commercial Reprocessing Plant: Requirements
DC-203001	Design Criteria--Commercial Refabrication Plant: Requirements
DC-204001/ SD-204001	Site Description--Commercial Recycle Plant
DC-207001	Design Criteria--Commercial Recycle Plant: Safeguards
DC-208001	Design Criteria--Commercial Recycle Plant: Safety Requirements
SD-208001	System Description--Commercial Recycle Plant: Plant Safety (Security and Protection)
DC-209501	Design Criteria: General Design Philosophy
DC-210001	Design Criteria: Spent Fuel Element Handling
SD-210001	System Description: Spent Fuel Element Handling
DC-220001	Design Criteria: Head-End Processing System
SD-220001	System Description: Head-End Processing System
DC-230001	Design Criteria: Solvent Extraction
SD-230001	System Description: Solvent Extraction
SD-241001	System Description: UNH Receiving and Storage
SD-242001	System Description: Sphere Loading
SD-243001	System Description: Kernel Carbonization Conversion
SD-244001	System Description: Kernel Coating
SD-245001	System Description: Kernel and Particle Storage
DC-251001	Design Criteria: Particle Blending
DC-252001	Design Criteria: Fuel Rod Formation
SD-252001	System Description: Fuel Rod Formation
DC-253001/ 254001	Design Criteria: Fuel Rod Storage and Loading
SD-253001/ 254001	System Description: Fuel Rod Storage and Loading
DC-255001	Design Criteria: Fuel Rod Carbonization and Heat Treatment

Table 26 (Continued)

SD-255001	System Description: Fuel Rod Carbonization and Heat Treatment
DC-256001	Design Criteria: Final Element Assembly
SD-256001	System Description: Final Element Assembly
SD-257001	System Description: Scrap Recovery
DC-260001	Design Criteria: Heating, Ventilation, and Air Conditioning
SD-260001	System Description: Heating, Ventilation, and Air Conditioning
DC-265001	Design Criteria: Off-gas Processing
SD-265001	System Description: Off-gas Processing
SD-270001	System Description: Liquid Waste
DC-276001	Design Criteria: Liquid Waste Calcination
SD-276001	System Description: Liquid Waste Calcination
DC-280001	Design Criteria: Decontamination and Maintenance
SD-280001	System Description: Decontamination and Maintenance
DC-287001	Design Criteria: Process Support (Analytical)
SD-287001	System Description: Process Support (Analytical)
DC-288001	Design Criteria: Process Support (Plant Control)
SD-288001	System Description: Process Support (Plant Control)
SD-290001	System Description: Utility Systems

TABLE 27
DRAWINGS ISSUED FOR THE CONCEPTUAL DESIGN STUDY

System	Block Diagram	Flow Diagram	Piping and Instrument Diagrams	Arrangement
Fuel receiving, storage, and shipping	4			11
Head end	7		22	6
Solvent extraction	8	8	15	4
Fissile particle fabrication	7	6	6	
Fuel element fabrication	9	6	5	
Scrap recovery	12		20	
HVAC		4	8	23
Off-gas	4	6	13	
Liquid waste	5	5	13	
Solid waste	3	3	6	
Decontamination and maintenance				1
Analytical	8			
Cold chemical and utilities			1	
Total	67	38	109	45

9.2. FUEL HANDLING

Fuel handling involves the receipt and unloading of shipping casks, storage of the spent fuel, transfer to the process, decontamination and refurbishing of the shipping casks and fuel shipping containers, storage of refabricated fuel, and loading into the shipping cask. The design of this system is complete except for a few piping and instrument diagrams on the associated decontamination systems. The following drawings illustrate the design of the fuel handling system: PA-21100-1, -2, and -3; PA-216001, PPF-130, PPF-160, and PPF-180.

9.3. HEAD END

The head-end system encompasses the process steps of fuel element crushing, burning, particle crushing, leaching, and input accountability. The design of this system is essentially complete. The equipment specifications have been prepared and are ready for cost estimating. Arrangement drawings have been issued but may be modified by the dictates of the plant arrangement. The block flow diagrams (Drawing B2-2-200) show the various head-end process steps.

9.4. SOLVENT EXTRACTION

The solvent extraction system is designed to process the U-233 and U-235 in separate trains. Modifications of the acid Thorex and Purex processes are used with pulse columns specified as the solvent extraction contactors. Drawing BD-2-300 consists of the block flow diagrams for the solvent extraction system. The engineering work on the solvent extraction system has been completed.

9.5. FISSILE PARTICLE FABRICATION

The fissile particle preparation system contains individual process lines for U-233 and U-235. This system includes UNH batching, denitration,

resin loading, kernel carbonization and conversion, and kernel coating. Drawings BD-2-420, -430, -440, and -441 illustrate the major process steps in fissile particle preparation. The process flow diagrams are complete except for some modifications; the piping and instrument diagrams are also complete. The equipment specifications have progressed to the point of sizing the equipment items, and equipment arrangement work has been initiated.

9.6. FUEL ELEMENT FABRICATION

Process steps included within the fuel element preparation system are fuel particle blending, fuel rod formation, loading of fuel rods into the graphite blocks, in-block fuel rod carbonization and heat treatment, and final fuel element assembly. Drawings BD-2-510, -520, -540, -550, and -560 are the block flow diagrams for this system. The process flow and the piping and instrument diagrams have been completed, the preparation of equipment specifications is well advanced, equipment arrangement is nearing completion.

9.7. SCRAP RECOVERY

In the scrap recovery system, material from the refabrication area that does not meet specifications is processed to recover the fissile material and at least part of the fertile material. To the extent possible, scrap material is processed in a manner that permits its reinsertion into an earlier step in the refabrication area. This minimizes the quantity of material recycled to the reprocessing portion of the plant. In addition, only nitrate solutions are recycled to reprocessing. Piping and instrument drawings have been prepared and work has been initiated on developing the equipment specifications.

9.8. HEATING, VENTILATION, AND AIR CONDITIONING (HVAC)

The function of the HVAC system is to provide suitable environments for occupied areas, to remove heat from the process cells, and to confine

contamination by controlled directional air flow and by filtration. As the various areas are defined for the individual process systems, HVAC drawings are prepared. To date four such drawings have been completed. In addition, typical control and instrument drawings and mechanical equipment arrangement drawings have been prepared for supply air systems, exhaust systems, heat chambers, filter units, etc. Duct work drawings have been prepared for the fuel handling area.

9.9. OFF-GAS

In the off-gas system, gaseous effluents from the process equipment are collected and treated for the removal of gaseous and particulate fission products prior to atmospheric release via the plant stack. In addition, the nitrogen oxides are reduced to acceptable release limits. Gaseous fission products removed are iodine, krypton, radon, and tritium. Krypton is removed by the KALC process and the others by adsorption on zeolites or molecular sieves. The off-gas system is divided into four subsystems for handling the off-gases from the burners, leachers, reprocessing vessels, and refabrication gases. The process flow and piping and instrument diagrams are complete. Work on the equipment specifications is well advanced, and equipment arrangement has been initiated.

9.10. LIQUID WASTE

In the liquid waste system, the waste streams arising from the reprocessing operation are processed to produce recovered nitric acid for recycle to the process, decontaminated water that is vaporized and discharged through the plant stack, and concentrated high- and intermediate-level waste streams. Drawing BD-2-700 shows the process steps in liquid waste treatment. Process flow and piping and instrument diagrams have been prepared, and the development of equipment specifications is nearing completion.

9.11. SOLID WASTE

The solid waste system includes the solidification of high- and intermediate-level liquid wastes as well as its packaging and interim on-site storage, the incorporation of tritiated water into concrete, and the incineration of contaminated combustible material and its packaging. The high-level waste calcination process uses a fluidized bed calciner producing a granular calcine. In this area, process flow and piping and instrument diagrams have been developed, the equipment has been sized, and preliminary equipment arrangement drawings have been prepared. Work has been initiated on waste incineration. Arrangement drawings for the underwater storage of packaged calcined waste, SiC hulls, and retired U-235 fissile particles are well advanced.

9.12. MISCELLANEOUS

The plant analytical facilities have been defined. The plant control system (data acquisition and dissemination) has been specified and the cost estimating effort is well advanced. A draft of the QA plan for the recycle plant project has been prepared. Process equipment decontamination and maintenance cells within the process building have been defined and layout drawings (280001) have been prepared.

As the work on the various process systems is completed, the related utility and cold chemical requirements are determined. Preliminary sizing of the steam supply and cooling water equipment has been accomplished as well as that for bulk chemicals. A cold chemical piping and instrument diagram for leacher acid makeup has been completed.

9.13. SITE

A preliminary drawing of the overall site arrangement was prepared. This drawing, however, is being modified to reflect changes resulting from

the subsequent work on equipment arrangements prepared for the individual systems. Layout drawings have been prepared for several of the site support facilities including the administration building, training center, maintenance shops, locker rooms, and cafeteria.

REFERENCES

1. Faires, V. M., Design of Machine Elements, MacMillan and Company, New York (1955), p. 84.
2. Nash, W. A., Strength of Materials, Schaun Publishing Company, New York (1957), p. 40 (problem 9).
3. Timoshenko, S. P., and J. N. Goodier, Theory of Elasticity, McGraw-Hill Book Company, New York (1970), p. 138.
4. Kovalski, B. S., and F. F. Sorokovenko, "Design, Calculation, and Testing of Machines," Russian Eng. J. XLIX (No. 10), 6 (1974).
5. ASIM Bulletin B438-70, p. 639.
6. Jenike, A. W., "Storage and Flow of Solids," University of Utah Engineering Experiment Station Bulletin 123, March 1970.
7. "Thorium Utilization Program Quarterly Report for the Period Ending August 31, 1974," USAEC Report GA-A13178, General Atomic Company, October 31, 1974.
8. Stula, R. T., "10-cm Primary Burner Run 46," General Atomic unpublished data, October 1, 1974.
9. Stula, R. T., "10-cm Primary Burner Auger System Evaluation," General Atomic unpublished data, June 25, 1974.
10. Stula, R. T., "10-cm Primary Burner Runs 49, 50, and 51," General Atomic unpublished data, October 18, 1974.
11. Zimmerman, R. D., "16-in. Primary Burner Operating Cycle - Conceptual Design Basis," General Atomic unpublished data, May 2, 1974.
12. Wender, L., and G. Cooper, A. I. Ch. E. J. 4, 15 (1958).
13. "Bed-to-Wall Heat Transfer Coefficient for Fort St. Vrain Pilot Plant Primary Burner," ICPP Memo DLA-5-74.
14. Stula, R. T., "10-cm Primary Burner Run 44 - 8/21/74," General Atomic unpublished data, September 3, 1974.

15. Jakob, M., Heat Transfer, Vol. I, John Wiley and Sons, New York (1949), p. 552.
16. Mc Adams, W. H., Heat Transmission, McGraw-Hill Book Company, New York (1954).
17. Zimmerman, R. D., "Burner Operating Temperature," General Atomic unpublished data, September 13, 1974.
18. Standifer, R. L., Chem Eng. Progr. Symp. Ser. 66 (No. 105), 198 (1970).
19. Wen C. Y., and R. F. Hashinger, A. I. Ch. E. J. 6, 220 (1960).
20. Zenz, F. and D. F. Othmer, Fluidization and Fluid-Particle Systems, Reinhold Publishing Corp., New York (1960).
21. Todes, O. M., in Applications of Fluidized Beds in the Chemical Industry, Izd. "Znanie," Leningrad, Part II, pp. 4-27.
22. Goroshko, V. D., R. B. Rozenbaum, O. M. Todes, Izv. Vysshikh Uchebn. Zavedenii, Neft i Gas No. 1, 125 (1958).
23. Rozenbaum, R. B., and O. M., Todes, Dokl. Akad. Nauk SSR 115, 504 (1957).
24. Rickman, W. S., "10-cm Primary Burner Run F4RHB-M36," General Atomic unpublished data, April 22, 1974.
25. Nicholson, E. L., L. M., Ferris, and J. T. Roberts, "Burn-Leach Processes for Graphite-Base Reactor Fuels Containing Carbon-Coated Carbide or Oxide Particles," USAEC Report ORNL-TM-1096, Oak Ridge National Laboratory, April 1965.
26. Perry, J. H., Chemical Engineers Handbook, 5th Edition, McGraw-Hill Book Company, New York (1973).
27. Park, U., "10-cm Secondary Burner Induction Coil Design With a Susceptor Plate," General Atomic unpublished data, October 17, 1974.
28. Davidson, J. F., and D., Harrison, Fluidization, Academic Press, New York (1971).
29. Einstein, V. G., Dissertation, Inst. Fine Chem. Technol., Moscow (1967).
30. Zabrodsky, S. S., Int. J. Heat Mass Transfer 16, 241 (1973).
31. Variggin, N. N., and I. G. Martjushin, Khin. Mashinostr. No. 5, 6 (1959).
32. Wen, C., and M. Leva, A.I. Ch. E. J. 2, 482 (1956).

33. Wender, L., and G. Cooper, A.I. Ch. E. J. 4, 15 (1958).

34. Dow, W. M., and M. Jakob, Chem. Eng. Progr. 47, 637 (1951).

35. Van Heerden, G., P. Nobel, and D. W. Van Krevelen, Chem. Eng. Sci. 1, 51 (1951).

36. Van Heerden, G., P. Nobel, and D. W. Van Krevelen, Ind. Eng. Chem. 45, 1237 (1953).

37. Toomey, R. D., and H. F. Johnstone, Chem. Eng. Progr. Symp. Series 49, 51 (1953).

38. Levenspiel, O., and J. S. Walton, Chem. Eng. Progr. Symp. Series 50, 1 (1954).

39. Nicholson, E. L., L. M. Ferris, and J. T. Roberts, USAEC Report ORNL-TM-1096, Oak Ridge National Laboratory, April 2, 1965.

40. "HTGR Base Program Quarterly Progress Report for the Period Ending August 31, 1972," USAEC Report Gulf-GA-A12222, Gulf General Atomic, September 30, 1972, pp. 76-78.

41. "HTGR Base Program Quarterly Progress Report for the Period Ending May 31, 1972," USAEC Report Gulf-GA-A12150, Gulf General Atomic, June 30, 1972, pp. 69-70.

42. Benedict, G. E., "Solvent Extraction Experimental Run Plan," General Atomic unpublished data, May 29, 1974.

APPENDIX A

ENGINEERING DRAWINGS FOR INSOLS DRYING SYSTEM

DWG NO.	TITLE
5267004	Fluid bed insols dryer assembly
5267005	Fluid bed vessel
5267006	Nitrogen heater assembly (5 sheets)
5267007	Base cone - fluid bed vessel
5267008	Cyclone transition
5267009	Product collection vessel
5267010	Centrifuge feed transition
5267011	Y-transition
5267012	Absolute filter housing
5267013	Humidity sensor duct assembly
5267014	Humidity sensor duct assembly
5267016	Cyclone to Y-transition
5267017	Base cone elbow

APPENDIX B

ENGINEERING DRAWINGS FOR TARGET RECYCLE PLANT FOR REPROCESSING AND REFABRICATION OF HTGR FUEL

DWG NO.	TITLE
PA-211001	Spent fuel receiving plan
PA-211002	Ground floor plan, shipping and receiving
PA-211003	Sections
PA-216001	Refabricated fuel element handling and transfer
PPF-130	Fuel recycle facility fuel receiving - material handling process flowsheet No. 3
PPF-160	Fuel recycle facility fuel receiving - material handling process flowsheet No. 4 (Sheet 1 of 2)
	Fuel recycle facility fuel receiving - material handling process flowsheet No. 5 (Sheet 2 of 2)
PPF-180	Fuel recycle facility fuel receiving - material handling process flowsheet No. 7
BD-2-200	Block flow diagram, fuel element crushing, System 200 (Sheet 1 of 7)
	Block flow diagram, fuel element burning-classifying, System 200 (Sheet 2 of 7)
	Block flow diagram, U-233 material leaching-accountability, System 200 (Sheet 3 of 7)
	Block flow diagram, fissile material leaching, System 200 (Sheet 4 of 7)
	Block flow diagram, U-235 material crushing-burning, System 200 (Sheet 5 of 7)
	Block flow diagram, U-235 material leaching-accountability, System 200 (Sheet 6 of 7)
	Block flow diagram, solids assay, System 200 (Sheet 7 of 7)

DWG NO.	TITLE
B2-2-300	Block flow diagram, U-233 solvent extraction, 1st cycle (Sheet 1 of 8)
	Block flow diagram, U-233 solvent extraction, 2nd cycle (Sheet 2 of 8)
	Block flow diagram, U-233 solvent extraction, 3rd cycle (Sheet 3 of 8)
	Block flow diagram, U-235 solvent extraction, 1st cycle (Sheet 4 of 8)
	Block flow diagram, U-235 solvent extraction, 2nd cycle (Sheet 5 of 8)
	Block flow diagram, thorium concentration (Sheet 6 of 8)
	Block flow diagram, 1st cycle, solvent cleanup system (Sheet 7 of 8)
	Block flow diagram, 2nd cycle, solvent cleanup system (Sheet 8 of 8)
BD-2-420	Sphere loading and drying (Sheet 3 of 7)
BD-2-430	Kernel carbonization and conversion (Sheet 4 of 7)
BD-2-440	Fissile kernel coating (Sheet 5 of 7)
BD-2-441	Fertile kernel coating (Sheet 6 of 7)
BD-2-510	Particle blending
BD-2-520	Fuel rod formation (Sheets 1 of 3, 2 of 3, and 3 of 3)
BD-2-540	Fuel rod loading
BD-2-550	Fuel rod carbonization and heat treatment
BD-2-560	Final element assembly (Sheets 1 of 2 and 2 of 2)
BD-2-700	Low level liquid waste (Sheet 1 of 5)
	Block flow diagram, high level liquid waste (Sheet 2 of 5)
	Block flow diagram, intermediate level liquid waste (Sheet 3 of 5)
	Block flow diagram, solvent disposal (Sheet 4 of 5)
	Block flow diagram, service waste (Sheet 5 of 5)
PA-280001	Decontamination and maintenance

APPENDIX C

TOPICAL REPORTS PUBLISHED DURING THE QUARTER

Brooks, L. H., C. A. Heath, B. Kirstein, and D. G. Roberts, "Carbon-14 in the HTGR Fuel Cycle," USAEC Report GA-A13174, General Atomic Company, November 29, 1974.